# SOLID SUSPENSION AND GAS DISPERSION IN GAS-SOLID-LIQUID STIRRED VESSELS WITH HIGH SOLID CONCENTRATION

**MEYSAM DAVOODY**

**DEPARTMENT OF CHEMICAL ENGINEERING**
**FACULTY OF ENGINEERING**
**UNIVERSITY OF MALAYA**
**KUALA LUMPUR**

**2017**

# SOLID SUSPENSION AND GAS DISPERSION IN GAS-SOLID-LIQUID STIRRED VESSELS WITH HIGH SOLID CONCENTRATION

**MEYSAM DAVOODY**

**THESIS SUBMITTED IN FULFILLMENT OF THE REQUIREMENTS FOR THE DEGREE OF DOCTOR OF PHILOSOPHY**

**DEPARTMENT OF CHEMICAL ENGINEERING**
**FACULTY OF ENGINEERING**
**UNIVERSITY OF MALAYA**
**KUALA LUMPUR**

**2017**

Name of Candidate: Meysam Davoody

Registration/Matric No: KHA120098

Name of Degree: PhD in Chemical Engineering

Title of Thesis: **SOLID SUSPENSION AND GAS DISPERSION IN GAS-SOLID-LIQUID STIRRED VESSELS WITH HIGH SOLID CONCENTRATION**

Field of Study:

I do solemnly and sincerely declare that:

(1) I am the sole author/writer of this Work;
(2) This Work is original;
(3) Any use of any work in which copyright exists was done by way of fair dealing and for permitted purposes and any excerpt or extract from, or reference to or reproduction of any copyright work has been disclosed expressly and sufficiently and the title of the Work and its authorship have been acknowledged in this Work;
(4) I do not have any actual knowledge nor do I ought reasonably to know that the making of this work constitutes an infringement of any copyright work;
(5) I hereby assign all and every rights in the copyright to this Work to the University of Malaya ("UM"), who henceforth shall be owner of the copyright in this Work and that any reproduction or use in any form or by any means whatsoever is prohibited without the written consent of UM having been first had and obtained;
(6) I am fully aware that if in the course of making this Work I have infringed any copyright whether intentionally or otherwise, I may be subject to legal action or any other action as may be determined by UM.

Candidate's Signature Date:

Subscribed and solemnly declared before,

Witness's Signature Date:

Name:

Designation:

## ABSTRACT

Mechanically agitated vessels are used widely for gas-liquid-solid mixing operations in processing plants. In such systems, increase in solid concentration increases the energy required to suspend the solids off the tank bottom. Therefore, improving agitator energy efficiency is essential for operating at high solids concentrations. Most of previous studies are limited to low solids concentrations in solid-liquid systems. Therefore, it is imperative to determine the best possible impeller and tank geometries, and optimum operating conditions for tanks handling high concentration slurries, such as those found in mineral processing plants. This study aims at proposing optimum industrial agitator designs for systems handling high concentration slurries (up to 40% v/v) in the presence of gas. In this regard, a combination of both operational (solid concentration) and design (impeller type and baffling condition) parameters were considered for investigating specific impeller power ($P_j/M_s$) and gas hold-up. The apparatus utilized in this study includes a 0.4 m diameter flat bottom cylindrical perspex tank. The agitation was provided by a shaft which was placed in vertical axis of the tank and driven by a 3.0 kW motor. The power efficiency factor ($\varepsilon_{jsg}^{-1}$ (kg/W)) serves as an indication of the quantity of solid particles that could be suspended per unit of power consumed by impeller. Accordingly, it was found that the $\varepsilon_{jsg}^{-1}$ values can be maximized by operating the mixing tank with an optimum range of solids concentration, which is around $C_v$ = 0.2 - 0.3 v/v for the systems studied in this work. It was observed that larger diameter mixed flow impellers were more energy efficient when the tank was operated under aerated condition with an optimum concentration of solids. Increase in particle size resulted in lower $\varepsilon_{jsg}^{-1}$ values and this phenomenon was more prominent in unbaffled tanks. Another term, known as baffling efficiency factor, 'R', was used to study how baffle removal influences the energy efficiency of impellers in three-phase systems. It was observed that absence of

baffles could exert negative effects on energy efficiency of axial- and mixed-flow impellers at particular operating conditions. The investigations also included the effect of baffle removal on solid dispersion. Gas holdup, Sauter mean bubble diameter ($d_{32}$), and gas-liquid interfacial area ($\alpha_{g-l}$) were also studied. The results indicated that $d_{32}$ values decrease with an increase in particle size and solids concentration. Then, an optimum solids concentration was identified at which the performance of the impeller expressed in terms of power efficiency and ability to generate sufficient gas-liquid interfacial area is maximized. Mathematical models were developed to predict the optimum solids concentration, $d_{32}$, and $\alpha_{g-l}$, and their predictions exhibited reasonable agreement with the experimental results. In the last part of this paper, an example is shown to highlight the advantages of implementing the optimization strategies proposed in this work.

## ABSTRACT (In Malaya language)

Kelalang teraduk mekanikal digunakan secara meluas dalam operasi percampuran gas-cecair-pepejal di kilang pemprosesan. Dalam sistem tersebut, peningkatan kepekatan pepejal akan meningkatkan tenaga yang diperlukan untuk mengapungkan pepejal dari bahagian bawah tangki. Oleh itu, penambahbaikan tenaga kecekapan pengaduk adalah penting untuk sistem beroperasi pada kepekatan yang tinggi. Kebanyakan kajian sebelum ini adalah terhad kepada kepekatan pepejal yang rendah dalam sistem pepejal-cecair. Oleh itu, adalah penting untuk menentukan pendesak dan geometri tangki yang sesuai serta keadaan operasi yang optimum supaya tangki dapat mengendalikan sluri yang berkepekatan tinggi seperti yang terdapat di kilang pemprosesan mineral. Dalam kajian ini, reka bentuk optimum untuk pengaduk industri bagi sistem yang mengendalikan sluri berkepekatan tinggi (sehingga 40% v/v) dengan kehadiran gas akan dicadangkan. Dalam hal ini, gabungan dua parameter operasi iaitu (kepekatan pepejal) dan reka bentuk (jenis pendesak dan keadaan mengherankan) dipertimbangkan untuk mengkaji kuasa khusus pendesak ($P_j/M_s$) dan isipadu gas terkumpul. Alat yang digunakan dalam kajian ini termasuklah 0.4 m diameter bahagian bawah silinder perspek tangki. Pengadukan telah dihasilkan oleh aci yang diletakkan di dalam paksi menegak tangki dan didorong oleh motor 3.0 kW. Istilah yang ditakrifkan sebagai faktor kecekapan kuasa, $\varepsilon_{jsg}{}^{-1}$ (kg/W) berfungsi sebagai petunjuk kuantiti zarah pepejal yang boleh terapung bagi setiap unit kuasa yang digunakan oleh pendesak. Oleh itu, didapati bahawa nilai $\varepsilon_{jsg}{}^{-1}$ boleh dimaksimumkan dengan mengendalikan tangki pencampuran dengan pelbagai kepekatan pepejal optimum iaitu sebanyak $C_v$ = 0.2-0.3 v/v digunakan untuk kajian. Melalui pemerhatian didapati bahawa pendesak bercampur aliran yang berdiameter besar lebih cekap tenaga apabila tangki itu beroperasi di bawah keadaan berudara dengan kepekatan pepejal yang optimum. Peningkatan saiz zarah menyebabkan nilai $\varepsilon_{jsg}{}^{-1}$ menjadi lebih

rendah dan fenomena ini lebih menonjol di dalam tangki yang tiada sesekat. Istilah lain yang dikenali sebagai faktor kecekapan membingungkan ‘R’ telah digunakan untuk mengkaji bagaimana penyingkiran sesekat mempengaruhi kecekapan tenaga pendesak dalam sistem tiga fasa. Pemerhatian mendapati bahawa ketiadaan sesekat mempengaruhi kecekapan tenaga pendesak dalam sistem tiga fasa. Ianya juga mendapati bahawa ketiadaan sesekat boleh memberi kesan negatif ke atas kecekapan tenaga paksi dan pengaduk bercampur-aliran pada keadaan operasi tertentu. Penyelidikan juga termasuk kesan penyingkiran sesekat pada serakan pepejal. Dalam bahagian seterusnya kajian, gas holdup, Sauter mean diameter gelembung ($d_{32}$), dan kawasan sentuhan gas-cecair ($\alpha_{g\text{-}l}$) dikaji. Keputusan dinyatakan nilai-nilai $d_{32}$ berkurangan dengan meningkat saiz dan kepekatan zarah. Kemudian, satu kepekatan pepejal optimum telah dikenal pasti di mana prestasi pendesak dalam kecekapan kuasa dan keupayaan untuk menjana mencukupi kawasan sentuhan gas-cecair adalah dimaksimumkan. Model matematik telah dibangunkan untuk meramalkan pepejal berkepekatan optimum, $d_{32}$, dan $\alpha_{g\text{-}l}$, dan ramalan yang dihasilkan menunjukkan kaitan munasabah dengan keputusan eksperimen. Dalam bahagian akhir kertas kerja ini, contoh ditunjukkan untuk menyerlahkan kelebihan melaksanakan strategi pengoptimuman yang dicadangkan dalam kerja ini.

## ACKNOWLEDGEMENT

I would like to express my sincere gratitude to Professor. Ir. Dr. Abdul Aziz Bin Abdul Raman for his invaluable assistance and would like acknowledge his support during this study. As my supervisor, he provided constant academic and moral supports throughout the project. Appreciation is also extended to Dr. Rajarathinam Parthasarathy, my second supervisor, for his valuable guidance.

My sincere gratitude goes to the University of Malaya, for granting me the opportunity to pursue my PhD program, allowing access to laboratories, equipments, library resources and all other supports during the period of study.

I am also grateful to the University of Malaya High Impact Research Grant (HIR-MOHE-D000038-16001) from the Ministry of Higher Education Malaysia which financially supported this work.

My heartfelt appreciation goes to my dear wife Parastou for her emotional and spiritual support during the program. She helped me immensely in diverse ways.

# TABLE OF CONTENT

# LIST OF FIGURES

# LIST OF TABLES

# LIST OF ABBREVIATIONS

## Nomenclature and Symbols

Greek Letters

| | | |
|---|---|---|
| $\sigma$: | Surface tension | [$Nm^{-1}$] |
| $\varepsilon$: | Energy dissipation rate per unit mass | [W/kg] |
| $\varepsilon_{jsg}$: | Specific impeller power input at $N_{jsg}$ | [kg/W] |
| $\varepsilon_{js}$: | Specific impeller power input at $N_{js}$ | [kg/W] |
| $\varepsilon_{jsg}^{-1}$: | Power efficiency factor: Mass of the suspended solids per unit of Power at $N_{jsg}$ | [kg/W] |
| $\emptyset_g$: | Gas holdup | - |
| $\rho_s$: | Solid phase density | [$kg/m^3$] |
| $\rho_l$: | Liquid phase density | [$kg/m^3$] |
| $\rho_G$: | Gas phase density | [$kg/m^3$] |
| $\rho_w$: | Density of water | [$kg/m^3$] |
| $\rho_{slurry}$: | Density of slurry | [$kg/m^3$] |
| $\rho_{l\,eff}$: | Effective liquid density | [$kg/m^3$] |
| $\mu_l$: | Liquid phase viscosity | [Pa.s] |
| $\mu_g$: | Gas phase viscosity | [Pa.s] |
| $\mu_{slurry}$: | Viscosity of slurry | [Pa.s] |
| $\tau$: | Torque | |
| $\boldsymbol{\nu}$ : | The kinematic viscosity of liquid | [$m^2s^{-1}$] |

## Letters and Subscripts

| | | |
|---|---|---|
| $\alpha_{g\text{-}l}$: | Gas-liquid interfacial area | [$m^{-1}$] |
| C: | Impeller clearance | [m] |

| | | |
|---|---|---|
| $C_v$: | Solid volume fraction | [v/v] |
| $(C_v)_{OSC}$: | Optimum solids concentration | [v/v] |
| D: | Impeller diameter | [m] |
| d: | Particle size | [m] |
| $d_{32}$: | Sauter mean bubble diameter | [m] |
| $d_{max}$: | The maximum stable diameter | [m] |
| g: | Gravitational acceleration | [$m/s^{-2}$] |
| $H_B$: | Bed height | [m] |
| $H_S$: | Suspension/slurry height | [m] |
| k: | Impeller constant | |
| $M_s$: | Mass of solids | [kg] |
| N: | Impeller speed | [rps/rpm] |
| $N_{jsg}$: | The impeller speed for complete off-bottom suspension in three-phase system | [rpm] |
| $N_{js}$: | The impeller speed for complete off-bottom suspension in two-phase system | [rpm] |
| $N_p$: | Power number | |
| $N_{RE}$: | Reynolds number | |
| P: | Power | [W] |
| $P_g$: | Gassed power | [W] |
| S: | Dimensional coefficient | |
| R: | Baffling efficiency factor | |
| $Q_g$: | Gas flow rate | [vvm] |
| T: | Tank diameter | [m] |
| V: | Tank volume | [$m^3$] |
| $V_l$: | Liquid volume | [$m^3$] |

| | | |
|---|---|---|
| X: | Solid loading ratio | [kg/kg] |
| W: | Impeller’s blades width | [m] |

**Abbreviations**

| | | |
|---|---|---|
| OSC: | Optimum solids concentration | [v/v] |
| vvm: | Volumetric flow rate of gas per minute per volume of liquid in the tank | |

# CHAPTER 1: INTRODUCTION

## 1.1 Background

Mineral processing, catalytic gas-phase reactions, oxidation, hydrogenations, fermentation, and wastewater treatment represent only a small number of the complex mixing processes in three phase stirred vessels that involve simultaneous dispersion of gas and suspension of solids in a liquid (Nienow and Bujalski, 2002). Efficiency of mixing is directly controlled by the liquid flow, which in turn is governed by a number of factors including solid concentration, gas flow rate, agitation speed, impeller type and its geometry. These factors, at the same time, determine the total energy input to the system, which is the basis for economic evaluation of the process. In such systems, process intensification is usually practiced by enhancing the production yield per unit volume per unit time without modifying the current plant. Yield enhancement is obtained by improving the efficiency of mixing in the system since reducing the volume of the current vessels is impractical. Thus, the process is intensified by enhancing the solids throughput and maintaining size of the tanks. As the concentration of solids in the system increases, however, the required speed for complete suspension of solids enhances accordingly, which in turn increases the power input to the system. This situation is even more severe in three phase systems where introduction of gas often leads to immediate sedimentation of solid particles and the agitation speed should be further increased to avoid particle sedimentation at the tank bottom. Therefore, it is imperative to identify suitable impeller configurations and operating conditions that enable a highly-dense three phase stirred tank to maintain the solid particles in suspension form by consuming the least amount of energy.

Various strategies have been proposed to minimize the power input to the slurry tanks. Kasat & Pandit (2005) concluded that the proper selection of impellers has immense impact on the performance of stirred vessels. Wu et al. (2010) obtained up to 70% saving in power consumption of solid-liquid stirred vessels by removing baffles. Recently Wang et al. obtained significant saving in impeller power input in solid-liquid systems through a combination of suitable operating conditions and baffling configuration. Yet, an effective approach to minimize the power draw of three phase stirred vessels operating at high solids concentrations is missing as the available documents are limited to two phase systems (Wang et al., 2014).

Process intensification is usually defined as enhancement in production yield per unit volume per unit time, which is achieved by either increasing solids concentration (throughout) or reducing volume of the existing vessel as stated in a number of studied (Drewer (2000); Wang et al. (2012b); Wang et al. (2014)).

## 1.2 Problem statement

Mixing efficiency in agitated vessels is directly controlled by liquid flow, which is governed by a number of factors including solids concentration, gas flow rate, agitation speed, impeller type and geometry. These factors, at the same time, determine the total energy input into the system, which is the basis for economic viability of the process. In such systems, process intensification is usually practiced by enhancing the production throughput per unit volume per unit time without modifying the existing equipment. Higher throughput can probably be obtained only by improving the mixing efficiency of the system since reducing the volume of the existing mixing vessels in the plant is impractical. In other words, enhancing the solids throughput without altering the size of mixing tanks can intensify a process. However, as the solids concentration increases, the impeller speed required to achieve complete suspension of solids increases accordingly,

leading to a subsequent increase in impeller power input. This occurrence is even more prominent in three-phase systems as the introduction of gas often leads to immediate sedimentation of particles thereby leading to further increase in impeller speed to avoid particle sedimentation at the tank bottom.

In addition, studying bubble size and gas-liquid hydrodynamics in presence of high concentrations of solids is challenging due to lack of proper tools for measuring bubble size in three-phase stirred vessels. As a result, the knowledge on gas-liquid interactions in three-phase systems involving high solids concentrations is far from complete, and consequently, proposing optimum conditions to achieve maximum efficiency in the system is challenging.

Therefore, it is imperative to identify suitable impeller configurations and operating conditions to maintain solids suspended in a three-phase stirred tank with the minimum energy consumption and maximum contact area between gas and liquid phases.

## 1.3 Aims and objectives

The present work aims at identifying optimum operating conditions at which the performance of the impeller expressed in terms of power efficiency and ability to generate sufficient gas-liquid interfacial area is maximized. This study will also work towards proposing mathematical models to estimate system's behavior in different conditions.

The main objectives of the present work are to achieve the followings:

- To determine suspension of solids in three-phase stirred vessels
- To determine optimum solids concentrations in two- and three-phase systems based on power efficiency
- To determine the effects of various operating and design parameters on the optimum solids concentrations

- To determine the effects of solids concentration and size on Sauter mean bubble size, gas holdup, and gas-liquid interfacial area
- To propose mathematical correlations to predict key parameters in design and operation of three-phase mixing tanks

## 1.4 Scope of the study

The scope of this study is limited to determining solids suspension and gas-liquid hydrodynamics in stirred vessels. Water, compressed air, and glass beads were used to represent liquid, gas and solid phases, respectively. All experiments were conducted in batch mode. Systems were running for sufficient time to achieve steady state conditions before solids suspension, gas holdup, and gas bubble size were determined. All runs were also carried out at $N_{js}$, ensuring that solids were fully suspended during all tests.

## 1.5 Organization of the thesis

This thesis is organized in the following order:

**Chapter 1:** This chapter briefly discusses the current gap in operation of three-phase agitated vessels handling high solids-concentrations, and highlights the research's objectives.

**Chapter 2: Literature Review**

This chapter discusses past work on three-phase mixing. It also describes various methods of measuring the complete off-bottom suspension speed, bubble size, gas hold-up, and determination of impeller's power consumption in two- and three-phase mixing vessels. This chapter aims at identifying the gaps in the current literature.

**Chapter 3: Methodology**

This chapter provides the details of the experimental set-up and procedure used in the present work.

**Chapter 4: Results and discussion**

The impeller's specific power to achieve complete off-bottom suspension is expressed based on the total mass of the suspended solids. Accordingly, an optimum solid concentration ($(C_v)_{OPT}$) was identified at which the consumed power by impellers was supplied most efficiency. Effect of gas introduction, gas flow rate, particle size, impeller type, and baffling configuration on Cv was thoroughly investigated. Investigations also included the effect of solids concentration on gas holdup, average gas bubble size ($d_{32}$), and eventually gas-liquid interfacial area ($\alpha_{g-l}$). Chapter is finalized by proposing mathematical correlations to predict critical parameters in various operating conditions.

**Chapter 5: Conclusions and Recommendations for future works**

Conclusions from this study are summarized in this chapter and recommendations are made for future work.

# CHAPTER 2: LITERATURE REVIEW

## 2.1 Introduction

This chapter initially reviews the various techniques proposed for determination of critical impeller speed, gas holdup, and average bubble size in two- and three-phase stirred vessels. A general literature review is also provided on the effect of various operating and design factors on impeller's power input in stirred vessels.

Mineral processing, catalytic gas-phase reactions, oxidation, hydrogenations, fermentation, and wastewater treatment represent only a small number of complex mixing processes carried out in three-phase stirred vessels that involve simultaneous dispersion of gas and suspension of solids in a liquid (Nienow & Bujalski, 2002). Flow field is the main force that lifts solid particles from the tank bottom and disperses them throughout the liquid medium. The mechanical energy supplied to a given vessel highly contributes to the degree of turbulence in the flow field, and higher impeller energy input can lead to higher degree of suspension due to formation of more powerful anisotropic turbulent eddies. Therefore, the impeller power consumption is a major operating parameter in stirred tanks, which is directly influenced by factors such as agitation speed, solids concentration, impeller type and baffling configuration.

## 2.2 Hydrodynamics of particle suspension

Drag and lift forces produced by the mobile fluid and the bursts of the turbulent eddies are the major factors responsible for suspension of solids. It's been also proposed that

particles with density equal to that of liquid keep rotating in the tank once complete off-bottom suspension is achieved (Paul et al., 2004).

### 2.2.1 Hydrodynamics of suspension in gas-solid-liquid systems

A wide variety of processes require the suspension of solid particles in liquid. Examples include crystalisation, dissolution, ion-exchange, polymer dispersion, coal-water slurries, solid catalysed liquid reactions and cell suspension in fermentation. Agitation is usually necessary to prevent separation of the two phases due to density differences. This chapter is concerned with systems where the solids are heavier than the liquid. The duty of the agitators then to lift them from the base of the vessel and keep them suspended.

It is important to establish the optimum operating condition. The state of "just-suspension" is usually defined as the point when the particles are completely lifted off the base. Before *complete suspension* is achieved the entire solids surface area is not available for processing; and increasing the agitation beyond this state does not remarkably improve mass transfer.

Investigators generally use the impeller speed as the dependent variable because it is the easiest to change, but there is no fundamental reasoning for choosing this quantity as the dependent one. In the literature, the critical speed at just-suspension is usually designated as $N_{js}$.

The impeller and tank geometry have been shown to have a significant role in determining the quality of suspension in a stirred vessel. Properties of the liquid and solids also affect the agitation intensity.

The work of Zwietering (1958) is frequently cited in solid suspension studies as it still represents the most complete investigation of $N_{js}$. He defined the complete suspension criterion such that no particle remains stagnant on the tank base for longer than a few (l or 2) seconds. This is termed the "1-2 second criterion" and it can be determined relatively

easily by visual observation of the base. This allowed over 1000 experiments to be performed with a wide range of variables covered. Using dimensional analysis, the classic empirical correlation (Eq 2-1) was obtained after expansion of the dimensionless groups:

$$N_{js} \propto S d_p^{0.21} \left(\frac{\Delta\rho}{\rho_l}\right)^{0.43} X^{0.12} D^{-2.21} \qquad \textbf{2-1}$$

The values of the exponents on the right hand side of the equation are independent of the impeller geometry, tank size or D/T and the impeller clearance. Variations in geometry is incorporated in the value of the constant S. For disc turbines Zwietering did not find the effect of clearance (C) on S between *T/7* < C < *T/2*.

The dimensionless proportionality constant $N_{Po}$ represents the ratio of the pressure differential, formed by the flow of liquid in the vessel to the inertial forces. It is commonly known as the power number. The power number is a function of the impeller Reynolds number $N_{Re}$. In mixing vessels, the laminar region is when $N_{Re}$ is less than 10, the transitional region is when $N_{Re}$ is between 10 and 4000 and the fully turbulent region is when $N_{Re}$ is greater than 4000 (Metzner and Otto, 1957). At $N_{Re}$ below 10 and above 100, the $N_{Po}$ values in the non-Newtonian liquid are the same as those in the Newtonian liquid. In the range between 10 and 100, the impeller in the non-Newtonian liquid consumes less power than the Newtonian fluid. This indicates that the transition from laminar to turbulent flow in the non-Newtonian liquid is delayed until a $N_{Re}$ of about 45 is reached as compared to 10 in the Newtonian liquid.

Nienow (1968) performed an experimental study with disc turbines with a new range of density difference, particle size and concentration, and obtained the relation:

In Zwietering's equation the exponent of the D term for disc turbine after including the dependence of S on it ($S \propto (T/D)^{1.5}$ ) is -2.35, hence, there is very good agreement

between the two equations. However, Nienow (1968) found a significant influence of the clearance on $N_{js}$, although it was not included in Eq 2-1.

Chapman et al. (1983) reported a study with a number of different impeller types and a range of particle and liquid properties and reported similar results. The general relation obtained is:

$$N_{js} \propto d_p^{0.15} \left(\frac{\Delta\rho}{\rho_l}\right)^{0.4} X^{0.12} D^{a} \qquad \textbf{2-2}$$

where the exponent "α" was dependent on the impeller geometry. For 6DT the value was 2.45 and for 4-blade mixed-flow impellers it was -1. 5. From Zwietering's data a value of -1.67 was obtained for propellers. The effect of clearance on $N_{js}$ for 6DT was confirmed. The liquid kinematic viscosity was increased from $10^{-6}$ to 5 x $10^{-6}$ $m^2/s$, and there was no significant effect on $N_{js}$. Minor geometrical variations on the vessel bottom such as the presence of a centre bearing on the base were capable of having very dramatic effects on suspension. The exponent for the Δρ term was obtained using density differences between 50 and 1900 $kg/m^3$.

The authors found that Zwietering's equation failed for particles with shape drastically different from spherical or granular. The example given was anthracite which was predominantly flat and very angular. Zwietering (1958) did indicate that the correlation should be applicable to small scale, flat bottom tank and does not recommend its use when geometric or experimental conditions are very different from those covered in that work.

Raghavo Rao et al. (1988) working with 6-blades mixed flow impellers obtained similar exponent values for $d_p$ and X and an exponent of -1.16 for D when the impeller is pumping downward. The reason given for a lower exponent value for D with downward pumping impellers compared to 6DT was that the length of the flow path does not change appreciably with changes in the 6MFD diameter because liquid flow is between the

impeller to the base; and a small change in path may only occur because of changes in the blade width.

There is a wealth of information on the effect of impeller type on power consumption in solid-liquid agitated vessels. The choice of a proper impeller to satisfy suspension requirements is critical since different impellers generate different flow patterns leading to different hydrodynamics, thus affecting the energy efficiency of the system. Extensive studies have been conducted previously using low to medium solids concentrations, and it was generally agreed that the pitched-blade impellers perform more efficiently than disc turbines, and the pitched turbine down flow types consume less energy than pitched turbine flow impellers (Ibrahim and Nienow, 1996; Frijlink *et al.*, 1990).

Raghavo Rao *et al*. (1998) concluded that three factors are responsible for the poor mixing efficiency of a disc turbine. These are: (a) only partial energy delivered by the circulation loop is available for solids suspension; (b) liquid-phase turbulence is created at the impeller tip but it decays along the path of liquid flow; (c) energy is lost during the two changes of the flow directions, first near the wall opposite of the impeller and then at the corner of the base and wall. However, Wu *et al*. (2002) did some work on extremely high solids concentration (Cv = 0.49 v/v) and concluded that based on power efficiency at high solids loading, radial impellers are superior to the axial flow impellers to suspend solids. This is contrary to what is generally noticed at low solids loading. However, information regarding the effect of impeller type on solids suspension at high solids concentration cannot be considered to be complete.

The complete suspension criterion would suffice for most processes provided the liquid phase is well-mixed. In continuous processes such as continuous crystallization or leaching it would be desirable to have homogeneous suspension. Such a condition requires very high energy input if ever achieved by mechanical agitation. Homogeneity

is defined through measurements of the local solids concentration at different positions in the vessel. Bourne & Sharma (1974) reported that an approximation to homogeneous suspension may become possible in flat bottom tanks equipped with a draught tube, and better levels of homogeneity without stagnant zones can be obtained with contoured tanks at lower energy inputs. However, for actual operations, in addition to the homogeneous suspension criterion, homogeneity of the product withdrawn will also need to be monitored.

### 2.2.2 Mechanism of suspension

There is a considerable range of theoretical work on solid suspension. In general, modelling of solid suspension is based either on the concept of turbulence or the drag forces exerted by the mean bulk flow on the particles. Energy balances performed in accordance with the assumptions made yield equations which are usually capable of describing experimental measurements with varying degree of success. However, no universal form is yet available.

The models are generally similar in their functional relationships, making experimental differentiation between them difficult, especially given the quality of data. But major differences occurred when predictions of energy requirements are made at the large scale with these models.

It has been proposed that the mechanism for suspension does not depend solely on either turbulence or mean fluid flow alone, but a condition requiring a critical degree of both. It was suggested that in order to obtain more clarification on the exact nature of the suspension mechanism, it would be ideal to test systems which can generate pure turbulence or mean bulk flow.

#### 2.2.2.1 Gas-liquid mixing

The physics of dispersion in a mechanically agitated vessel can be understood from the impeller hydrodynamics. When an impeller moves through liquid (or vice versa), the stagnation of flow at the edge of the blade produces a pair of spinning vortices behind it. They are also termed "trailing vortices" and for a Rushton turbine, with the presence of radial flow, they elongate up to three blade lengths before dissipating. A similar type of tertiary flow can be obtained with other impellers. The high centrifugal accelerations of these spinning vortices create a low pressure region and gas is immediately attracted towards it once introduced into the system. The gas collects as cavities behind the blades, through which bubbles are released into the bulk stream.

The shapes and sizes of cavities depend on two factors: 1) The intensity and shape of the vortices which are influenced by the impeller geometry and speed (Tatterson et al., 1980), and fluid properties. It was determined that a Froude number of 0.015 was required for bubbles to be captured at all to form cavities, otherwise the large buoyancy of bubbles compared with the centrifugal force allow them to pass to the downstream (Van't Riet & Smith, 1973). 2) The actual amount of gas fed to the impeller. In addition, the rate of aeration (Bruijin et al., (1974)), the sparger geometry (Bujalski et al. (1988)), and its position with respect to the impeller (Nienow et al. (1977)), and the impeller speed are also important as they determine where in the stream of bulk motion the gas is released and to what extent recirculation of gas contribute to the total supply.

In addition to being the source of gas bubbles, a cavity's shape and size can affect the impeller pumping capacity or the direction of fluid discharged, which effectively determines the gas distribution. The impeller hydrodynamics directly governs the impeller's energy consumption.

The 6DT is the most widely used impeller for gas-liquid dispersion. Before cavities were first discovered it was believed that feeding the gas beneath the disc encourage break-up of bubbles. The 6DT is still considered one of the best for gas dispersion. Impellers producing axial flow which were less favoured because of instability in their dispersion characteristics have recently received more attention, for applications in three-phase mixing, due to their superior performance over the 6DT in suspending solids. 3-blade propellers, however, are usually ruled out since hydrodynamic instability is more severe with the small number of blades (or small O/T). The 6-blade mixed-flow impellers with a large O/T (> 1/2) have shown good potentials.

According to the literature, it can be concluded that mixed-flow impellers are more efficient in suspension of solids in stirred tanks, while radial-flow impellers will offer better performance in dispersing gas phase in the liquid volume.

#### 2.2.2.2 Three-phase mixing

Solid-gas-liquid mixing occurs in various hydrogenations and oxidations, fermentation, evaporative crystallization and froth floatations agitations. The impeller is required to simultaneously disperse gas and suspend solids.

In comparison to two phase solid-liquid or gas-liquid systems, the number of papers in the literature on the hydrodynamics of three-phase mixing is few. The next section reviews some of the previous findings on this topic. The central questions are if the solid particles affect the gas-liquid behaviour and if the presence of gas influences solid suspension. It is of practical importance to determine the minimum speeds for gas dispersion and solids suspension with the coexistence of a third phase. The minimum speed for just-suspension under gassed condition is usually designated as ($N_{jsg}$).

Complications arise in selecting an impeller for performing the dual function in three phase systems due to quite different design specifications for solid suspension and gas dispersion. Current data suggests that downward pumping impellers. which are very energy efficient for solids suspension under unaerated condition, but very poor for gas-liquid dispersion, could be utilized at low gas inputs when the fluid dynamics are not dominated by asymmetric flow pattern.

### 2.3 Critical impeller speed ($N_{js}$ , $N_{jsg}$)

Suspension of particles in a liquid medium is one of the widely used function of a stirred vessel. The applications include processes such as adsorption, crystallization, dissolution and catalytic reaction. Due to its industrial relevance, the subject of solid suspension in stirred vessel has been widely studied.

When suspending solid particles, the degree of suspension can be divided into two states, namely, complete suspension in which all the particles are at suspension and homogeneous suspension in which the solid particles are distributed evenly in the vessel. It is well recognized that the point where solid particles are just suspended is the most important state because until such condition is reached, the total surface area of the solid particles are not effectively utilized for mass transfer operations. The speed at which this condition occurs is universally referred as just suspension speed, and $N_{js}$ and $N_{jsg}$ are the commonly used notation to indicate this speed at absence and presence of gas, respectively.

Except for the specific processes that require complete homogeneity, such as crystallization, keeping the solids completely suspended from the tank bottom is sufficient as it provides adequate contact area between solid and liquid phases. Significant drawbacks can appear upon misidentifying the minimum impeller speed required to

achieve complete off-bottom suspension. Operating the mixing vessels at speeds higher than $N_{js}$, can result in higher suspension degree and mass transfer yet. At the same time, higher turbulence shear rate generated at higher speeds can result in particle attrition, which is not beneficial for biological processes. In addition, higher agitation speed forces the impeller to consume more power, which significantly contributes to the operation's capital costs.

It is very common to process high concentrations of solids (up to C = 0.45 v/v) in gold cyanidation processes to enhance recovery rate of gold. By operating the vessel at speeds lower than $N_{js}$, fillets of stationary solid particles start to form at the corners of tank's bottom, which can affect the selectivity and production yield. It should be noted that this condition may be allowed for certain cases where the significant savings of impeller's power consumption heavily outweighs the problem of a small portion of inactive solids.

Given the fact that the most common methods for determination of $N_{js}$ are subjective and may defer from a person to another, it is logical to comment that accurate determination of impeller's critical speed is challenging. Yet, it seems that under-estimation of $N_{js}$ is more desirable compared to over-prediction as excessive agitation speed drastically increases the power consumption of the setup, and consequently, results in increased capital costs. High recovery of gold can be obtained by employing a series of stirred tanks with diameter of 8 m. Under this condition, over-estimation of critical impeller speed result in huge excessive capital costs, while operating at speeds lower than $N_{jsj}$ leads to reduction in gold recovery. It's been reported that 10% to 100% over-estimation of critical impeller speed can increase the unit's energy costs from $ 0.5 M to % 10.3 M/year (Jafari, (2010)). In addition, extra costs associated with repairing and maintenance of the mixing vessels adds to the economical drawbacks of vessels operating at speeds higher than required.

Determining the just suspension speed is dependent on how the state is defined. One of the most widely accepted definition (or criterion) for $N_{js}$ is given by the pioneer worker in this field, Zwitering (1958) whose work on solid suspension is rarely missed by subsequent researchers in this field. He defined $N_{js}$ as the speed where no particles remain stagnant at the bottom of the tank for more than (1-2) seconds and the criterion is often referred as '1-2 seconds criterion'. There are other definitions for just suspension speed condition which will be thoroughly discussed in the next parts.

### 2.3.1 Critical impeller speed in presence of gas

The addition of gaseous phase in solid-liquid systems alters the solid suspension behavior. For example Frijlink et al. (1990) reported that $N_{jsg}$ increases with increasing gas rates for constant solid concentration when agitated with Rushton turbine. The effect of gas rate on just suspension speed in three-phase systems ($N_{jsg}$) is commonly related with just suspension speed ungassed condition ($N_{js}$) by many workers.

From the literature review it can be seen that impeller type, solid concentration and gas rates are the main factors that affect suspension characteristics in stirred vessels. Solid concentration and gas rates also play a major role in any industrial application. Therefore in this study a wide range of solid concentration and gas rates are evaluated for all the curve blade design. Detailed description of the range of experiments and other relevant information are discussed in Chapter 3 of this report.

Mixing efficiency in a stirred tank can be improved by increasing the total volume of the fluid circulated by the agitator. The stream produced by agitator should be strong enough to reach the distant corners of the vessel.

It is very important to operate the mixing tanks at just-suspended speed as this condition provides maximum contact area between phases. Nienow et al. (1968) reported that

maximizing interfacial areas is an effective strategy to increase the rate of heat and mass transfer in stirred vessels. On that note, several works pertaining to the suspension of solids have studied the effect of various operating and design factors on the complete off-bottom suspended condition to make sure results can contribute to increase in heat and mass transfer rates.

To better understand the critical impeller speed in three phase mixing vessels, various states of gas dispersion and solid suspension that can be found in a three-phase stirred vessel, originally described by Pantula and Ahmed (1998), are shown in Figure 2.1. The labels $H_S$, H, and $H_B$ refer to heights of suspended solids bed, slurry, and settled solid bed, respectively. At low agitation speeds, sparged gas bubbles pass through the impeller without much dispersion and liquid flows around the outer part of the blades undisturbed by the gas, resembling the impeller flooding condition. At this stage, the cavities are either non-existent (Figure 2.1a) or ragged (Figure 2.1b), the impeller is unable to disperse gas, and solids rest motionless at the tank bottom. An increase in agitation speed, transforms ragged cavities into large cavities because gas bubbles are captured by the vortices behind the impeller blades. In this region, some radial liquid motion occurs and bubbles are pushed to the tank walls. Transition from stage shown in Figure 2.1b to 2-1c can be regarded as the onset of impeller loading. The liquid circulated at this condition can lift some settled particles from the tank bottom but the fraction of suspended solids is still insufficient to influence the gas-liquid hydrodynamics. Further increase in impeller speed transforms the large cavities into vortex cavities, leading to the better dispersion of the bubbles and small recirculation patterns (Figure 2.1d). The corresponding impeller speed is known as the critical impeller speed for complete gas dispersion, $N_{CD}$, and is defined as the speed at which an impeller is able to supply sufficient energy to effectively distribute gas bubbles throughout the liquid volume. Even though gas bubbles are sufficiently dispersed within the vessel at $N_{CD}$, complete suspension of solids from the

tank bottom is not achievable. It was Nienow (1968) who initially reported that $N_{CD}$ is independent of particle conditions (concentration, density, $d_p$, etc.,) and achievable at speeds lower than $N_{js}$. As impeller speed increases further, more and more particles are lifted by the circulated liquid flow up to a point that no particle remains stationary at the tank bottom (Zwietering criterion) or the last layer of sedimentation bed disappears (Hicks criterion). This speed is marked as the just suspended speed in the three-phase system ($N_{jsg}$) (Figure 2.1e). At this speed, gross recirculation of gas bubbles into the impeller region occurs. Therefore, this speed is also referred as recirculation speed ($N_R$) in gas-liquid studies. Further increase in impeller speed results in a uniform distribution of solid particles (Hs/H = 1) and the formation of a secondary bubble loop above the impeller. This speed is labeled as the critical impeller speed for ultimate homogeneous solid suspension in a three-phase system, $N_{usg}$, (Figure 2.1f).

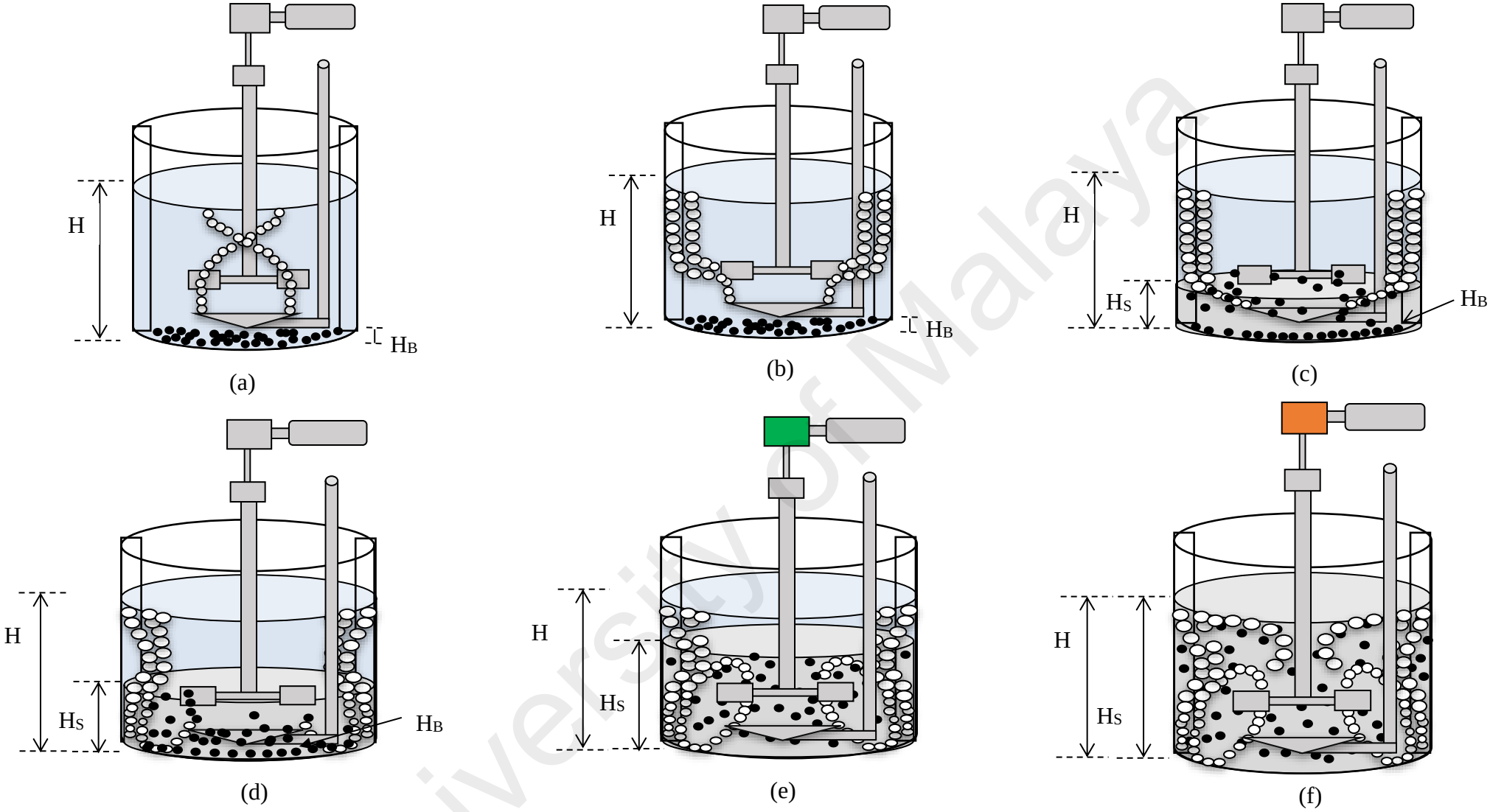


Figure 2.1 States of solids suspension and gas dispersion, HS = Suspended solids bed hight, H = Slurry height, HB = Settled solid bed height

### 2.3.2 Determination of critical impeller speed

A wide range of methods and approaches has been proposed for determining the critical impeller speed (Zwietering, 1958) (Hicks et al., 1997) (Musil & Vik, 1978) (Bohnet & Niesnak, 1980) (Micale et al., 2002) (Zhu & Wu, 2002) (Jirot et al., 2005) (Ren et al., 2008) (Brucato et al., 2010) (Tamburini et al., 2011) (Tamburini et al., 2012) (Selima et al., 2008) (Rewatkar et al., 1991) (Bourne and Sharma, 1974) (Buurman et al., 1986) (Kraume, 1992) (Hosseini et al., 2010) (Mersmann et al., 1998). The most common method for determination of $N_{js}$ is the visual technique proposed by Zwietering (1958), which defined impeller critical speed as the speed at which no particle remained stationary at the tank bottom for more than 1-2 seconds. A major problem with is technique is the excessive energy that it requires to suspend a small portion of that are not lifted due to poor circulation of water particles in stagnant zones. In this regard, Kasat and Pandit (2005) pointed out that in order to suspend these fillets that contain negligible number of particles, the agitation speed should be increased up to 20-50% higher to what is required to achieve complete off-bottom suspension ($N_{js}$). Wu et al. (2009a,b) approved this observation and commented that small quantity of solids that remain motionless at the stagnant regions may not be lifted even at high speeds. Thus, degree of suspension should not be assessed on the basis of insignificant portion of solid particles.

It is also worth mentioning that for the process where diffusion is not a limiting factor, maintaining the solids in 'complete off-bottom suspended' condition (Figure 2.1e) is adequate. Increasing agitation speed just to encourage homogenous mixing (Figure 2.1f) consumes more energy, which is wasteful as it does not improve the mass transfer or reaction rate. The green and red colors of motors in Figures 2.1(e) and 2-1(f) visually indicate that operating the motor at the 'complete-off bottom suspension' condition is more energy efficient. Therefore, all experiments and analyses in this study were carried out under 'complete off-bottom suspended' condition at $N_{js}$ or $N_{jsg}$.

A less subjective method is to measure particles concentration near the base of the vessel by conductivity or optical probes (Musil and Vik (1978)) (Bourne and Sharma (1974)). When the impeller speed is first increased the particle concentration increases as solids are gradually lifted off the base. At $N_{js}$ the concentration just above the base is generally at the maximum since all the particles are suspended (Musil and Vik (1978), Bourne and Sharman (1974)). Some workers associate this to the point to a sharp change in the slope of the curve concentration versus N. Bourne and Sharma (1974) reported identical values of $N_{js}$ determined using the visual method or by measuring concentration, but others (Rao et al. (1988)) have indicated that the value of $N_{js}$ is higher when subject to personal judgment.

A possible explanation for this discrepancy is that the visual observer has the tendency to over-estimate $N_{js}$ in assuring that the criterion is met. The particle concentration technique is obviously more involved than the visual method, but it can be used for vessels which are not transparent and with any type of base geometries. It is also more suitable for large scale studies where proper observation of the base may not be feasible. However, measuring points should be properly located near the base to account for possible changes in the distribution of solids, due to changes in the operating variables. On the other hand, with the visual method discussed in the preceding paragraph, one is able to observe the entire base, and see the overall distribution of solids. Judgments will naturally be based on the last suspension point-viewed for the system of interest.

Hicks et al. (1997) defined $N_{js}$ as the impeller speed at which the last layer of sedimentation bed disappears. They measured the sedimentation bed height at different speeds, and concluded that measuring impeller critical speed based on the bed height is the most energy efficient strategy to provide sufficient contact area between phases in a mixing tank. This approach usually offers lower $N_{js}$ values compared to the conventional techniques, and because of that, has been used in several studies involving high solids

concentrations (Wu et al. (2010); Wang et al. (2014); Wang et al. (2012a); Wang et al. (2012b)).

Einenkel and Mersmann (1977) identified $N_{js}$ as the speed at which high of interface between the solid-liquid mixture and the clear liquid was equal to 90% of the total operating height. Later, it was reported that the critical speed values obtained using this method were generally 20-25% higher than those recorded by Zwietering technique Kraume (1992) and Kasat & Pandit (2005). The fact that some particles may stay stationary at the tank bottom when few small solids have already reached the critical interface height was mentioned as the main reason behind this difference.

Focusing the observation near or at the tank base neglects the behaviour of solids in the other parts of the vessel. Einenkel & Mersman (1977) considered the bulk coverage of the solids by defining $N_{js}$ as the speed at which the height of the liquid at the top is 1/10 of the total liquid height. But uncertainties may arise in distinguishing the interface between the clear liquid zone and the slurry. Another reason that this technique is not all that advantageous is that the speed where the height criterion is met does not guarantee complete suspension of the particles. For particles with high settling velocity it is very likely that some of the solids would still be immobilized at the base of the tank although others may have been fluidized to the top, in which case a significant portion of the total surface area available would be improperly utilized.

Rewatkar & Joshi (1991) proposed that impeller critical speed should be considered as the agitation speed after which an increase in speed did not influence values of impeller power number. The $N_{js}$ values determined using this method were found to be in good agreement with those identified using the Zwietering method.

Based on the highlighted studies, it can be concluded that sedimentation bed height proposed by Hicks et al (1997) is the most suitable approach for determination of $N_{js}$ and $N_{jsg}$ in this study as it has exhibited acceptable and consistent results in the previous works

involving high solids concentrations (Wu et al., 2010a) (Wang et al., 2012a) (Wang et al., 2012b) (Wang et al., 2014).

## 2.4 Impeller power consumption

### 2.4.1 Unaerated Power Consumption

Power input in a stirred vessel is the energy per unit time transferred from the rotating impeller to the medium being agitated. Pioneer researchers in this field like Rushton et. al (1950a, 1950b) identified that power consumption in stirred vessels are dependent on impeller type, tank geometry, impeller diameter, impeller speed and liquid rheology. From dimensional analysis, Bates et.al (1966) concluded that for geometrically similar vessels, the following relationship applies:

$$\left[\frac{P_0}{\rho_c N^3 D^5}, \frac{\rho_L N D^2}{\mu_L}, \frac{N^2 D}{g}\right] = 0 \qquad \textbf{2-3}$$

where

$\frac{P_o}{\rho_c N^3 D^5}$ = $N_P$ = Power Number

$\frac{\rho_L N D^2}{\mu_L}$ = $N_{Re}$ = Reynolds Number

$\frac{N^2 D}{g}$ = $N_{Fr}$ = Froude Number

Reynolds Number, $N_{Re}$ is used to characterize the flow in the vessel as either laminar, turbulent or in the transition region while $N_{Fr}$ is useful in studying motion during scale-up. Meanwhile Power Number, $N_p$ is a dimensionless quantity commonly used to

characterize a particular impeller and the value is commonly determined using water as a medium. $N_{po}$ is commonly expressed as function of $N_{Re}$. The relationship between those dimensionless numbers can be obtained by rewriting equation 2-4 in following form

$$N_{P0} = K(N_{RE})^a(N_{Fr})^b \qquad \textbf{2-4}$$

Where K, a and b are constants for a particular vessel and geometry

It has been reported that at high $N_{Re}$ (>$10^4$ ) the Power Number becomes constant (Bates et al 1966). At a similar D, N and $\rho_L$ different impellers have different $N_p$ values. Many researchers studied various factors that influence $N_p$ values and found that impeller to tank diameter ratio, impeller clearance rate, blade thickness, number of blades, blade type and baffles are among the main factors that influence $N_p$ values. Some of the past work done in this respect are discussed below.

Shiue and Wong (1984) reported that $N_p$ for 6RT ranges from 4.3- 5.5 when D/T (impeller diameter to tank diameter ratio) was varied. For similar variations of D/T ratios, $N_p$ values for 6 Curved Blade (CB) and 4 Curved Blade (CB) (without central disc) remain quite stable at 4.1 and 1.6, respectively. Similar studies were conducted by Sano & Usui (1985) for turbine blades. They proposed the following correlation for D/T range between 0.3 and 0.7, W/T between 0.05 and 0.4 and number of blades, $n_p$ between 2 and 8. This equation is best used for tanks of 0.2 – 0.4 m diameter (equation 2-5), with W referring to impeller blade width.

$$N_p = 3.6\left(\frac{D}{T}\right)^{-0.96}\left(\frac{W}{T}\right)^{0.75} n_p^{0.8} \qquad \textbf{2-5}$$

Meanwhile Gray et.al (1982) proposed the following correlation for 6RT:

$$N_p = 5.71\left(\frac{C}{D}\right)^{0.29} \text{ for } \frac{C}{D} < 1.0 \qquad \textbf{2-6}$$

$$N_p = 5.71 \text{ for } \frac{C}{D} > 1.0 \qquad \textbf{2-7}$$

Other than D/T , W/T , C/D and $n_p$ values, the effect of thickness of the disc and the shape of the impeller on $N_p$ were also keenly investigated by researchers. For example, Nienow & Wisdom (1976) attributed Power Number difference between disc type and flat type blade to low pressure cavities behind the blade that causes form drag. As for the thickness of the blade, Bujalski et.al (1987) showed that disc style turbine follows equation 2-8.

$$N_p \propto \alpha\left(\frac{X}{D}\right)^{-0.2}\left(\frac{T}{\mu_L}\right)^{0.065} \qquad \textbf{2-8}$$

As for the present study is concerned, the $N_p$ analysis will be conducted on the effects of number of blade, shape of curve and effect of central disc for curve blade impellers.

### 2.4.2 Aerated Power Consumption

Under aerated conditions, power input, $P_g$, by an impeller normally drops compared to the power input, $P_o$ at similar impeller speed under unaerated conditions. This drop is normally presented in a plot of $P_g/ P_o$ as a function of $N_F$ ( Flow Number, $Q/ ND^3$ ). One such plot is shown in Figure 2.2.

Figure 2.2 shows that curve blade impeller have lesser aerated power consumption drop compared to Rushton turbine. For Ruston turbine, the power reduction reaches down to 30% of the ungassed power draw while for curved blade, the reduction is around 80 to 90%, even at high gassing rate. Many empirical correlations are available for estimating aerated power input, $P_{g,}$ in stirred vessels. Many studies have confirmed that the reduction in power input is due to the form drag resulting from formation of gas cavities behind the blades and it is not due to the reduction in bulk density of the medium as once thought (Burujin et.al, 1974, Nienow et. al 1977).

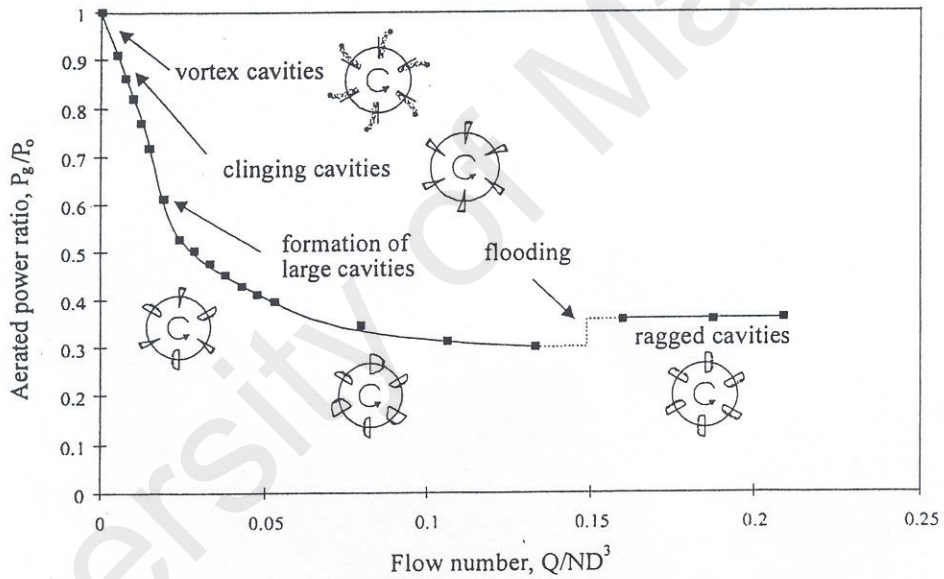


Figure 2.2 Ratio of gassed and ungassed power as a function of flow number for Rushton turbine impeller at 500 rpm (Source: Nelson and Ahmad, 1998).

The shape of the power reduction plot as shown in Figure 2.2 under gassed condition can be explained by studying the formation of various cavity structures. Figure 2.3 shows a typical aerated power reduction against the type of cavities formed. It can be seen that shape and size of the cavities determine the level of fall in power reduction. It is also observed that the relationship between $P_g/ P_o$ versus flow number is not unique. The main reason for this behavior is that the gas in the impeller zone does not only come from the

amount that is being sparged but also includes the 'old' gas recirculated Q', to the impeller zone. Therefore, at a sparging rate Q, the actual flow rate is Q+ Q'. Therefore any attempt to correlate power drop to sparging rate should also consider the amount recirculated to obtain the unique relationship. Warmoeskerken et.al (1986) proposed a corrected flow number based on external distribution factor and gas hold up and plotted $P_g/ P_o$ versus flow number. The plot for different impeller speed was found to fall on a single curve up to the flooding line.

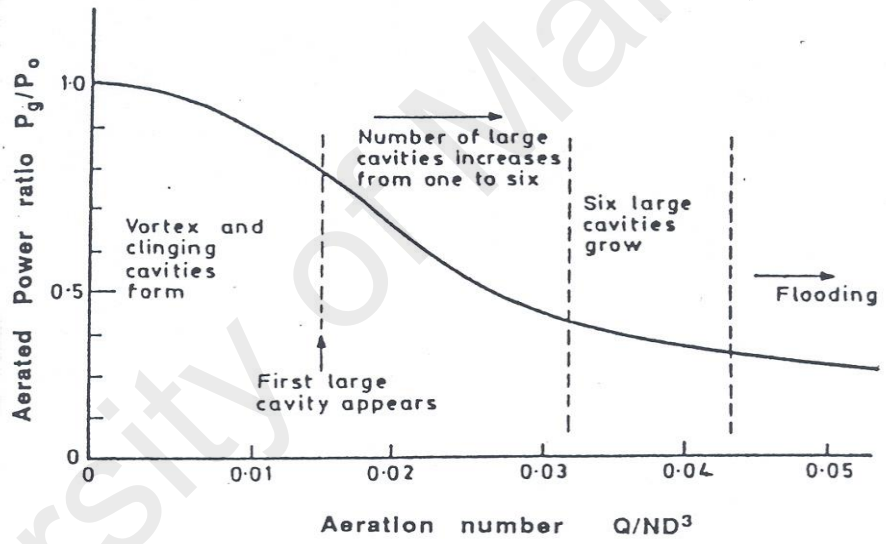


Figure 2.3 Typical Pg/ Po versus Flow Number (Q/ND3) plot for constant impeller speed and respective formation of gas cavities

### 2.4.3 Effect of solids concentration

Solids concentration is a significant factor that influences the energy input in solid-liquid mixing vessels. It is always of interest to increase the solids concentration in the agitation vessel since throughput can be increased subsequently and tank infrastructure can be efficiently employed. However, a higher solids loading (such as 0.20 – 0.50 v/v) could

result in more intensive energy input. Bubbico et al. (1998) explained that extra energy input with high solids loading is due to the extra energy required to compensate the energy loss in solid-liquid friction, particle-particle collision and particle-equipment collisions. Bubbico et al. (1998) and Raghava Rao et al. (1988) all agreed that the amount of energy loss due to this mechanism is ignorable at low solids concentration (< 0.04 v/v) and becomes appreciable when high solids loading is present. Drewer et al. (1994) indicated that there is a critical or maximum solids concentration where suspension is unattainable. Wu et al. (2002) suggested that the maximum solids concentration at which slurry suspension can be maintained in an agitated vessel given by the following relationship:

$$\frac{C_v}{C_{vb}} \approx 0.9 \qquad \textbf{2-9}$$

where $C_v$ (v/v) is the solids concentration, $C_{vb}$ (v/v) is the solids volume-packing coefficient. It is challenging to operate the slurry mixing tank at an extremely high concentration since the power input at the just-off-bottom solids suspension condition (i.e. Pjs) increases exponentially as the concentration approaches the solids volume-packing coefficient Cvb (Drewer *et al*, 1994, 2000; Wu *et al*, 2002); an upper limit of $C_v$, that is practically achievable, was found to be between 0.50 – 0.55 for a typical packing coefficient ranging from 0.55 to 0.60 (Wu *et al*, 2010b). Wu *et al.* (2002) also pointed out that in the region of Cv/Cvb > 0.9, bogging of the agitator would eventually occur due to the excessively high power consumption.

It is also well known that concentrated suspensions exhibit non-Newtonian properties leading to complex circulation behind the blades of impellers. Slurries with viscous non-Newtonian characteristics are problematic due to poor mixing and reduced heat and mass transfer rates (Kasat and Pandit, 2005).

It can be observed that the majority of the previous works are limited to either low concentrations solids or two-phase (solid-liquid) systems, while the mixing tanks involved in mineral processing usually operate at high concentrations of solids. This gap warrants further investigations on suspension of high concentration slurries in presence of gas.

### 2.4.4 Effect of baffle removal

The effect of baffle installation cannot be ignored in the optimization of mechanically agitated vessels. The role of baffles in mechanically agitated vessels is to prevent swirling and vortexing of liquid (Lu et al., 1997). With the installation of baffles, it is generally agreed that enhanced mixing occurs which consequently increases mass- and heat transfer. However, excessive or insufficient baffling may result in the reduction of mass flow and localizing circulation in the agitation system (Nishikawa *et al.*, 1979). Nishikawa *et al.* (1979) also indicated that if the width of the baffle is larger than 0.1T, the fully baffled condition will be obtained with 3 baffles or more. Lu *et al.* (1997) also studied the effects of width and number of baffles in mechanically agitated vessels with standard Rushton turbine impellers in the agitation systems with and without the presence of gas, and concluded that the insertion of the appropriate number of baffles obviously results in improvement in the extent of liquid mixing. Nevertheless, excessive baffling would interrupt liquid mixing and lengthen the mixing time. A consequence of lengthening of the mixing time is the reduction in the efficiency of the agitation system (Lu *et al.*, 1997).

Unbaffled agitated vessels or weakly baffled tanks were found to be more energy efficient than those with full baffles for single phase system. This is based on studies that are associated with radial impellers and axial impellers conducted by Markopoulos *et al.*

(2004) and Markopoulos *et al.* (2005) respectively. Although, the removal of baffles leads to an increase in mixing time, it is also a very effective way to drastically reduce the specific energy for suspending solids particles off the tank bottom (Wu *et al.*, 2010a). Wu *et al.* (2010a) pointed out that the increased mixing time is not usually a problem since the time scale for reaction and the slurry residence time in some mineral processes can be much longer than the mixing time. Typically, for example, in gold leaching processes, residence time requirements in practice vary from a few hours to several days, which is an order of magnitude longer than the mixing time, which is typically in minutes (Marsden & House, 2006; Wu *et al.*, 20010b). Wu *et al.* (2010b) concluded that a superior way to improve energy efficiency is to remove the baffles for those tanks if the mixing rate is not critical in cases such as slurry-holding tanks or reactors where chemical reactions are slow.

Thus, the available literature suggests that operating mixing tanks in absence of baffles can result in significant savings in overall power consumption of the vessels. However, it should be noted that removal of baffle can cause formation of a vortex inside the tank which might reduce mass transfer rate. This issue is not problematic for mineral processing as the time required for an efficient mass transfer is much longer than the mixing time. Therefore, this study will investigate baffle removal as a strategy to minimize power consumption in three-phase mixing tanks.

### 2.4.5 Effect of impeller configuration and tank geometry

The impeller and tank geometry are important in solid suspension because the liquid flow behavior which is responsible for solid suspension is highly dependent on the shape of the system within which it is confined.

The Rushton turbine has been shown to be inefficient for particle suspension, and liable to cause considerable surface aeration (Ibrahim & Nienow, 2009) (Rewatkar & Joshi, 1991). Axially discharging impellers, particularly, the three-blade propeller, were found to be the most energy efficient for producing complete off bottom suspension (Ibrahim & Nienow, 2009). Raghavo Rao et al. (1988) reported that mixed-flow impellers pumping in the downward direction consume one fifth of the energy of the disc turbine and one third of the energy for the mixed-flow pumping upwards for particles 2000 μm in diameter at 6.6% concentration. They explained that during downward pumping the fluid immediately flows toward the base and is directly available for suspension whereas in upward pumping the length of liquid path and number of direction changes are greater.

The axial flow impellers have a low power number to flow number ratio and are called flow impellers. The repeated findings that impellers from the latter category produce better suspension for the same energy supply implies that it is the flow and not shear that controls the suspension of solids. It was also suggested, however, that the reduced path length between the discharge and the solids with axial flow impellers may lead to less turbulence decay which consequently improves the suspension.

The impeller and tank geometry are important in solid suspension because the liquid flow behavior which is responsible for solid suspension is highly dependent on the shape of the system within which it is confined. The Rushton turbine has been shown to be inefficient for particle suspension, and liable to cause considerable surface aeration (Yawalkar et al. (2002)). It is possible to categorized the disc turbine as a shear type impeller which has a high power number to flow number ratio.

The other important geometric variable is the position of the impeller with respect to the tank base. The plots presented by Zwietering (1958) and later workers implied that $N_{js}$ decreases with decrease in clearance for a variety of impellers. It's been recommended

the optimal clearance as the minimum allowed either by the tank geometry or the settled solids bed height, based on results with 3-blade propellers of D = *T/3* in a flat bottom and cone-and-fillet.

The geometry affects the last suspension points of the particles on the base. With disc turbines the solids were observed to collect in the centre, except at very low clearances where the flow pattern changed and they are thrown to the sides (Nienow (1968)). For the downward pumping propellers, Zwietering noted that if $D/T < 0.45$ the particles were observed to suspend last from the peripherial areas, whereas if $D/T > 0.45$ the solids moved inwards and centrally upwards into the impeller.

The other important geometric variable indicated earlier is the position of the impeller with respect to the tank base. The plots presented by Zwietering (31) and later workers implied that $N_{js}$ decreases with decrease in clearance for a variety of impellers.

Raghavo Rao et al. (1998) concluded that three factors are responsible for the poor mixing efficiency of a disc turbine. These are: (a) only partial energy delivered by the circulation loop is available for solids suspension; (b) liquid-phase turbulence is created at the impeller tip but it decays along the path of liquid flow; (c) energy is lost during the two changes of the flow directions, first near the wall opposite of the impeller and then at the corner of the base and wall. However, Wu et al. (2002) did some work on extremely high solids concentration (Cv = 0.49 v/v) and concluded that based on power efficiency at high solids loading, radial impellers are superior to the axial flow impellers to suspend solids.

In another study, Dohi et al. (2004) reported that large impellers (D/T = 0.5) consumed less power for both gas dispersion and solids suspension compared to smaller impellers (D/T = 0.3). According to Nienow et al. (1977) larger impellers are less sensitive to gassing conditions and can handle suspension better in aerated systems. The significant advantages of large impellers over the traditional design have been observed in both

aerated and unaerated systems (Nienow ,1968) (Chapman et al., 1983) (Dohi et al., 2004). It is also reported that large impellers are more energy efficient compared to the combination of three impellers on one shaft (Dohi et al., 2004). With regards to impeller clearance, the literature suggests that decreasing the distance between the impeller and tank bottom can reduce critical impeller speed (Zwietering, 1958)(Nienow ,1968)(Dohi et al., 2004).

The addition of gas phase in solid-liquid systems alters the solids suspension behavior. It's been reported that $N_{jsg}$ increases with increasing gas flow rate for a constant solids concentration when agitated with Rushton turbine (Dohi et al., 2004) (Dohi et al., 1999). The choice of impeller type also directly influences the suspension performance of a mixing vessel. Ibrahim and Nienow (2009) noticed that, at low gas flow rates, $N_{jsg}$ can be lower than $N_{js}$ if agitation is provided by a large pitched blade impeller (D/T=0.5) pumping in either directions. On contrary, $N_{jsg}$ was found to increase steadily with an increase in $Q_g$ in the case of Rushton turbine. In addition, they observed that the introduction of gas did not lead to torque fluctuations or tank vibration in a vessel equipped with a Rushton turbine, while mixed- and axial-flow impellers were prone to significant flow instabilities. According to Rewatkar et al. (1991), $N_{jsg}$ increases with a decrease in the distance between the sparger and impeller. They also reported that the difference between $N_{js}$ and $N_{jsg}$ increases with an increase in solids concentration due to changes in fractional gas holdup. It is clear that solids concentration, gas flow rate, and impeller configurations contribute significantly to the mixing behavior and power efficiency of a stirred vessel.

In summary, observations of Wu et al. (2002) are contrary to what is generally noticed at low solids loading. However, information regarding the effect of impeller type on solids suspension at high solids concentration in presence of gas is absent in the literature, which warrants further investigation.

### 2.4.6 Effect of particle size

Particle size is one of the most important physical properties for solid suspension. Drewer et al. (1994) reported that due enhanced gravitational force, stronger liquid circulation is required for suspension of larger particles, which consequently led to consumption of more power to maintain the solids at suspension. According to Bubbico et al. (1998), the supplied energy to the system is partially dissipated by large solid particles as the energy lost through solid-liquid and solid-solid contacts became more significant by using larger particles. The available literature on the effects of particle size on agitation speed and power is mostly limited to solid-liquid systems handling low solids concentration under fully baffled conditions, which warrants further investigation in three-phase systems handling high solids concentrations.

## 2.5 Gold cyanidation process

Gold cyanidation process is an industrial example of a three-phase system that involves high concentrations of solids. Gold is usually extracted from its ore through cyanidation process. In this three-phase process, gold is extracted by a reaction between solids and cyanide in presence of Oxygen dissolved in liquid phase. In order to obtain excellent mixing and high recovery of gold, a cascade of stirred tanks, usually 10, are used.

Gold cyanidation process suffers from high material and operation costs due to high consumption of reactants. Various parameters contribute to efficiency of three-phase reactions in the extraction process. In this regard, total power consumption of the mixing vessel and with mass transfer rate play major roles in determining the efficiency of reaction and the total capital and operation costs.

Gold cyanidation process has been studied comprehensively before, but the majority of the documented literature have tried to improve the process efficiency by studying reaction mechanism. Since no significant improvement is reported yet, it is necessary to seek alternative strategies to minimize the costs associated with this extraction reaction. By adjusting the design and operating parameters, it is possible to identify optimum condition at which the stirred tank can operate with maximum efficiency. Absence of reliable experimental results on effect of design factors (e.g. baffling configuration and impeller type) and operating parameters (solids concentration and gas flow rate) on solid suspension, gas dispersion, and impeller's power input warrant the necessity of further investigations.

## 2.6 Gas-liquid hydrodynamics

The performance of a three-phase agitated reactor is determined by the efficiency of the impeller in generating a large gas-liquid interfacial area and at the same time utilizing the maximum contact area available between gas/liquid phases and solid particles for transfer processes. Average bubble size and volume fraction of the gas retained in the dispersion (gas hold-up) are the two important parameters that determine the gas-liquid interfacial area.

Sparging gas at a low flow rate into a solid-liquid system with suspended solids causes sedimentation of solids at a given impeller speed. Particles are no longer fully suspended under this condition. Further increase in gas flow rate leads to more solids sedimentation. The reduced pumping capacity of the impeller due to the formation of ventilated gas cavities behind the impeller blades is pointed out to be the main reason for the collapse of suspension (Warmoeskerken et al., 1984).

In a solid-liquid system, drag forces due to liquid flow and associated turbulent eddies are responsible for solids suspension. The decrease in impeller pumping capacity and power due to gassing decreases the magnitude of drag force and the intensity of eddies, thereby leading to the loss of suspension. A higher impeller speed is required to maintain the solids suspension in gassed systems. Thus, the interactions of gas-liquid-solid phases in a stirred vessel is complex, and a reliable approach is required to investigate the design parameters Sauter mean bubble diameter ($d_{32}$), gas holdup ($\emptyset_G$), and gas-liquid interfacial area ($a_{g\text{-}l}$) especially for systems involving high solids concentrations.

### 2.6.1 Gas holdup

Gas hold-up is an important measurement of gas-liquid dispersion performance in stirred vessels. Low gas hold-up indicates poor dispersion property and could lead to poor mass transfer performance. Gas hold-up, $\varepsilon_g$ is commonly stated in percentages and defined as the following:

$$\emptyset_g = \frac{H_A - H}{H_A} \qquad \textbf{2-10}$$

where $H_A$ and H denote the heights of the aerated liquid and the clear liquid, respectively.

$\emptyset_g$ is determined by measuring increment in level of the medium being agitated with a presumption that the value of gas being 'hold-up' will produce similar volume displacement in the overall agitated medium. Literature review shows that gas hold-up has been studied as a function of gas flow rate, vessel geometry, impeller type and geometry, liquid phase properties and sparger type. Detail discussion on available literatures that relates to the operating functions are as follows:

### 2.6.1.1 Effect of gas rates

The effect of gas flow rate at a constant speed is shown in Figure 2.4. Gas hold-up increases with increasing gas flow rate until flooding point is reached when the gas flow rate is $Q_2$. At this point, the impeller is said to be flooded and any further increase in gas rate does not result in increased gas holdup value. On the other hand when the gas rate approaches zero, there is a finite value of gas hold-up, $Ø_{g\,o,}$ which is due to the air bubbles being sucked into the vessel from the surface (surface entrainment).

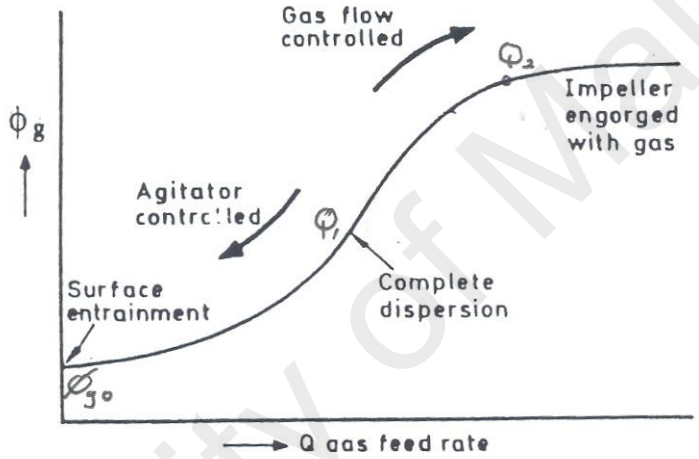


Figure 2.4 Effect of gas flow rate on gas hold-up at constant impeller speed

The bubbles in the tank are said to be completely dispersed when the flow rate reaches $Q_1$. A detailed description of 'complete dispersion' will be given in a later section. The term 'agitator controlled' indicates that at lower gas rates, the gas hold-up values are dependent on impeller speed whereas at higher gas rates the gas hold-up values are gas rate dependent.

### 2.6.1.2 The effect of impeller speed

The effect of impeller on gas hold-up at constant gas flow rate is shown in Figure 2.5. The gas hold-up at low rotational speed is insignificant. As the impeller speed increases

the gas hold-up also increases. The increment is due to shearing effect by the impeller and also improved dispersion of bubbles as the result of increased liquid circulation in the tank.

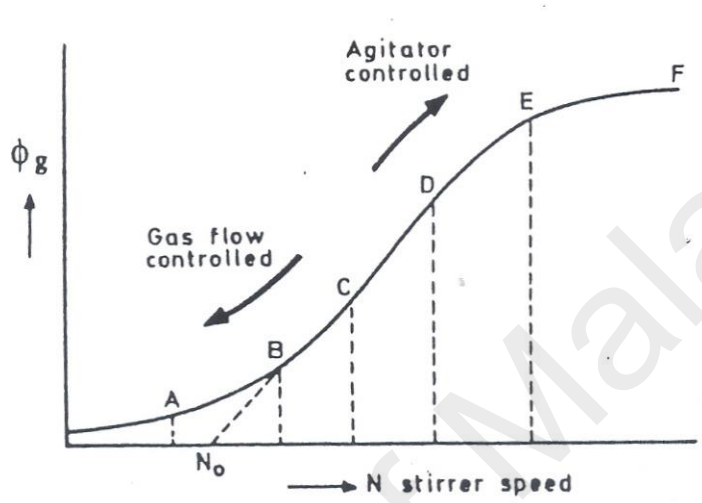


Figure 2.5 Effect of impeller speed on gas hold-up at constant flow rate

### 2.6.1.3 Effect of impeller type

In general it can be considered that an impeller with high power input capability can be considered to create better gas dispersion and this should result in higher gas hold-up. Chapman et al. (1983) studied different types of impeller for gas hold-up and found that at the same specific energy dissipation rate, impeller type does not have any influence on gas hold-up. Generally the literature review also suggests that the flow pattern and direction of flow also contribute greatly to gas hold-up characteristics of a particular impeller. Up flow impeller was found to have superior dispersion characteristics than the radial flow impellers at similar energy input level.

#### 2.6.1.4 Effect of solid presence

Presence of solid in gas-liquid dispersion process can be expected to influence the dispersion performance of impeller as a result of ratification of viscosity and local density or vortex structures in the vicinity of the impeller blades (Frijlink et. al, 1990) (Ibrahim & Nienow, 2009). Furthermore, unsuspended solids may form a false bottom and effectively reduce the impeller clearance, C, and affect the power input characteristics, which in turn affect the gas hold-up values. However no outright conclusion can be made on effect of solid particles on gas hold-up values as it seems to be a function of gas flow rate, solid particle shape, size and concentration, impeller type and direction of pumping. For example Kurten and Zehner (1979) found that the presence of solid in concentration of 5-10% (weight) reduces the gas hold-up. At high gas velocity, the presence of solid increased the gas hold-up values.

Table 2.1 lists some of the previous works on suspension of solids in two- and three-phase stirred tanks. It is obvious that suspension of high concentration of solids in the presence of gas has not been investigated before.

Table 2.1 Specifications of two- and three-phase systems in previous works

| Author | System | Impeller type | Tank diameter, T, (m) | Liquid phase | | | Solid phase | | | Gas phase | | |
|---|---|---|---|---|---|---|---|---|---|---|---|---|
| | | | | Type | Density | Liquid height | Type | Density (kg/ $m^3$) | Concentration | Type | Density | Gas flow rate |
| Raghava Rao et al (1988) | S-L | RT, PBD, PBU | 1.5 | Water | 1000 | = T | Quartz | 2520 | 0-50% w/w | - | - | - |
| Drewer et al. (1994) | S-L | RT, PB | 0.2 | Water | 1000 | = T | SGBB | 2500 | 4.3-48.5% v/v | - | - | - |
| Drewer et al. (2000) | S-L | RT, PBD, Propeller | 0.2-0.4 | Water | 1000 | = T | SGBB | 2500 | C < 50% v/v | - | - | - |
| Hicks et al. (1997) | S-L | P-4, HE-3 | 0.29 | Water | 1000 | = T | Sand, resin | 1053-2590 | C < 10% w/w | - | - | - |
| Selima et al. (2008) | S-L | PB | 0.98 | Water | 1000 | =1.38T | Phosphate particles | 2650 | 6-10 % w/w | - | - | - |
| Wu et al. (2010) | S-L | RT, PB, Propeller | 0.39-5.5 | Water | 1000 | = T | SGBB | 2500 | C < 40% v/v | - | - | - |
| Wang et al. (2014) | S-L | RT, PB, A310 | 0.39 | Water | 1000 | = T | SGBB | 2500 | 0-40% v/v | - | - | - |
| Ibrahim & Nienow (2009) | G-S-L | RT, PBU, InterMIGs, HE-3 | 0.29 | Water | 1000 | = T | SGBB | 2500 | 0-5 % w/w | Air | 1.225 | 0.25-3 vvm |
| Dohi et al (2004) | G-S-L | Maxblend, Fullzone & PBD | 0.2-0.4 | Water | 1000 | = T | SGBB | 2500 | 0-30 % v/v | Air | 1.225 | 0.01-0.092 $ms^{-1}$ |

Table 2.1 (Cont.)

| | | | | | | | | | | | | |
|---|---|---|---|---|---|---|---|---|---|---|---|---|
| Dohi et al.(1999) | G-S-L | PBD, Pfaudler | 0.2 & 0.8 | Water/ Methanol | 998/792 | = T | SGBB & polymeric particles | 2500/1495 | 0-20 % v/v | Air | 1.225 | 0-0.092 $ms^{-1}$ |
| Li et al. (2015) | G-S-L | CB/ Hydrofoils | 0.3 | Water | 1000 | =1.8T | SGBB | 2500 | 3-9 % v/v | Nitrogen | 1.165 | 1.4-4.2 vvm |

SGBB: spherical glass ballotini beads, G: gas, S: solid, L: liquid, RT: Rushton turbine, PBD: Pitched blade (down-pumping), PBU: Pitched blade (up-pumping), CB: Curved blade impeller

In summary it can be concluded that the presence of solid could result in either increase or decrease in gas hold-up values, depending on factors that were mentioned earlier. In this work a wide range of solid concentration and gas flow rates will be evaluated for all the impellers for their respective gas hold-up behavior when solids are present.

#### 2.6.1.5 Prediction of gas hold-up

Theoretical prediction of gas hold-up is rarely available due to lack of three dimensional flow information in the vessels. However numerous correlations are available in empirical form. The correlation for gas hold-up can be reduced into two types as follows:

(Type 1)

$$\emptyset_g \sim \left[\frac{P_g}{V}\right]^x U_g^y \qquad \textbf{2-11}$$

(Type 2)

$$\emptyset_g \sim N^x U_g^y \text{ or } \emptyset_g \sim N^x Q^y \qquad \textbf{2-12}$$

Equation 2-11 implies that $Ø_g$ is dependent on specific power input and superficial gas velocity, meanwhile equation 2-12 implies that gas hold-up is dependent on impeller speed and gas flow rate (or superficial gas flow rate). Some of the correlations available for Rushton turbine are listed in Table 2.2. All the listed correlations in the table are for liquid-gas system only.

Attempts also have been made to improve gas hold-up correlations by taking impeller and bulk flow regimes into account. An example of such work is by Smith (1991) who proposed following correlation:

$$\emptyset_g = 0.85\left[\frac{N^2 Q \rho_L}{g\mu_L}\right]^{0.354}\left(\frac{D}{T}\right)^{1.25} \quad \textbf{2-13}$$

From the discussion earlier it can be seen that only empirical correlations dominated the prediction of $Ø_g$. Power input, impeller speed and gas flow rate are found to influence the $Ø_g$ values. In this study, therefore, all these variables will be studied for each impeller being evaluated.

Limited correlations are presently available for predicting gas hold-up when solid particles are present in the system, and these correlations are applicable for a range of solid particles concentration, type, shape and diameter studied. The correlations are similar to the one proposed for gas-liquid system with additional features for solid particle presence as shown in the following general form:

$$\emptyset_g = A\left(\frac{P}{V}\right)^B V_g^c (1+\varepsilon_s)^D \quad \textbf{2-14}$$

Equation 2-14 is applicable for both two and three phase gas hold-up prediction. In a detailed study involving gas-liquid-solid, gas hold-up prediction, Cleszkowski and Dylog (1994) proposed a correlation as given in equation 2-15 below. This equation is valid for P/V =10 to 200 W/m$^3$, $V_s$ = 0.005 to 0.02m/s and $\varepsilon_s$ = 0 to 0 .2.

$$\emptyset_g = 0.177\left(\frac{P}{V}\right)^{0.39} V_g^{0.58}(1+\varepsilon_s)^{-2.9} \quad \textbf{2-15}$$

Archis et.al (2002) studied gas hold-up values in tank reactors and conducted analysis using similar correlation.

Table 2.2 Correlations for determination of gas holdup in gas-liquid systems

| Author (s) | System | Impeller | T(m) | D/T | N, rps | $U_g$, mm/s | Correlation |
|---|---|---|---|---|---|---|---|
| Yoshida and Miura, (1963) | Water, NaOH, glycerol | 12-flat blade | 0.25<br>0.59 | 0.4 | 1-5.83 | 1.7-7.6 | $\emptyset_g = constant\ N^{0.8}U^{0.75}D^{1.2}$ |
| Rushton and Bimbinet, (1968) | Water, Corn-syrup | Rushton turbine | 0.23<br>0.91 | 0.18-0.53 | | 3.0-30.0 | $\frac{\emptyset_g}{1-\emptyset_g} = 0.31\left(\frac{P_g}{V}\right)^{0.31} U_g^{0.6}$ |
| Chapman et al., (1983). | Water | Various types | 0.56 | 0.5 | 2.3-9.3 | 2.3-9.3 | $\emptyset_g = 17.9\left(\frac{P_g}{V}\right)^{0.31} U_g^{0.67}$ |
| Sterback and Sachova, (1976) | Water, Glycerol | 4-flat blade | 0.16 | 0.57 | 5.3-15 | 7.2-21.6 | $\emptyset_g = 9\times10^{-5}\left[\frac{\rho_L U_g D}{\mu_L}\right]^{0.77}\left[\frac{\rho_L N^2 D^3}{\sigma}\right]$ |
| Loiseau et al. (1977) | Organic and ionic solution | Rushton turbine | 0.22 | 0.33 | 5-27.5 | 6.4-47.0 | $\emptyset_g = 0.011\left[\frac{P_g}{v}\right]^{0.27}\left[\frac{U_g}{\sigma}\right]^{0.36} - \mu_L - 0.056$ |
| Hassan and Robinson, (1977) | Water non-ionic solution | Rushton turbine | 0.15<br>0.29 | 0.33 | 3.3-35 | 3.5-6.8 | $\emptyset_g = 0.113\left[\frac{QN^2}{\sigma}\right]^{0.57}$ |

| | | | | | | | |
|---|---|---|---|---|---|---|---|
| Yung et al., (1979) | Water, Glycol, Acetone, NaCl | Rushton turbine | 0.4 | 0.23-0.45 | 3.33-23.3 | 1.0-21.0 | $\emptyset_g = 0.52\left[\frac{\rho_L N^2 D^3}{\sigma}\right]^{0.65}\left[\frac{Q}{ND^3}\right]^{0.5}\left[\frac{D}{T}\right]^{1.4}$ |

### 2.6.2 Bubble size and gas-liquid interfacial area

Gas–liquid mass transfer is a crucial factor in the design of chemical and biochemical processes where dispersed phase is a reaction-limiting factor. In general, the gas–liquid interfacial area is a function of unit's geometric size, operating parameters, physical and chemical properties of phases. In several applications, mass transfer rate is determined by volumetric mass transfer coefficient, which is a function of specific interfacial area. So to optimize the processes on the mass transfer phenomena, it is essential to know the bubble size distribution and interfacial phenomena in the particular system at different operating conditions. In a three-phase stirred vessel, bubble size distribution plays a crucial role in the transport phenomena and governs the overall rate of reaction, while gas holdup along with bubble size determines the efficiency of gas-liquid interactions (Busciglio et al., 2013). In such systems, these two parameters are mainly determined by agitation level and gas flow rate. When solids are present, the role played by these variables in determining the gas-liquid interfacial area is modified to a large extent by solids. In addition to participating in chemical reactions or transfer processes, solid particles also influence the gas dispersion process (Chapman et al., 1983). Evidences for such an interaction have been reported in studies involving three-phase fluidized bed columns which have hydrodynamic characteristics similar to those of multiphase stirred vessels but with no agitation. Increasing the impeller speed is the easiest way of increasing the gas hold-up and decreasing the bubble size and thus achieving a large interfacial area.

#### 2.6.2.1 Measurement techniques

There are several studies on bubble dynamics in gas-liquid systems in the literature. Various techniques have been used for studying gas dispersion characteristics and bubble size measurements in gas-liquid systems. These approaches include photographic

techniques (Machon et al., 1997) (Bouaifi & Roustan, 1998) (Bouaifi et al., 2001)( Winterton & Munaweera, 2001) (Bailey et al., 2005) (Horn et al., 2007)( Montante et al., 2008)( Sommerfeld & Bröder, 2002) ( Lau et al., 2013), wire mesh sensors (Lucas et al., 2005)( Manera et al., 2009), imaging probes (Honkanen et al., 2010), pressure probes (Linek et al., 1996), conductivity probes (Gao et al., 2001), resistivity probes (Bombač et al., 1997)( Bombač et al., 2000), impedance probes (Paglianti & Pintus, 2001), suction probes (Parthasarathy & Ahmed, 1994)(Kamiwano et al., 2003), computed tomography (Wang et al., 2000)(Khopkar et al., 2005)( Hampel et al., 2007)( Ford et al., 2008) (Boden et al., 2008), transmitted light probe (Calderbank, 1958) and particle image velocimetry (PIV) (Laakkonen et al., 2005). These measurement techniques can be divided into two categories invasive and non-invasive methods. A majority of non-invasive methods that rely on capturing images from outside of tank (e.g. photography and image analysis or light attenuation) require transparent walls and liquids. Invasive techniques, such as needle probe or heat transfer probe, are limited to low solids concentration and not applicable to wall vicinity. More details on the measurement techniques for gas-liquid systems can be found in the comprehensive review by Boyer et al (2002).

Increasing the impeller speed is the easiest way of increasing the gas hold-up and decreasing the bubble size and thus achieving a large interfacial area. However there are no predictive methods available to estimate the effect of impeller speed on physical interfacial area as there is no detailed information on bubble size. Previous studies in this area involved the measurement of mainly the interfacial area and the gas hold-up. A number of correlations are available in the literature which relate the interfacial area and the gas hold-up to the specific power input or the impeller speed. In most of these correlations the bubble size has been either assumed to be a constant or not taken into account.

The main reason for the absence of information on bubble size is the experimental difficulties involved in its measurement. Thus, this study tries to design and propose a novel imaging technique using which, bubble size can be studied in presence of high concentrations of solids.

#### 2.6.2.2 Mathematical correlation

Calderbank (1958) was the first to measure average bubble size in a stirred tank. He used light attenuation and suction probe techniques to measure gas-liquid interfacial area and gas holdup, respectively. He then proposed following correlation for determination of Sauter mean bubble diameter by integration of the local data obtained to the entire tank volume:

$$d_{32} = 4.15 \frac{\sigma^{0.6}}{\left(\frac{P_g}{V}\right)^{0.4} \rho_l^{0.2}} \emptyset_g^{0.5} + 9 \times 10^{-4} \qquad \textbf{2-16}$$

where σ is surface tension ($Nm^{-1}$), $P_g$ is gassed power input (W), V is tank volume ($m^3$), $\rho_l$ refers to liquid density ($kg/m^3$), and $Ø_g$ is gas holdup.

This equation includes the role of gassing rate and predicts that $d_{32}$ values decrease with an increase in agitation power consumption. Working on a dual impeller system, Bouaifi et al. (2001) observed the same relationship between Sauter mean bubble diameter and agitation power. Ever since, a number of studies have used this correlation to determine the $d_{32}$ values (Laakonken, 2005; Busiclio, 2013; Alves, 2002; Bouifi, 2001; Machon 97; Kawase 87). However, a reliable correlation to determine average bubble diameter in presence of high concentrations of solids is absent in the literature.

A major obstacle in proposing reliable correlations is lack of proper setup to study gas-liquid interaction in three-phase systems. A survey has revealed that very few attempts have been made to develop a recording setup to capture the size distribution of gas bubbles in the presence of particles.

In summary, it is well-known that operating stirred tanks at just suspended condition ($N_{jsg}$), at which no particles remain stationary at the tank bottom, is the best way to provide maximum contact area between solid and liquid phases. In a gas-solid-liquid system operating at $N_{jsg}$, gas bubbles are engulfed by clouds of rotating solids, which makes them almost invisible from outside especially in critical regions such as zones above the impeller level.

Therefore, it is mandatory to design a reliable technique for measuring bubble size in three-phase stirred vessels handling high solids concentrations.

#### 2.6.2.3 Effect of operating parameters

Barigou and Greaves (1991, 1992) measured the bubble size distribution at about 22 locations including the impeller region in a stirred vessel using a capillary suction probe. They found that the distributions near the impeller at low speed exhibit positive skew which are positioned at the lower size scale of the bubble spectrum. With increase in impeller speed the size distribution was found to move towards the lower end of the spectrum.

Takahashi and Nienow (1993) measured the sizes of the bubbles generated by a Rushton turbine by photographing them through the tank wall. In addition to the decrease in the mean bubble size with increase in agitation their observations include an increase in the mean bubble size with increase in gas density which was attributed to impeller cavity size modifications. In a following work Takahashi and Nienow (1993) reported that, at a given

impeller speed, the mean bubble size above the impeller is greater than that at the impeller plane due to the coalescence effect. They also concluded that coalescence effect in deionised water is pronounced even in the impeller plane as bubbles coalesce rapidly as they emerge from the impeller and travel towards the vessel wall.

Parthasarathy and Ahmed (1994) investigated the effect of impeller speed on the size distribution of bubbles in a noncoalescing system using a photographic method. They found the size distribution of bubbles generated by a porous sparger changed as a function of the impeller speed. Bubble size distribution that was approximated by a log-normal distribution at low speed become bimodal due to bubble break-up at higher impeller speeds. With further increase in impeller speed, the bimodal distribution changed into a unimodal distribution but with a lower mean size. It was noted that this lower mean size unimodal distribution is an equilibrium distribution resulting from the bubble break-up and coalescence processes.

In another study on bubble size in electrolyte and alcohol solutions at a given specific energy dissipation rate, Machon et. al., (1997) have suggested that the equilibrium bubble size distribution in a stirred vessel is influenced significantly by the turbulence level, but not as much by the surface tension of the liquid medium. They reported that the concentration of the solutes like electrolytes and alcohols in the liquid medium has a major role in coalescence suppression and therefore in determining the resulting mean bubble size.

## 2.7 Summary

From the literature review, it can be concluded that information on the suspension of high concentration slurry is extremely limited. The behavior of high concentration suspension is difficult to predict because the presence of a large amount of solids exerts a strong

impact on the fluid circulation. This situation becomes more pronounced in three-phase systems as introduction of gas leads to immediate sedimentation of solids. The effects of various variables such as impeller type, baffling configuration, solids concentration, and gas flow rate on impeller power consumption in a gas-solid-liquid system are still not established, particularly for the systems involving high solids concentration. Therefore, in this study, the investigation focuses on the suspension of high-concentration slurry and specific power input to evaluate the solid-suspension operation in gas-solid-liquid mixing vessels.

The above review also shows that the knowledge on gas-liquid interactions in three-phase systems involving high solids concentrations is far from complete. Consequently, mathematical correlations that can predict system's behavior under various operating conditions are not available. This problem is mostly associated with the lack of reliable recording setups for observing changes in bubble size in the system. In order to fill the gap, this study aims at proposing an in-situ measurement technique by which bubble size and gas-liquid interfacial area can be measured for a wide range of solids concentration in three-phase stirred vessels, and uses the $a_{g\text{-}l}$ values to identify optimum conditions at which impeller's performance in terms of power efficiency and ability to provide optimum gas-liquid contact area can be maximized. These results can also lead to development of reliable mathematical models which can estimate average bubble size and gas-liquid interfacial area in three-phase systems handling high concentrations of solids. Since studies on the effects of high concentration of solids on bubble size and gas-liquid interfacial area are very limited, it is hoped that results of present work can lead to optimum usage of multi-phase slurry tanks such as those frequently used in mineral processing.

# CHAPTER 3: METHODOLOGY

## 3.1 Experimental setup

The transparent cylindrical vessel used in this work was 0.4 m (T) in diameter with unaerated liquid height equal to the tank diameter. The vessel was made of scratchproof Perspex with a thickness of 5 mm. Four equally spaced baffles with a width of 4 cm (0.1T) were attached to the inside wall along the entire depth of the tank to minimise vortex effects. The agitation was provided by a shaft, which was located at the vertical axis of the tank and driven by a 3.0 kW motor. The motor shaft was connected to the impeller via a shaft coupling. A 4.0 kW-frequency inverter was used to achieve different agitation speeds. The experimental setup used in this study is schematically shown in Figure 3.1. The main components of the set-up are listed in Table 3.1.

Impellers are divided mainly into two classes: axial-flow impellers and radial-flow impellers. Axial flow impellers generate currents parallel to the axis of the shaft whereas radial-flow impellers generate currents in a radial direction. Typical radial flow impellers include the Rushton turbine and the curved blade turbine, and common axial flow impellers include the pitched blade turbine. Radial flow impellers with straight or concave blades are usually employed for gas dispersion in low viscosity systems. The major applications of axial flow impellers are in solids suspension, where the axial flow of the liquid sweeps solids off the tank bottom. The axial flow is usually discharged downwards in this case. Axial flow impellers pumping upwards are usually employed in multiple impeller systems.

Three types of impellers used in this work were: Rushton turbine (RT), pitched blade impeller (PB), and Lightnin aerofoil (A310). These three impellers are commonly chosen

for studies involving suspension of high-concentration slurries because they have a range of power numbers ($N_P$) and flow patterns (Wang et al., 2012, Wang et al., 2014). The impeller clearance (C) was kept at 0.25 T in all experiments. However, C was kept at 0.33T in $N_P$ measurement experiments, so that $N_p$ values obtained in this work could be compared with those reported in literature.

Details of the impellers used in this study are shown in Table 3.2. It can be seen that the $N_p$ values determined are close to the ones that are generally reported in the literature. Compressed air was sparged into the tank through a ring sparger of a diameter of 0.5T located 5 cm above the tank bottom. The sparger had 34 symmetrical holes of 1 mm diameter each. The sparger holes were facing the tank bottom to ensure that they would not be clogged by suspended particles.

Unaerated and aerated liquid heights were measured to determine the gas holdup under different mixing conditions. These values were continuously measured using an ultrasonic level sensor (EchoSonic® LU23-29 Ultrasonic Level Transmitter, Flowline). The ultrasonic sound pulse generated by the instrument (pulsed four times per second) travels through air, gets reflected from the liquid surface and eventually returns to the transducer. The liquid level is determined based on the time taken by the pulse to travel to the liquid surface and return to the instrument. The liquid level measurement accuracy was further improved by placing the sensor inside a Perspex cylindrical chamber. The bottom of the chamber, which was in contact with the liquid surface, had a porous Perspex material to dampen out the fluctuations of the liquid surface during the experiment and provide a stable surface for measurement. To ensure that the liquid height values measured were valid, the measurements were repeated by placing the sensor at a point diametrically opposite to its original location and midway between two adjacent baffles. Comparing the values recorded at both locations, the reproducibility of the data was checked. Gas hold-up and impeller power input were measured in separate runs.

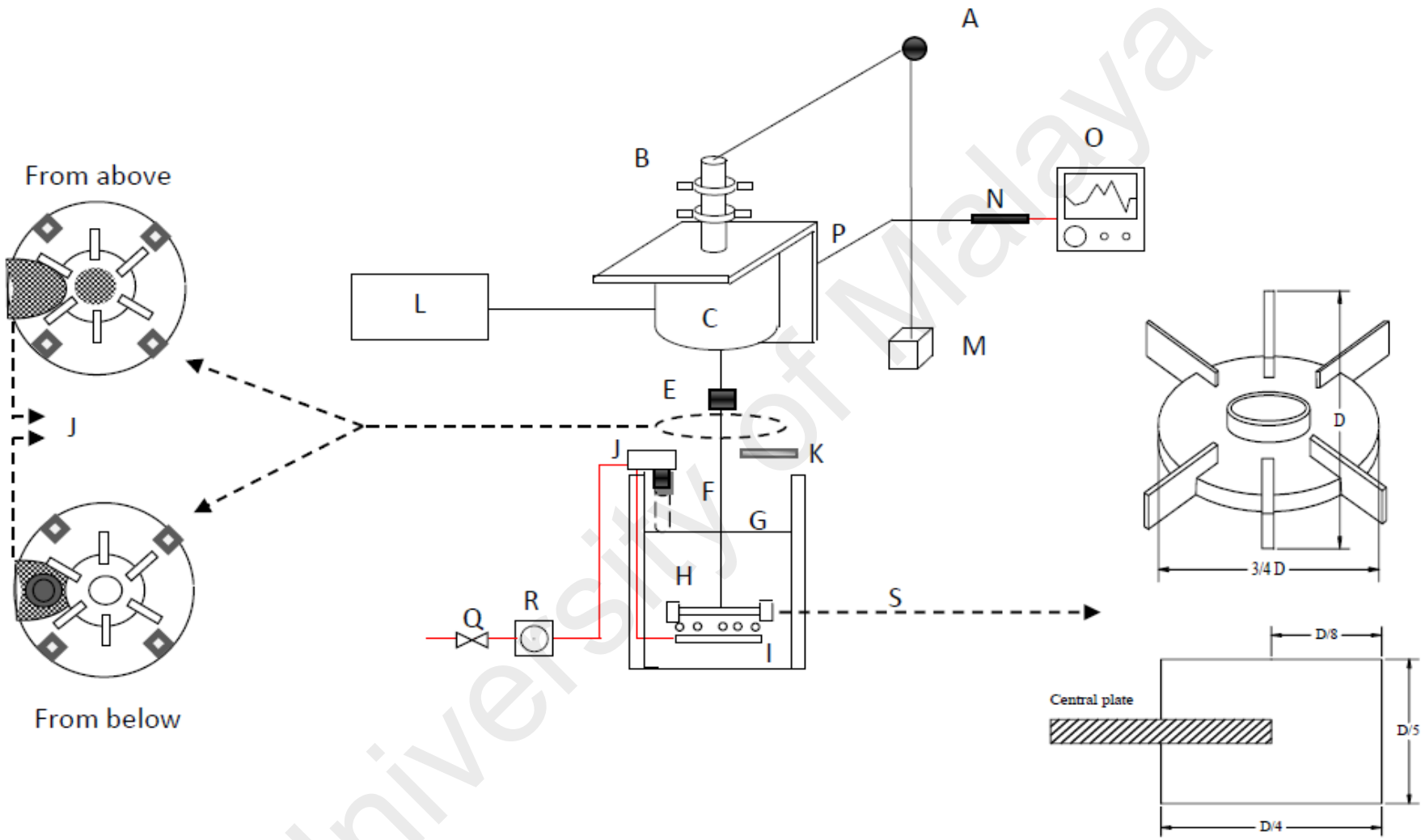


Figure 3.1 Schematic diagram of the experimental setup used in this study

Table 3.1 Specifications of the setup depicted in Figure 3.1

| Mark | Details | Mark | Details |
|---|---|---|---|
| A | Pulley | J | Level sensor |
| B | Bearings | K | Tachometer |
| C | Motor | M | Counterweight |
| D | Impeller diameter | N | Load cell |
| E | Impeller coupling | O | Recorder |
| F | Shaft | P | Lever Arm |
| G | Liquid level | Q | Gas pipe |
| H | Impeller | R | Rotameter |
| I | Sparger | S | Impeller details |

Table 3.2 Specifications of impellers used in this study

(Power numbers were measured using a clearance of 0.3T from the tank bottom)

| Impeller type | Flow pattern | No. of blades | D/T | Impeller abbreviation | Power Number ($N_p$) |
|---|---|---|---|---|---|
| Rushton turbine | Radial | 6 | 0.3 | 0.3 RT | 5.4 |
| Rushton turbine | Radial | 6 | 0.5 | 0.5 RT | 5.4 |
| 45° pitched blade turbine | Mixed | 6 | 0.3 | 0.3 PB | 1.24 |
| 45° pitched blade turbine | Mixed | 6 | 0.5 | 0.5 PB | 1.24 |
| Lightnin hydrofoil impeller | Axial | 3 | 0.52 | A310 | 0.33 |

In mixing studies, various dimensions are commonly stated as fraction or ratio of the tank diameter, T. Impeller clearance, impeller diameter, liquid height, baffle width, sparger diameter and clearance are some of the dimensions that need to be determined for the study. The dimensions for this study were determined after identifying the most used fractions and ratios in the literature so that comparisons and conclusions can be drawn more effectively at the end of the study. Figure 3.2 shows the ratios used in this study, which is followed by Table 3.3 which lists their details.

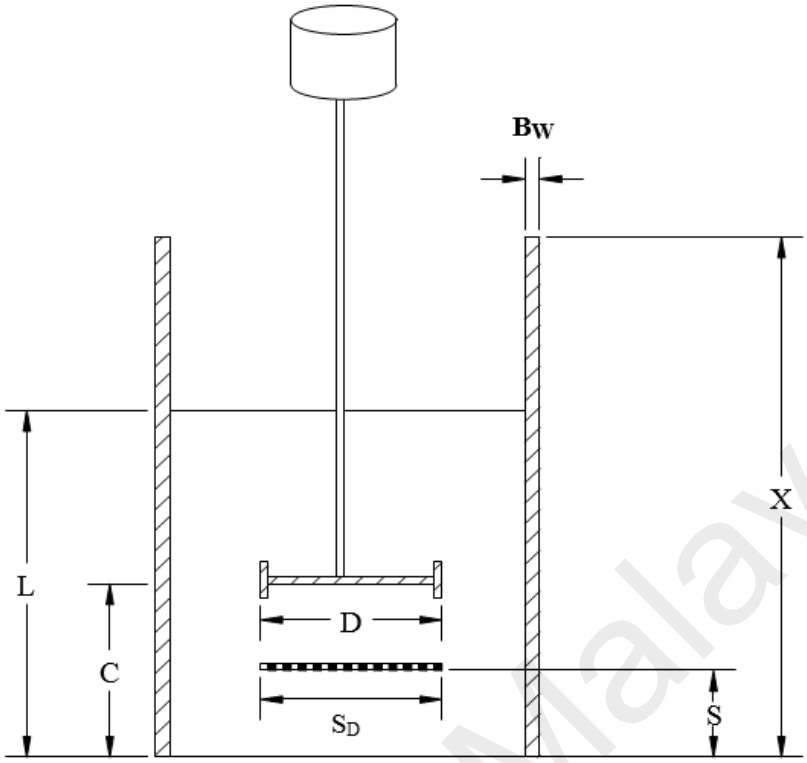


Figure 3.2 Geometrical dimensions in the stirred vessels used

Table 3.3 Details of dimensions

| Symbol | Description | Ratio | Length (cm) |
|---|---|---|---|
| T | Tank diameter | T | 40.0 |
| c | Impeller clearance | T/3 | 13.3 |
| D | Impeller diameter | T/3 | 13.3 |
| $S_D$ | Sparger diameter | T/3 | 13.3 |
| S | Sparger clearance | T/6 | 6.7 |
| X | Baffle height | 1.5T | 60.0 |
| $B_W$ | Baffle width | 0.1T | 4.0 |

## 3.2 Materials

Compressed air, tap water, and spherical glass ballotini beads ($\rho_s$ = 2500 kg/m$^3$) were used as gas, liquid, and solids phases, respectively. A particle size analyser (Mastersizer 2000) was used to determine the particle size. The $d_{10}$, $d_{50}$, $d_{90}$, and $d_{32}$ for the particles used in this study are listed in Table 3.4. Three different gas flow rates of 25, 37, and 50 L/m, which corresponded to 0.5, 0.75, and 1 vvm respectively, were used. Expressing the gas flow rate in terms of vvm rather than superficial gas velocity has been reported to be advantageous (Chapman et al., 1983)(Nienow et al., 1977) and therefore gassing rates in this work are reported in vvm. The gas flow rate was regulated using a set of rotameters, which had been calibrated with standard gas meters to relate the graduations on the rotameters to the actual gas flow rate in litres per minute.

Table 3.4 Solids properties: glass bead, SG = 2.5, values obtained using particle size analyser Mastersizer 2000

| Particle type | Density (kg/m$^3$) | $d_{0.1}$ (μm) | $d_{0.5}$ (μm) | $d_{0.9}$ (μm) | $d_{32}$ (μm) | Particle Abbreviation |
|---|---|---|---|---|---|---|
| BGB* | 2500 | 274 | 370 | 500 | 360 | BGB $_{370}$ |
| BGB | 2500 | 494 | 683 | 957 | 665 | BGB $_{683}$ |

*BGB: Blue glass beads

## 3.3 Determination of critical impeller speed in three-phase system

$N_{js}$ and $N_{jsg}$ were determined in this work using an approach proposed by Hicks et al. (1997), which considers the height of the motionless particles at the tank bottom as a criterion for the degree of suspension. The agitation speed was initially increased up to a point that no particle rested motionless at the tank bottom. At this stage, all paticles were

completely dispersed throughout the vessel and gas bubbles were completely dispersed (Figure 2.1f). Then, the agitation speed was gradually decreased until the first layer of the motionless particles appeared at the tank bottom (Figure 2.1d). The bubbles were fully distributed in the vessel but a fraction of solids was not lifted at this point. Impeller speed was again increased to lift the bottom layer to reach the just-suspended condition (Figure 2.1e). The speed at which the layer of unsuspended solids disappeared was recorded as the critical impeller speed. At speeds lower than $N_{jsg}$, a visible layer of motionless particles appeared at the tank bottom, and its height was labeled as $H_B$ in Figure 2.1. This figure shows that $H_B$ decreased with an increase in agitation speed and eventually disappeared at $N_{jsg}$. In contrary, suspension height ($H_s$) increased with agitation speed, achieving a certain height at $N_{jsg}$ and eventually becoming equal to the liquid height at $N_{usg}$ (Figure 2.1f).

### 3.4 Determination of impeller power input

The power drawn by the impeller for agitation at a particular speed was determined by measuring the equivalent weight generated by the torque as a load. The principle of the technique is presented in Figure 3.3.

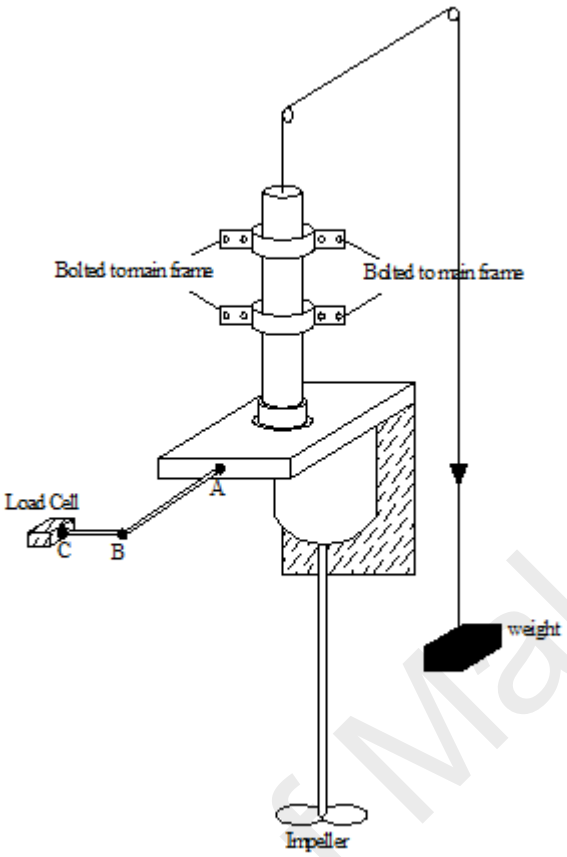


Figure 3.3 Principle of power measurement

The motor was attached to an L shape plate and the plate itself was connected to a shaft via pillow bearing as shown in Figure 3.3. When the impeller rotates, it imparts a force to the medium and in return the impeller also imparts an opposite force of similar magnitude. With the counter weight arrangement this rotational force will also be transmitted to the lever arm attached to the motor assembly. Load cell at the end of the lever arm stops the movement of the lever arm and also measures the magnitude and direction of the force.

Load cells are commonly used in weighing machine. It is basically a straight bar with resistance coils attached to it. When one end of the load cell is held steady and the other end is subjected to a force, the resistance of the coil changes. If the load cell is fed with a fixed current or voltage, the output current/voltage will vary according to changes in

resistance which in turn varies with magnitude of the force exerted on it. This is the principle of load cell operation. Before the load cell is put into use, a calibration is done with known weights and the corresponding output signal (for fixed voltage input of 12 V DC). The relationship between weight and the output signal is referred as the 'calibration factor'.

During the experiments, electrical signal from the load cell was recorded by a recorder and translated to force using the calibration factor mentioned above. Power drown, P by the impeller is then calculated using the following relationship:

$$P = 2\pi . N . \tau \qquad \textbf{3-1}$$

where N is impeller speed (rps) and $\tau$ is torque experienced by the impeller shaft, which was determined by:

$$\tau = F . dL \qquad \textbf{3-2}$$

where F is the force and $d_L$ is the lever arm length which is equal to the distance between the centre of agitator shaft and the point at which the load cell is connected to the lever arm, which is 0.23 m in this case. F can be determined by:

$$F = m . g \qquad \textbf{3-3}$$

where m is the load measured by the load cell and 'g' is the gravitational constant. Therefore, equation 3-2 can be written as:

$$\tau = m . g . dL \qquad \textbf{3-4}$$

Substituting equation 3-4 in equation 3-1, we can calculate the impeller power consumption P in terms of load (m) and impeller speed (N).

Then, the specific impeller power draw as a function of the total mass of the lifted solids ($\varepsilon_{jsg}$) can be calculated as:

$$\varepsilon_{jsg} = \frac{P_{jsg}}{M_s} = \frac{2\pi N m g d L}{M_s} \quad \textbf{3-5}$$

A calibration exercise was done using a Rushton turbine to ensure the power measured by the set-up is accurate. The power number of the impeller was determined for a speed between 300 rpm to 1000 rpm. Compared to literature, this power number value is comparable to established values.

After ensuring the viability of the technique using power number values for Rushton Turbine, calibrations were also carried out to determine reproducibility of the set-up. It was found that the reproducibility of the power measurement is within 5% for speed greater than 100 rpm.

### 3.5 Gas holdup measurement

The height of the liquid in the tank under aerated and unaerated conditions was measured using an ultrasonic sensor and used to determine the gas hold-up. These values were continuously measured using an ultrasonic level sensor (EchoSonic® LU23-29 Ultrasonic Level Transmitter, Flowline, made in USA). The ultrasonic sound pulse generated by the instrument (pulsed four times per second) travels through air. It gets reflected from the liquid surface and eventually returns to the transducer. The liquid level was determined based on the time taken by the pulse to travel to the liquid surface and return to the instrument. The location of the ultrasonic detector was determined by trial-

and-error to minimize the influence of other effects such as liquid level fluctuations on the measurement of the liquid dispersion height.

The measurement accuracy of liquid level was further improved by placing the sensor inside a perspex cylindrical chamber. The bottom of the chamber, which was in contact with the liquid surface, had a porous Perspex material to dampen the fluctuations of the liquid surface during the experiments and provide stable surface for measurement. To ensure that the measurement of liquid height was valid, the experiments were repeated by placing the sensor at a point diametrically opposite to its original location and midway between two adjacent baffles. The location of the ultrasound sensor in the tank is shown in Figure 3.4.The reproducibility of the data was checked by comparing the recorded values on both sides of the vessel. Gas hold-up and impeller power input were measured in separate runs.

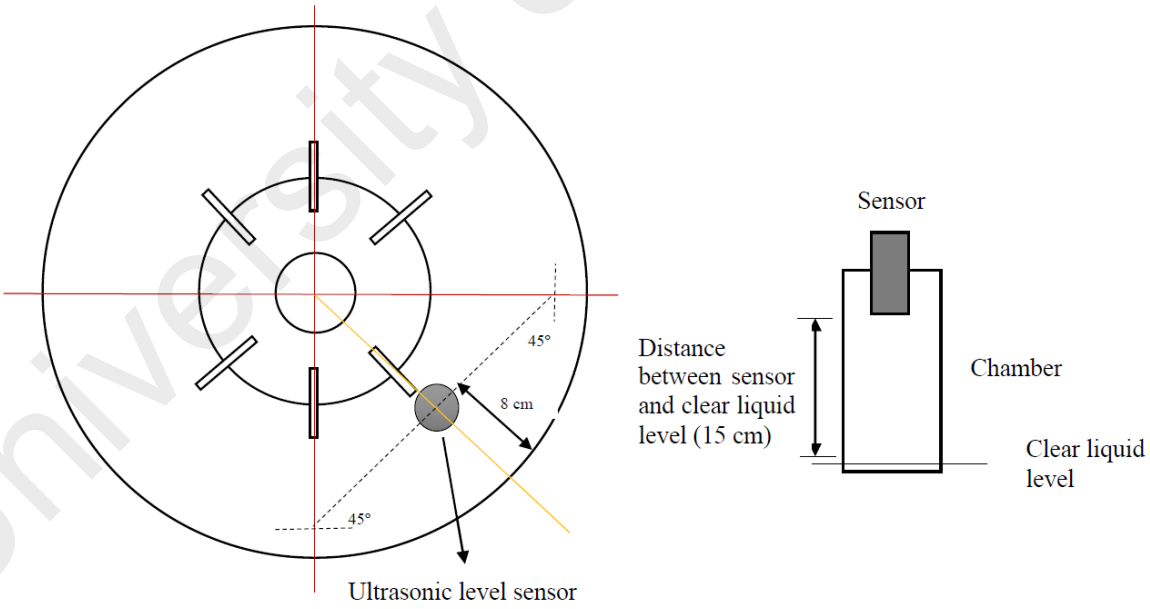


Figure 3.4 Position of level sensor in the mixing setup

### 3.6 Bubble size measurement

Bubble size is a crucial parameter in gas dispersion studies. Bubble size is also a reliable criterion in the evaluation of gas-liquid hydrodynamics as it directly influences gas holdup and interfacial area. In this study, bubble size was measured using a novel under-water video technique. The video recording setup included a camera, a flexible gooseneck cable, a camera cover, a TFT LCD monitor, a strobe light with adjustable flashing frequency, a transparent perspex rod, and a bracket. The setup is schematically shown in Figure 3.5.

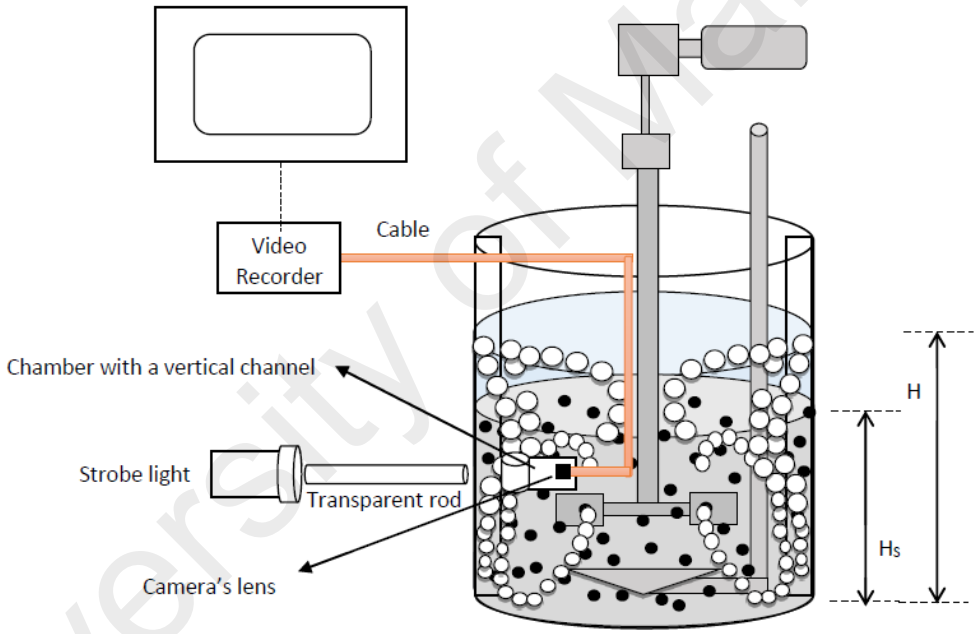


a

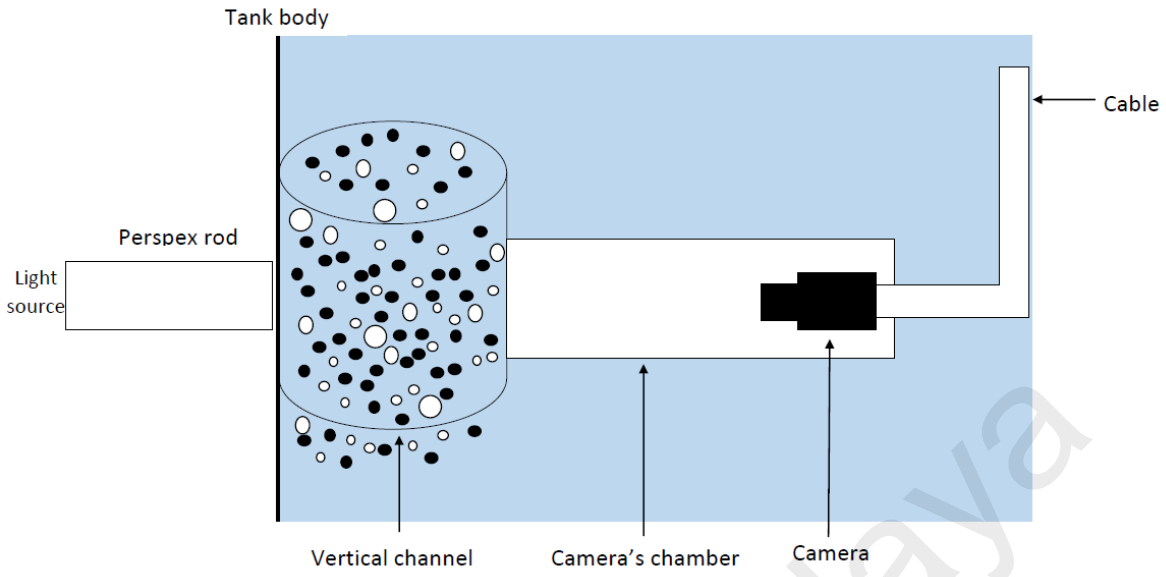


b

Figure 3.5 (a) Bubble size measurement technique (b) close-up view of the set-up used for capturing bubble images

The head of the camera was placed inside a Perspex cylindrical chamber attached with a vertical channel, and the camera was connected to the LCD monitor via a water-proof gooseneck cable. The cylindrical chamber protected the camera from water and provided sufficient focus range for camera's lens. The photographic unit was placed above the impeller level and its location was fixed in all runs using a bracket.

To improve the contrast between the bubbles and liquid phase, a diffused stroboscope light was used as the background light. Strobe light flashing frequency was adjusted to match that of the camera, which was 1875 frequency per minute (FPM) in this case. During the photography, camera unit was facing the tank wall, and a transparent perspex rod located outside the tank was used to transmit the diffused light from the strobe light to the tank. Outer surface of the Perspex rod was covered by black tape to minimize light loss. The rod also helped in centralizing the background light for the video images.

Once $N_{jsg}$ was achieved, the camera was turned on to record images of the multiphase flow that passed through the vertical channel. All recordings were made in a dark room. The video signals captured by camera were recorded by a video recorder and constantly monitored using a LCD monitor.

In all experiments, system was allowed to run for five minutes to reach a steady state, then videos were recorded for 30s. The recorded videos were played back, and several snapshots were captured. The images captured by the camera were then analysed using an image analysis software (ImageJ). Several snapshots were taken and images with clear bubbles were selected and saved as Tagged Interchange File Format (TIFF). Diameters of the spherical bubbles were measured using ImageJ software. The known diameter of the column served as the reference, based on which the diameter of the bubbles in the photos were estimated.

For each run, 200 unique bubbles were analysed to obtain a reliable bubble size distribution. The Sauter bubble size diameter ($d_{32}$) value was then determined using the following equation:

$$d_{32} = \frac{\sum_{i=1}^{i=n} d_{bi}^3}{\sum_{i=1}^{i=n} d_{bi}^2} \qquad \textbf{3-6}$$

where n and $d_b$ refer to the total number of bubbles and bubble diameter, respectively.

# CHAPTER 4: RESULTS AND DISCUSSIONS

## 4.1 Introduction

This chapter presents the results of the effect of operating and design parameters on impeller power consumption, and aims at proposing optimum operating conditions at which the consumed energy by the impeller is used most efficiently. Moreover, gas holdup, average bubble size, and gas-liquid interfacial area are also studied to have a better understanding of the effect of solids concentration on gas-liquid hydrodynamics. The chapter is finalized by proposing reliable mathematical correlations.

## 4.2 Power consumption

The impeller power consumption or the energy dissipation rate of the impeller, as some researchers prefer to call it, is the most widely reported of all the parameters measured in multiphase agitated contactors as it is of great importance to the hydrodynamics in such vessels. It controls the turbulence levels in the vessel, which influence bubble size, gas holdup, interfacial area and consequently the mass transfer rate. Power consumption measurements can be used as a means of comparing the characteristics of different types of impellers in the same vessel geometry to determine the superiority of a particular impeller design for a specific application. Power consumption is also used as a scale-up criterion. Therefore, to the engineer designing multiphase contacting vessels, impeller power consumption data and correlations are invaluable.

### 4.2.1 Power number

Power number for flat blade impellers were analyzed. Since the power number values for flat blade impellers are well established (especially for 6RT), it is used to validate the accuracy of the power measurement made in this work. The power number as a function of Reynolds Number (at various rotational speed) for all the impellers are given in Appendix A of this thesis. Figure 4.1 shows the power number variation as a function of Reynolds Number for 4,6,8 and 12 flat blade (FB) impellers.

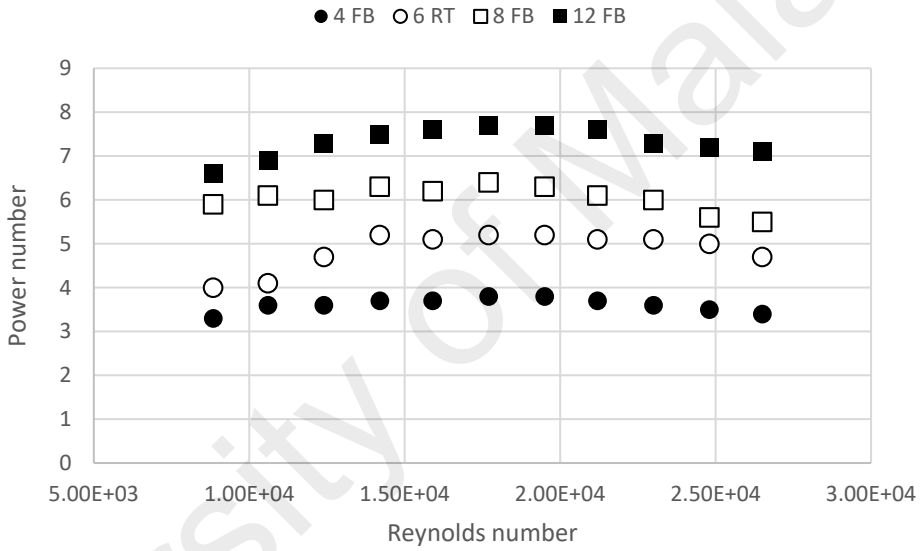


Figure 4.1 Power number versus Reynolds Number for 4, 6, 8 and 12 flat blade impellers

The $N_{po}$ values for all the impellers increases until $N_{RE}$ reaches $1.75 \times 10^4$ and beyond this point the power number reduces gradually with the reduction more pronounced in impellers with a higher number of blades. From the visual observation, the reduction in power number coincides when surface aeration sets in. The reduction in power number could be due to accumulation of air bubbles that are sucked into the tank from the surface of the liquid to the vicinity of the impeller (Warmoeskerken et al. (1984)). The sucked bubble inter the impeller zone, and dampen the pumping efficiency of the impeller, which

consequently results in reduced power numbers. Moreover, the surface aeration leads to net reduction in the displacement volume of the liquid phase, which consequently, reduces the overall power input into the system. The average power number for these impellers are given in Table 4.1.

Table 4.1 Average power number values for 4, 6, 8 and 12 flat blade impellers

| Impeller | Average power number |
|---|---|
| 4FB | 3.7 |
| 6RT | 5.4 |
| 8FB | 6.1 |
| 12FB | 7.5 |

When regressed , equation (4-1) with $R^2$ value of 0.99 was obtained.

$$\mathrm{Np} = 1.6\, n_p^{0.64} \qquad \textbf{4-1}$$

The $N_p$ value for 6RT obtained from this work is comparable to values obtained by other workers.

Not all the $N_p$ values for the type of impellers used in this work is available in the published literatures. For 6RT, the $N_p$ values are very well established, and can be used to validate the accuracy of the power measurement in this work. Bates et.al (1966) reported that for Reynolds number between $1.0x10^3$ to $1.0x10^5$, the $N_p$ for Rushton turbine was about 5.0. Meanwhile, Shiue and Wong (1984) reported that $N_p$ for 6RT ranges from 4.3 to 5.5 in turbulent regime. In this work the $N_{po}$ for Rushton Turbine was 5.4. This validates the accuracy of power measurement mechanism used in this work. In a more recent work, Wang et al. (2014) studied the Rushton turbine in a turbulent regime and reported $N_p$ of 5.6.

### 4.2.2 Critical Impeller speed

$N_{js}$ and $N_{jsg}$ were determined using an approach proposed by Hicks et al. (1997), who considered the height of the motionless particles at the tank bottom as a criterion for degree of suspension. The agitation speed was initially increased up to a point that no particle rest motionless at the tank bottom. At this stage, all solids were completely dispersed throughout the vessel and gas bubbles were completely dispersed. Then, the agitation speed was gradually decreased until the first layer of the motionless particles appeared at the tank bottom. The bubbles were fully distributed in the vessels but a fraction of the solids were not lifted at this point. Impeller speed was again increased to lift the bottom layer in order to reach the just-suspended condition. The speed at which the layer of unsuspended solids disappeared was recorded as the critical impeller speed. At speeds lower than $N_{jsg}$, a visible layer of motionless particles appeared at the tank bottom, and its height is labeled as $H_B$ in Figure 2.2. This figure shows that $H_B$ decreased with an increase in agitation speed and eventually disappeared at $N_{jsg}$. In contrary, suspension height ($H_s$) increased with agitation speed, achieving certain liquid height at $N_{jsg}$ and eventually becoming equal to liquid height at $N_{usg}$. The tanks were fully baffled and the agitation in this case was provided by RT impeller with D/T= 0.5 and off-bottom clearance of T/4. Compressed air was sparged at a flow rate of 0.5 vvm. A point between two baffles was chosen for measuring the bed height. The ratio of $H_B$ to the total liquid height ($H_B$/ H) is plotted in Figure 4.2 as a function of stirrer speed for different solid concentrations in the presence and absence of gas under baffled and unbaffled conditions. In these experiments solids were BGB $_{370}$, tap water and compressed air (0.5 vvm) were used as liquid and gas phases, respectively, agitation was provided by a large radial-flow impeller (0.5 RT), and impeller clearance was equal to T/4.

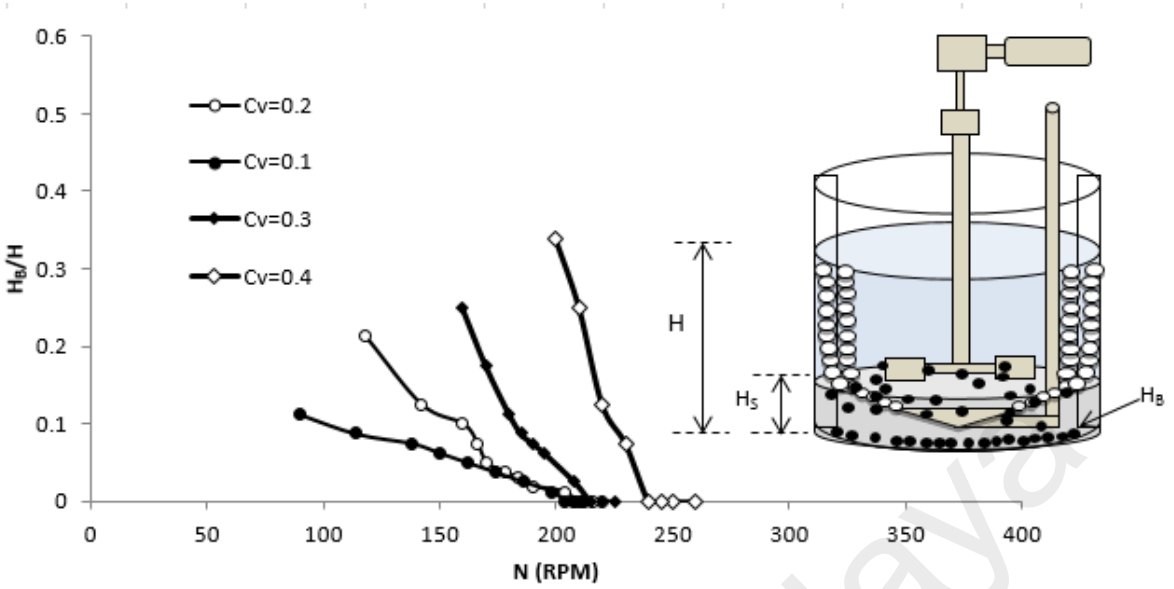


a

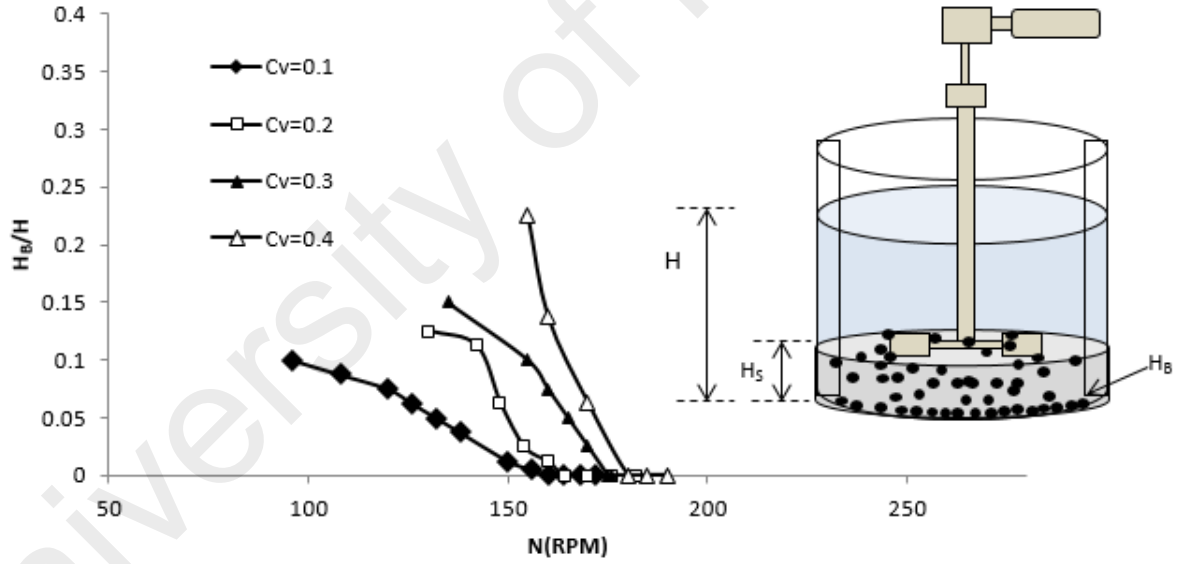


b

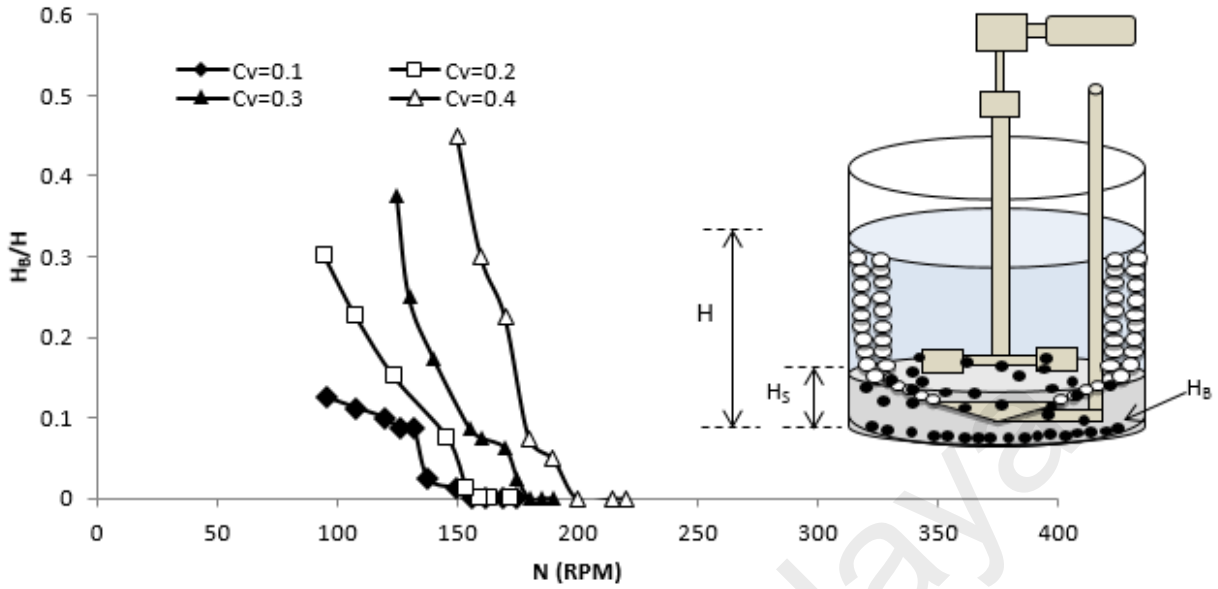


c

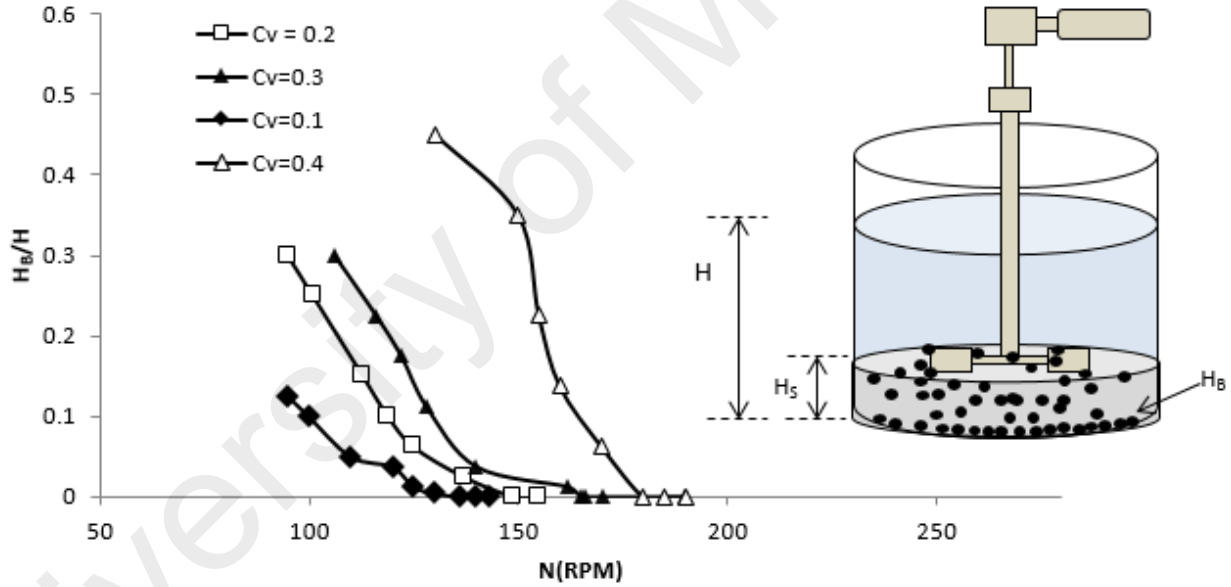


d

Figure 4.2 Determination of critical impeller speed in three-phase baffled tank (a) three-phase baffled tank (b) two-phase baffled tank (c) three-phase unbaffled tank (d) two-phase unbaffled tank

In these figures, critical impeller speed is the speed at which $H_B/H$ becomes zero. It is evident that the $H_B/H$ ratio increased with decrease in impeller speed. This method has exhibited reliable results for the determination of critical impeller speed in previous

studies on hydrodynamics of systems involving high solids concentrations (Wu et al., 2010a) (Wang et al., 2012) (Wang et al., 2014).

### 4.2.3 Effect of solids concentration on specific power input in two-phase system

The impeller power input required to just suspend particles off the tank bottom on the basis of unit slurry volume ($P_{js}/V$) is plotted against solids concentration $C_v$ (v/v) in Figure 4.3 for three impellers with different power numbers.

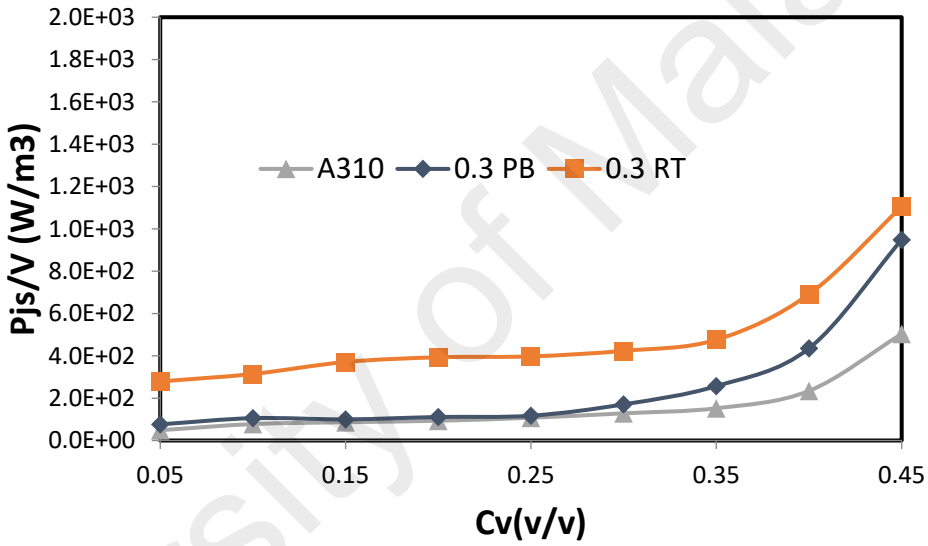


Figure 4.3 Effect of solids concentration on specific impeller power input in solid-liquid system

It was observed that $P_{js}/V$ gradually increased with an increase in solids concentration up to $C_v$ =0.3, after which it started to increase rapidly with solid loading. As explained earlier, it is possible to express the impeller power consumption based on $M_s$ ($\varepsilon_{js}$). Figure 4.4 presents the values of $\varepsilon_{js}$ for the 0.3 RT impeller and compares it with the specific power input based on the liquid volume.

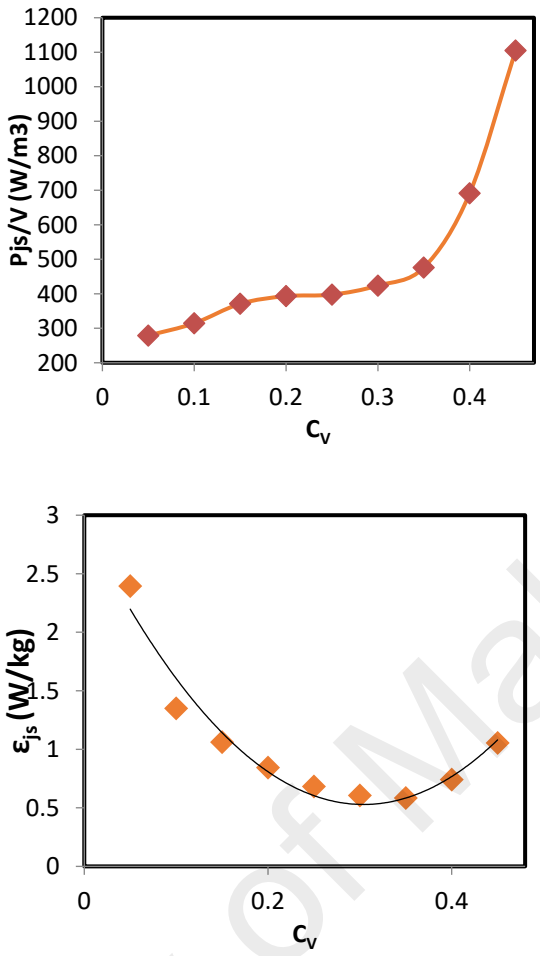


Figure 4.4 Effect of solids concentration on specific power input based on (a) liquid volume and (b) mass of suspended solids

Contrary to ($P_{js}/V$), $\varepsilon_{js}$ tends to decrease with an increase in solids concentration up to a certain point and then starts to increase. A skewed U-shape trend can be found for $\varepsilon_{js}$ as a function of $C_v$. The optimum value, which corresponds to the minimum specific power input, is identified as 35% for this particular mixing system. This $C_v$ for the optimum solids concentration is denoted as $(C_v)_{OSC}$ and it reflects the condition at which the energy supplied by the impeller rotation is utilized most efficiently. Figure 4.5 provides plots of $\varepsilon_{js}$ vs $C_v$ for all the impellers studied in this work.

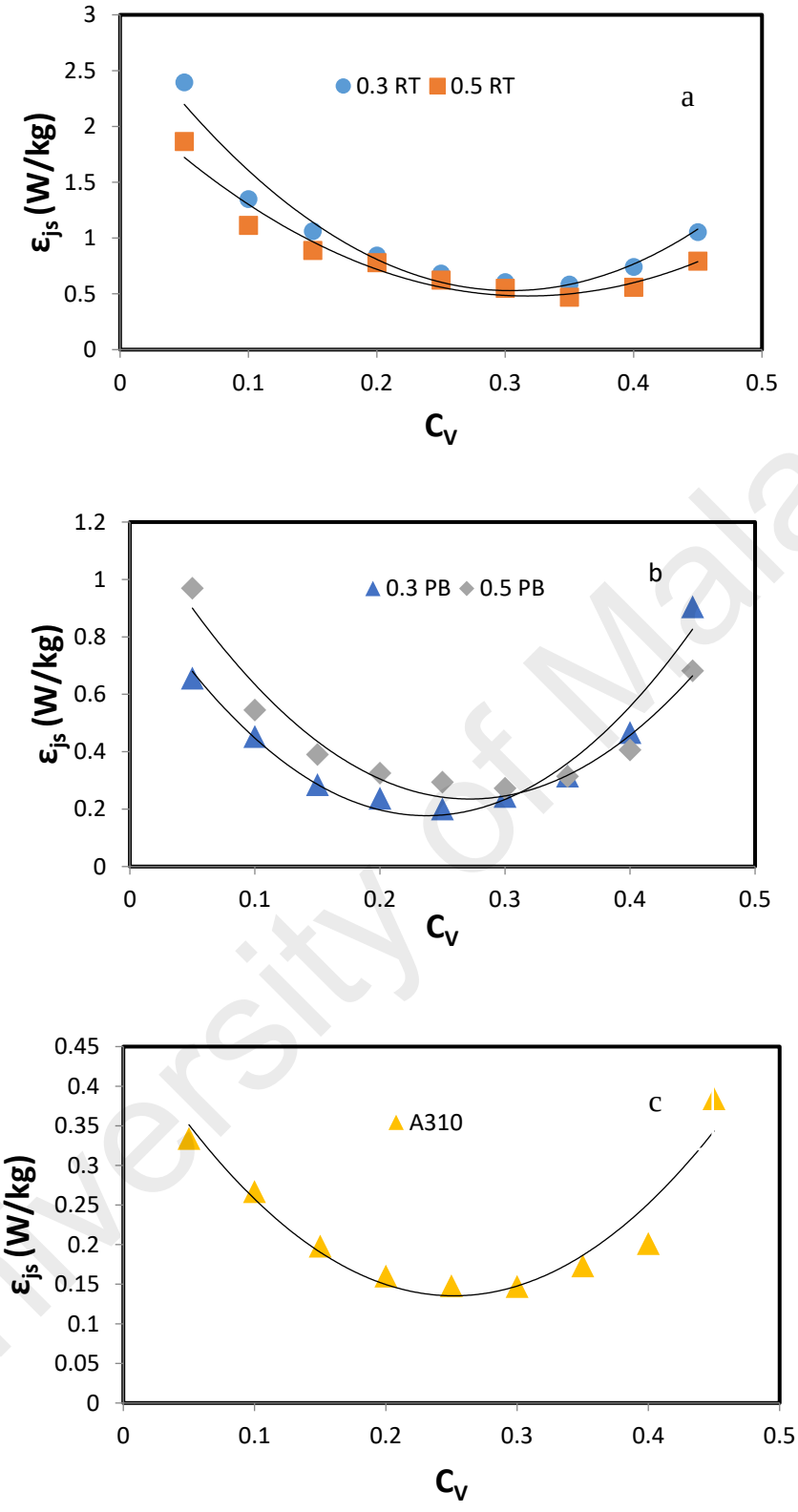


Figure 4.5 Effect of solids concentration on specific power input based mass of suspended solids for five impellers

It was obvious that all five impellers exhibited the same behavior, and consequently, there is a particular $C_v$ at which the supplied energy by the impeller was consumed the most efficiently. It was also evident that radial- and axial-flow impellers consumed the most and the least amount of energy for suspending 1 kg of solids respectively. According to Figure 4.5a, smaller RT impeller consumed more power per unit of suspended solids compared to the 0.5 RT impeller at any given solid loading. The opposite behavior was shown by the PB impeller (Figure 4.5b) at $0.05 < C_v < 0.3$ as the $\varepsilon_{js}$ values of the larger impeller were higher compared to those of the smaller impellers. Similar behaviour was observed by Ibrahim and Niewnow (1996) who explained that smaller RT impeller was less energy efficient in the presence of 5% (v/v) solids as it required higher speed and more energy to produce more flow per unit time to compensate for low volumetric discharge due to the large space between the blade tip and the wall that is filled by fluid. As for the PB impeller, the proportion of solids which remained deposited at the centre was higher with a larger impeller while the maximum flow was observed at the blade tip, which was further from the centre. The maximum flow from the PB impeller with smaller D/T was closer to the centre, hence it could sweep more solids to the sides. It could therefore be concluded that less additional energy was needed to lift the sedimentated solids from the sides when a smaller PB impeller was used compared to trying to overcome the central sedimentation with a larger impeller. According to our observations, at solids concentrations higher than 0.3, the larger mixed flow impeller operated more efficiently.

In summary, in terms of power efficiency in solid-liquid systems, these five impellers can be ranked in the following order from the most efficient to the least.

A310 > 0.3 PB > 0.5 PB > 0.5 RT > 0.3 RT

It is interesting to observe that impeller diameter has different impacts on power efficiency performance of radial- and mixed-flow impellers in solid-liquid systems.

### 4.2.4 Power efficiency factor

In order to provide a clearer picture of the improved impeller energy efficiency due to increased solids concentration, the inverse of $\varepsilon_{jsg}$ ($= \varepsilon_{jsg}^{-1}$) values was plotted against $C_v$ in Figure 4.6. $\varepsilon_{jsg}^{-1}$ (kg/W) represents the amount of solids that can be suspended per unit of impeller power input at just suspended conditions and is regarded as power efficiency factor.

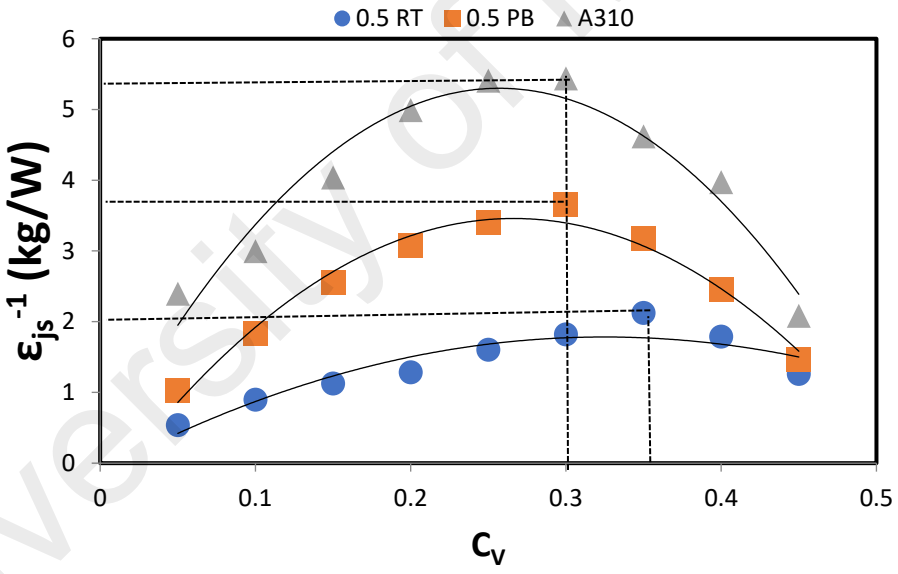


Figure 4.6 Values of power efficiency factor against solids concentration for three types of impellers in a solid-liquid baffled tank

It was observed that at any given solid loading, the hydrofoil impeller could suspend more solids compared to the other two impellers. At $C_v$ = 0.3, A310 impeller was able to suspend 5.43 kg of solids per one Watt of power, while the same amount of energy led to suspension of only 3.66 and 1.81 kg of solids when the tank was agitated by 0.5 PB and

0.5 RT impellers, respectively. Table 4.2 lists the values of power efficiency factor for five impellers operating at two different solid concentrations (dilute and optimum).

Table 4.2 Optimum solids concentrations in solid-liquid systems

| Impeller | $(C_v)_{OSC}$ | Power efficiency factor |
|---|---|---|
| 0.3 RT | 0.35* | 1.71 |
| | 0.05 | 0.41 |
| 0.5 RT | 0.35* | 2.12 |
| | 0.05 | 0.53 |
| 0.3 PB | 0.25* | 4.95 |
| | 0.05 | 1.52 |
| 0.5 PB | 0.3* | 3.66 |
| | 0.05 | 1.03 |
| A310 | 0.3* | 5.43 |
| | 0.05 | 2.5 |

* indicates this value is $(C_v)_{OSC}$

According to the data listed in Table 4.2, when 0.3 PB impeller was operating at $(C_v)_{OSC}$, for each Watt of power, the impellers was able to lift 4.95 kg of solids, while the same amount of energy only suspended 1.52 kg of solids at $C_v = 0.05$. The same comparison was made among the four impellers. With respect to the values of power efficiency factor, it could be concluded that the axial and mixed-flow impellers were more energy efficient compared to the radial flow impellers when the baffles were installed.

### 4.2.5 Validation of results in two-phase system

Recently, Wang et al (2014) proposed the following mathematical correlation for the determination of $\varepsilon_{js}$ in solid-liquid agitated systems:

$$\varepsilon_{js} = \left( \frac{Sd^{0.2}\left(\frac{g\Delta\rho}{\rho_l}\right)^{0.45}}{D^{0.85}} \right)^3 \left(\frac{N_P \rho_w D^5}{V\rho_s}\right) \left(\frac{100 C_v \rho_s}{(1-C_v)\rho_w}\right)^{0.39} \left(\frac{1}{C_v} + k\right) \upsilon^{0.3} \quad \textbf{4-2}$$

where $\varepsilon_{js}$ is specific energy dissipation rate (W/kg), $\rho_l$ is liquid density (kg/m$^3$), $\rho_w$ is density of water (kg/m$^3$), $\rho_s$ is solid density (kg/m$^3$), $\Delta\rho$ is the difference between liquid and solid densities (kg/m$^3$), d is particle diameter (m), D is impeller diameter (m), S is a dimensional coefficient which depends on impeller geometry, $\upsilon$ is kinematic viscosity (m$^2$s$^{-1}$), V is total volume of the liquid, $C_v$ is volumetric solids concentration (v/v), and k is a coefficient that represents a measure of the energy dissipation due by the particles.

Equation 4-2 was used to estimate $\varepsilon_{js}$ values for the solid-liquid system used in this work. Figure 4.7 compares the experimental data obtained for solid-liquid systems used in this work with the values predicted by equation 4-2. Reasonable agreement was found between them with a correlation coefficient of 0.89.

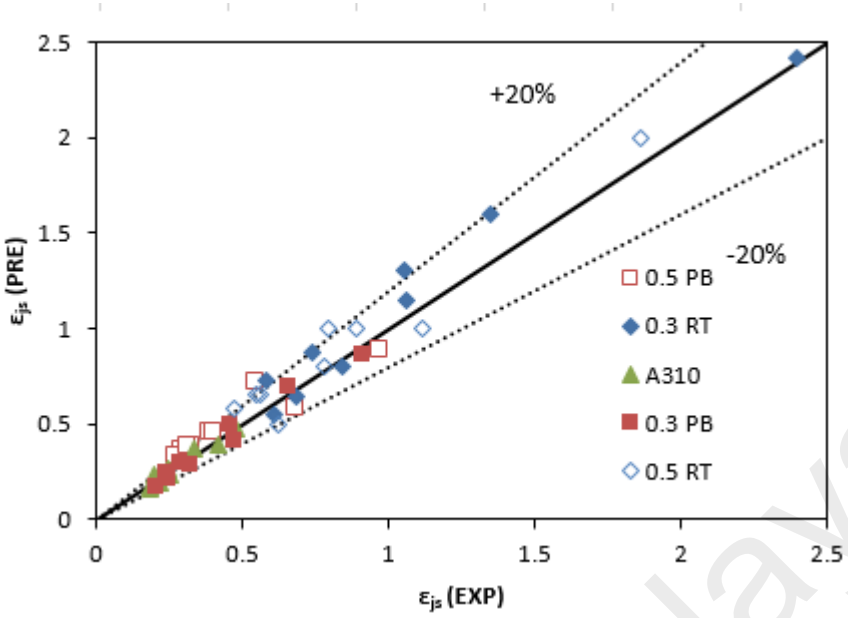


Figure 4.7 Comparison of experimental data for solid-liquid systems and the values predicted by equation 4-2 using a = 0.13, S = 4.39, k = 1.169, 1.315, 2.795, 2.227, 2.44 for A310, 0.5 PB, 0.3RT, 0.3PB, and 0.5 RT impellers, respectively

### 4.2.6 Gas-solid-liquid

In the next stage of the study all experiments were repeated in presence of gas to have a better understanding of how introduction of gas and gas rating can influence suspension of solids in multi-phase stirred tanks.

#### 4.2.6.1 Relations between $N_{js}$ and $N_{jsg}$

All $N_{js}$ and $\varepsilon_{js}$ experiments carried out in solid-liquid systems were repeated in the presence of gas using flow rates of 0.5, 0.75, and 1 vvm. The results for three phase experiments are presented in the following sections.

It is generally accepted that at a given agitation speed, introduction of gas leads to immediate loss of suspension of solids. Warmoeskerken et al. (1984) explained that the gas cavities formed behind the impeller blades lowers its pumping capacity up to a point

that the circulated flow was unable to keep the particles in suspension. Consequently, the impeller speed should be increased to achieve off-bottom solids suspension.

Nienow and Bujalski (2002) developed two correlations for the determination of $N_{jsg}$ for down-pumping (equation 4-3) and radial flow impellers (equation 4-4) based on gas hold-up:

$$N_{jsg} = N_{js}\left(0.83 + 0.31Q_g\right) \quad \textbf{4-3}$$

$$N_{jsg} = N_{js} + 0.85Q_g \quad \textbf{4-4}$$

Figure 4.8 compares the experimental results from this work with those estimated using Equations 4-3, and 4-4.

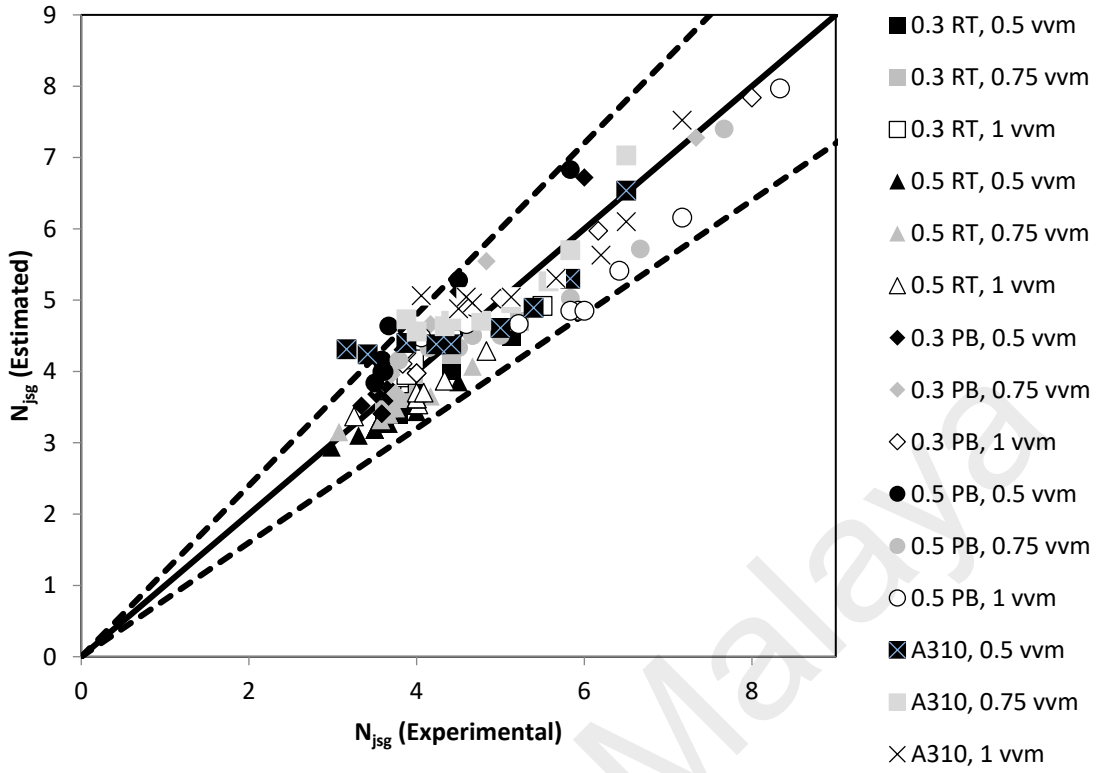


Figure 4.8 Comparison of Njsg experimental results and the estimations of Equations 4-3 and 4-4

Estimations of both equations fit the experimental results satisfactorily. Considering their acceptable accuracy, these equations were used in this work to develop a mathematical correlation for estimating $\varepsilon_{jsg}$ for the systems studied.

#### 4.2.6.2 Effect of impeller type and diameter

Five different impellers were used during experiments in order to study the effect of impeller type and diameter on specific power consumption. Results are discussed in the following sections.

#### 4.2.6.2.1 Normal mixed-flow impeller

The specific power input for 0.3 PB impeller based on the mass of the total suspended solids in the absence and presence of gas are shown as a function of the solids volume fraction in Figure 4.9. To provide a clearer picture of the improved impeller power efficiency, the inverse of $\varepsilon_{jsg}$ ($= \varepsilon_{jsg}^{-1}$) values are plotted versus $C_v$ in Figure 4.10. $\varepsilon_{jsg}^{-1}$ (kg/W) represents the amount of solids that can be suspended per unit of impeller power input at just suspended conditions, and is regarded as power efficiency factor.

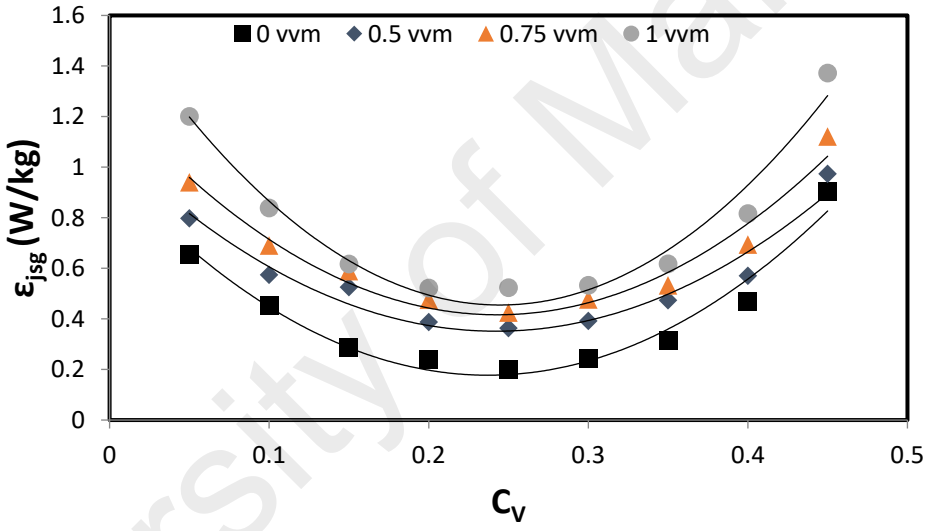


Figure 4.9 Effect of solids concentration on εjsg of 0.3 PB in the presence and absence of gas

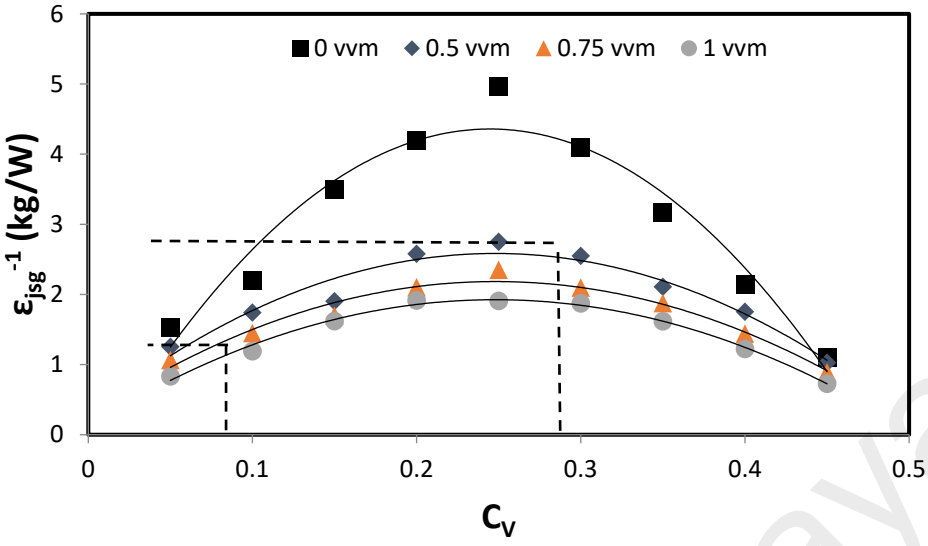


Figure 4.10 Effect of solids concentration on εjsg-1 for 0.3 PB in the presence and absence of gas

The $\varepsilon_{jsg}$ value for all $C_v$ increases with the introduction of gas (Figure 4.9). Also, $\varepsilon_{jsg}$ for a given $C_v$ increases with an increase in gas flow rate. As the solid concentration increases, impeller power efficiency increases up to a certain point ($(C_v)_{OSC}$), after which it starts decreasing (Figure 4.10). The mass of solids that can be suspended per unit Watt for a given $C_v$ decreases with increasing gas flow rate. For instance, for one unit Watt of power input at solids concentration of 0.1 (v/v), the amounts of solids that can be suspended are 2.2, 1.7, 1.44, and 1.23 kg for 0, 0.5, 0.75, and 1 vvm, respectively. It is interesting to see that for each Watt of power input at $Q_g$ = 0.5 vvm, 2.75 kg of solids could be suspended at $C_v$ = 0.25, while only 1.25 kg solids could be suspended at $C_v$ = 0.05. Therefore, similar to solid-liquid systems, it is possible to define an optimum solids concentration for three-phase systems at which the energy supplied by impeller rotation is consumed most efficiently.

#### 4.2.6.2.2 Large mixed-flow impeller

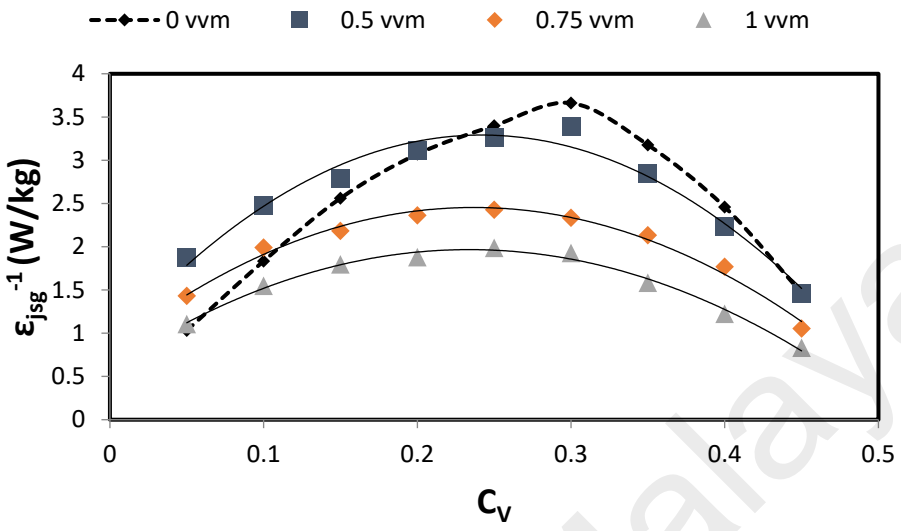


Figure 4.11 Variations of εjsg-1 values with solids concentration in various gas flow rates

A plot of $\varepsilon_{jsg}^{-1}$ versus $C_v$ for the 0.5 PB impeller shown in Figure 4.11 reveals a rather interesting behaviour. The operations under aerated condition are generally more energy efficient compared to that under unaerated condition (0 vvm). For example, 1.83 kg of solids per Watt could be suspended under unaerated condition at $C_v$ = 0.1. However, 2.46 kg of solids per Watt could be suspended at 0.5 vvm for the same $C_v$. This increase in power efficiency gradually diminishes either with an increase in gas flow rate or solids loading, especially above 20% (v/v). Similar trend was observed by Nienow et al. (1986) who reported that the presence of a small number of gas bubbles caused turbulence at the tank bottom leading to better suspension, especially just below the impeller, which is a problematic area for PB impeller under unaerated condition. In their study, Nienow et al. (1986) used a flat-bottom tank equipped with a 0.5 PB impeller and loaded with 5% (v/v) of solids. Our study indicates that the enhanced power efficiency in three phase system is dependent on the gas flow rate and solids loading. The three-phase system is more energy efficient at gas flow rates of 0.5, 0.75, and 1 vvm compared to the solid-liquid system

below $C_v$ = 0.21, 0.12, and 0.6 v/v, respectively. Figure 4.12 and Table 4.3 present the details of the effect of gas flow rate on $\varepsilon_{jsg}^{-1}$ for 0.5 PB impeller.

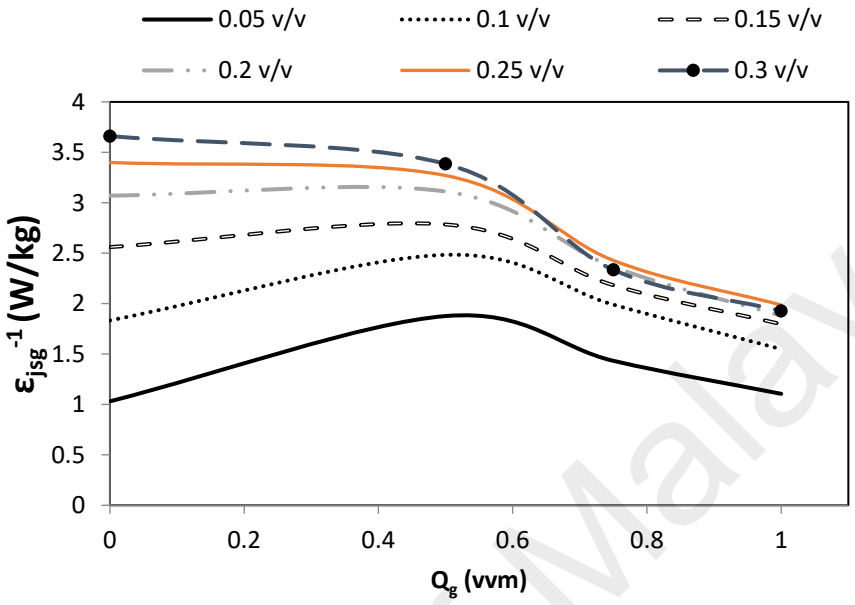


Figure 4.12 Variation of ($\varepsilon_{jsg}^{-1}$) values for 0.5 PB impeller with gas flow rate for different solids concentrations

Table 4.3 Selected data from Figure 4-12

| **$C_v$ (v/v)** | **$Q_g$ (vvm)** | **Mass of the suspended solids per unit power input (kg/W)** |
|---|---|---|
| 0.05 | 0.5 | 1.87 |
| 0.05 | 0 | 1.03 |
| 0.3 | 0.5 | 3.38 |
| 0.3 | 0 | 3.66 |

Figure 4.12 shows $\varepsilon_{jsg}^{-1}$ values as a function of gas flow rate at different solids concentrations for 0.5 PB impeller. As solid concentration increases, $\varepsilon_{jsg}^{-1}$ value at 0 vvm

increases confirming that impeller power efficiency is higher under unaerated conditions and at higher solids loadings. It is also interesting to notice that the curve for $C_v$ = 0.3 is below the curve for $C_v$ = 0.25 for gas flow rates higher than 0.5 vvm. It indicates that impeller power efficiency of three-phase system is higher at $C_v$ = 0.25 compared to $C_v$ = 0.3 for gas flow rates above 0.5 vvm, which is in agreement with the observation from Figure 4.12.

The data shown in Table 4.3 further illustrate the relationship between the gas flow rate, solids concentration and $\varepsilon_{jsg}^{-1}$ values for 0.5 PB impeller. Aeration improves the impeller power efficiency at $C_v$ = 0.05, but leads to an opposite result for $C_v$ = 0.3. It can be therefore concluded that the impeller power efficiency is higher with higher solid loadings in both aerated and unaerated systems. Moreover, the difference in $\varepsilon_{jsg}^{-1}$ values between aerated and unaerated conditions becomes smaller as $C_v$ increases (Figure 4.12).

#### 4.2.6.2.3 Normal radial-flow impeller

The experimental $\varepsilon_{jsg}^{-1}$ results for 0.3 RT impeller are shown in Figure 4.13a as a function of $C_v$. Although the curves for aerated conditions are inverse U-shaped and a maximum value could be identified in them, it is clear that the $\varepsilon_{jsg}^{-1}$ values for this impeller are almost independent of gas flow rate up to $C_v$ = 0.25, and varies above this $C_v$. The highest $\varepsilon_{jsg}^{-1}$ value is obtained at $C_v$ = 0.3 regardless of the aeration rate. Also, the curves for 0.5 and 0.75 vvm are close to each other up to $C_v$ = 0.3 v/v. At $C_v$ = 0.3, the impeller starts to exhibit sensitivity to gassing rate. This phenomenon starts from a lower $C_v$ for the case of 1 vvm. Rewatkar and Joshi (1991) reported that, in gas-liquid systems, where sparger was larger than the impeller, the gas was not easily captured by the impeller thereby leading to the disruption of trailing gas cavity formation, growth, and break-up. They mentioned that the agitation speed should be increased significantly before any noticeable

change in the gas flow patterns could be observed. In three-phase systems, an increase in impeller speed to improve gas dispersion will lead to suspension homogeneity (Figure 2.2d). For the sake of comparison, experimental $\varepsilon_{js}^{-1}$ results for unaerated system are shown with those for aerated system in Figure 4.13b. It is obvious that operating the RT impeller under unaerated condition leads to significantly higher power efficiency.

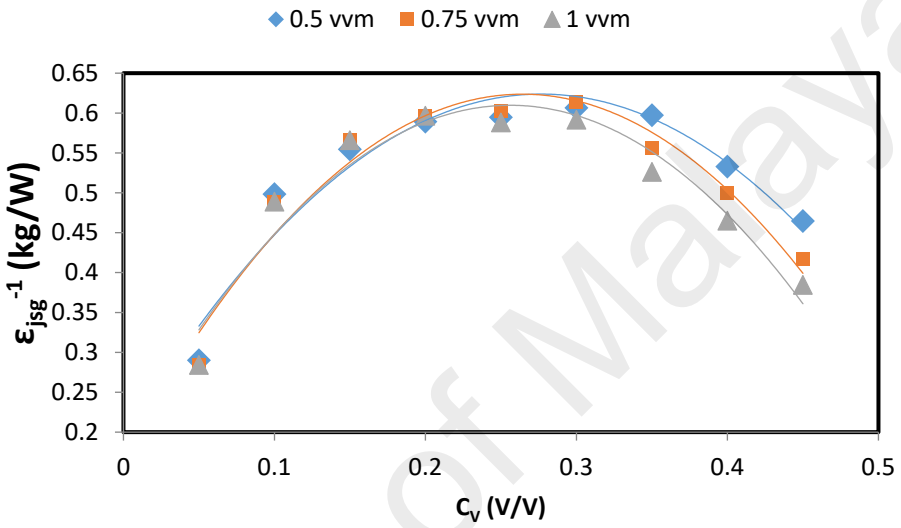


(a)

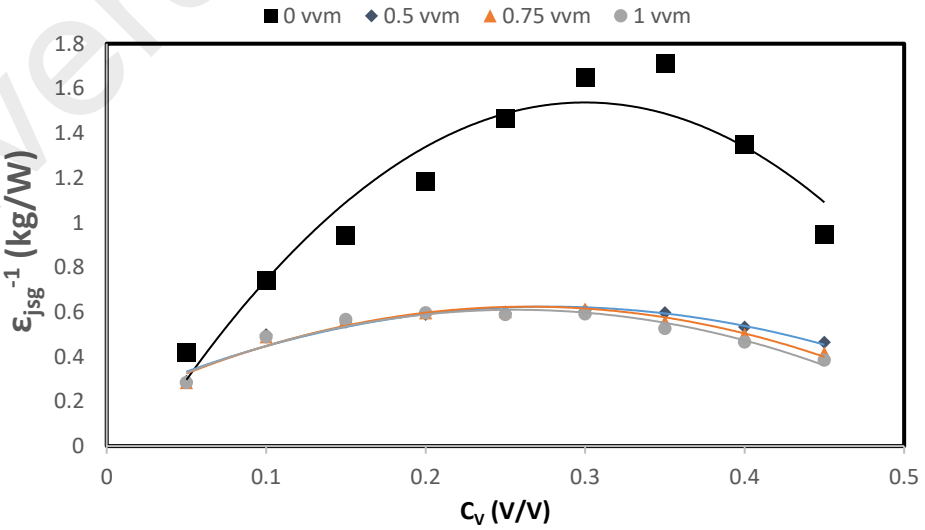


(b)

Figure 4.13 Variations of εjsg-1 values with solids concentration for 0.3 RT impeller (a) aerated system (b) aerated and unaerated systems

#### 4.2.6.2.4 Large radial-flow impeller

Figure 4.14 shows $\varepsilon_{jsg}^{-1}$ values for 0.5 RT impeller as a function of $C_v$ at different gas flow rates. The 0.5 RT impeller is able to suspend more solids per unit of power compared to 0.3 RT impeller. Comparing the data shown in Figures 4.13a and 4-14, at $C_v$ = 0.2, 0.59 kg of solids is suspended per unit Watt by 0.3 RT impeller whereas 0.68 to 0.93 kg solids is suspended per unit Watt by 0.5 RT impeller depending on the gas flow rate. Unlike the case with 0.3 RT impeller, gas flow rate has noticeable effect on $\varepsilon_{jsg}^{-1}$ value for 0.5 RT impeller starting from low solids concentrations.

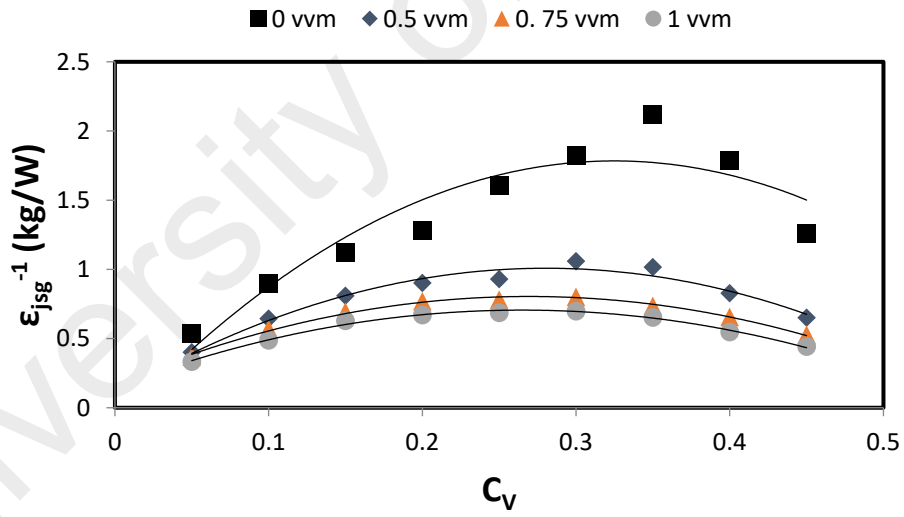


Figure 4.14 Effect of solids concentration on εjsg-1 for 0.5 RT under unaerated and aerated conditions

#### 4.2.6.2.5 Axial flow impeller

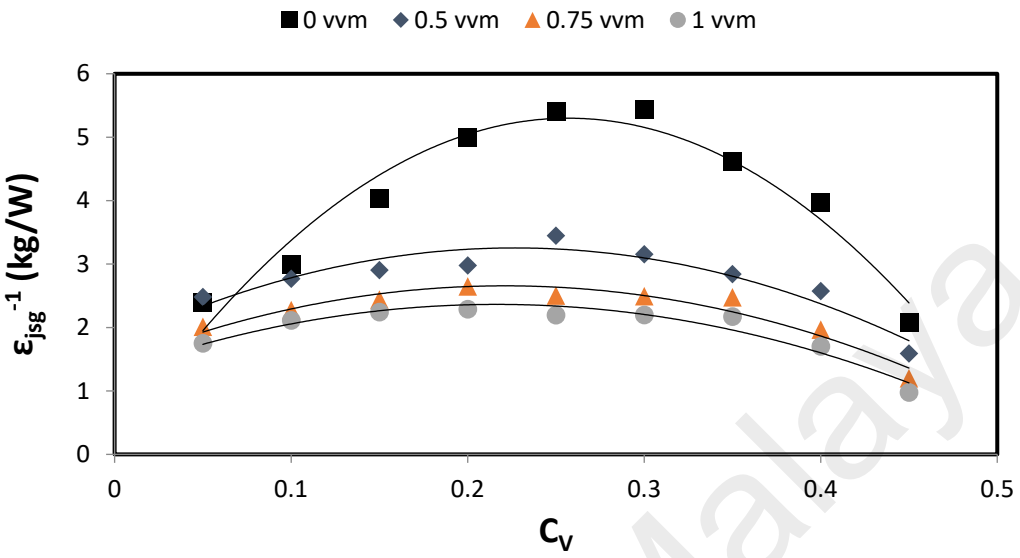


Figure 4.15 Effect of solids concentration on εjsg-1 of A310 under unaerated and aerated conditions

The $\varepsilon_{jsg}^{-1}$ results obtained with an A310 impeller are shown in Figure 4.15 as a function of $C_v$. The results for A310 are similar to those for 0.3 PB impeller shown in Figure 4.10. Both impellers exhibited unstable operating conditions and experienced high torque fluctuations, which could be attributed to low number of blades for A310 and small D/T ratio for the 0.3 PB impeller. Shaliza and Nienow (2009) observed similar phenomena at low solids concentration and explained that the formation of large cavities at high gassing rates made the gas dispersion asymmetric.

### 4.2.6.3 Effect of aeration on $C_{v\,(OSC)}$ in three-phase systems

In this section, the optimum solid concentrations for radial-, mixed-, and axial-flow impellers under aerated conditions are compared to understand the effect of aeration rates on power efficiency of these impellers. The results are shown in Table 4.4.

Table 4.4 Optimum solids concentrations in three-phase mixing systems

| Impeller | 0.3 PB | | | 0.5 PB | | | 0.3 RT | | | 0.5 RT | | | A310 | | |
|---|---|---|---|---|---|---|---|---|---|---|---|---|---|---|---|
| Aeration rate (vvm) | 0.5 | 0.75 | 1 | 0.5 | 0.75 | 1 | 0.5 | 0.75 | 1 | 0.5 | 0.75 | 1 | 0.5 | 0.75 | 1 |
| $C_{v\ (OSC)}$ | 0.25 | 0.25 | 0.25-0.2 | 0.3 | 0.25 | 0.25 | 0.3 | 0.3 | 0.3 | 0.3 | 0.3 | 0.3 | 0.25 | 0.2 | 0.2 |
| Corresponding $\varepsilon_{jsg}^{-1}$ value | 2.75 | 2.35 | 1.91 | 3.38 | 2.42 | 1.98 | 0.61 | 0.61 | 0.59 | 1.05 | 0.8 | 0.69 | 3.44 | 2.64 | 2.3 |

For A310, $(C_v)_{OSC}$ decreases from 0.25 to 0.2 when $Q_g$ increases from 0.5 to 1 indicating A310 loses its ability to suspend solids gradually with increasing gas flow rate. In case of PB impellers, the larger diameter 0.5PB impeller exhibits better gas dispersion ability compared to 0.3 PB impeller. Conversely, $(C_v)_{OSC}$ values for RT impellers are found to be independent of gassing rate and impeller diameter.

Among the impellers studied, 0.5 PB and 0.5 RT impellers exhibit both higher $(C_v)_{OSC}$ and $\varepsilon_{jsg}^{-1}$ values (Table 4.4). However, $\varepsilon_{jsg}^{-1}$ value for 0.5 PB impeller is higher than that of 0.5 RT impeller at all gas flow rates studied indicting its better gas dispersion and solids suspension abilities in three-phase systems. The $(C_v)_{OSC}$ values for 0.3 PB impeller and A310 are similar under aerated conditions. Both impellers exhibited poor gas dispersion ability especially at high solids loading leading to high torque fluctuations and impeller shaft instability, which could potentially lead to structural and motor damage.

Based on $(C_v)_{OSC}$ and $\varepsilon_{jsg}^{-1}$ data shown in Table 4.4, the five impellers used in this work could be ranked in descending order in terms of their ability to handle high solids loading under aerated conditions: 0.5 PB, 0.5 RT , 0.3 RT, A310 and 0.3PB. Although 0.3 RT impeller leads to lower $\varepsilon_{jsg}^{-1}$ values compared to A310 and 0.3 PB impellers at all gas flow rates used, its performance and stability under gassed condition at high solid loadings makes it as a preferable impeller compared to A310 and 0.3PB. By comparing this order with the one suggested above for two-phase systems, it can be concluded that the introduction of gas to stirred vessels with high solids concentration would predominantly influence the power drawn by impellers to achieve off-bottom solids suspension. Moreover, the range of $(C_v)_{OSC}$ in three-phase systems is 0.2 - 0.3 (v/v), which is lower compared to 0.2-0.35 (v/v) for two-phase systems.

Figure 4.16 compares the $\varepsilon_{jsg}^{-1}$ data for all five impellers as a function of gas flow rate for $C_v$ of 0.5, 0.25, and 0.4. In all three solid concentrations, A310 has the highest values

of power efficiency factor and 0.5 PB impeller has higher $\varepsilon_{jsg}^{-1}$ value compared to 0.5 RT and 0.3 RT impellers at any given gas flow rate. In addition, at $C_v$ = 0.05 and 0.25, the 0.3 PB impeller is more efficient compared to 0.5 PB impeller under unaerated condition. However, under aerated condition ($Q_g \geq 0.5$ vvm), the 0.5 PB impeller has higher values of power efficiency factor. From practical point of view, these three solid concentrations represent three different suspension regimes. At any gas flow rate, all five impellers exhibit the highest $\varepsilon_{jsg}^{-1}$ values around the optimum suspension region ($C_v$ = 0.25) indicating that the power drawn by the impeller could be efficiently used if the tank is operating with $(C_v)_{OSC}$.

The $\varepsilon_{jsg}^{-1}$ vs $C_v$ plots indicate that operating the mixing tanks at higher solids concentration than the ones that are currently handled is advantageous. The $(C_v)_{OSC}$ that corresponds to the highest $\varepsilon_{jsg}^{-1}$ value has practical implications to the design and operation of two- and three-phase mixing vessels. Any three-phase mixing tank that is designed and operated in accordance with the criteria described in this work could lead to a reduction in the operating cost and increase in impeller power efficiency without any major modifications to the operating plant.

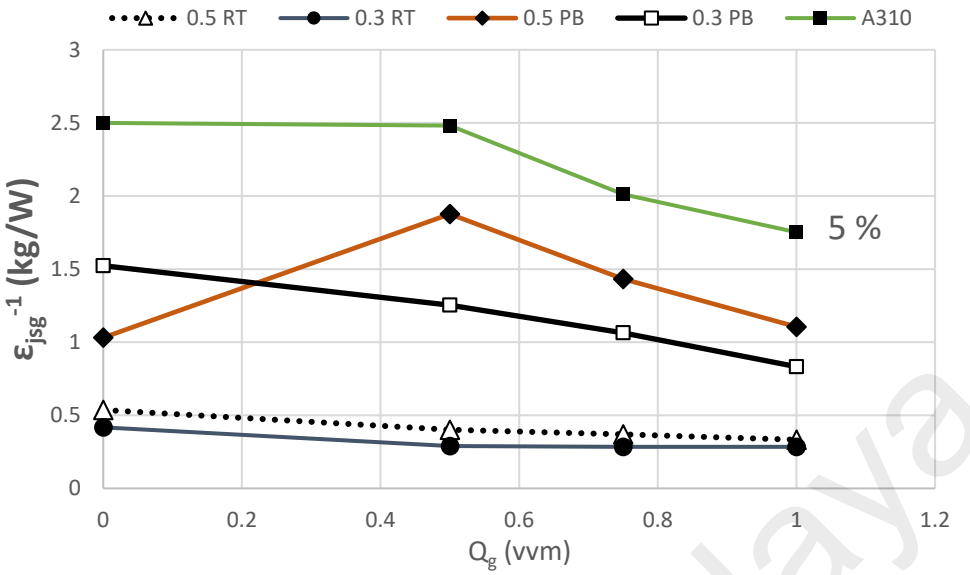


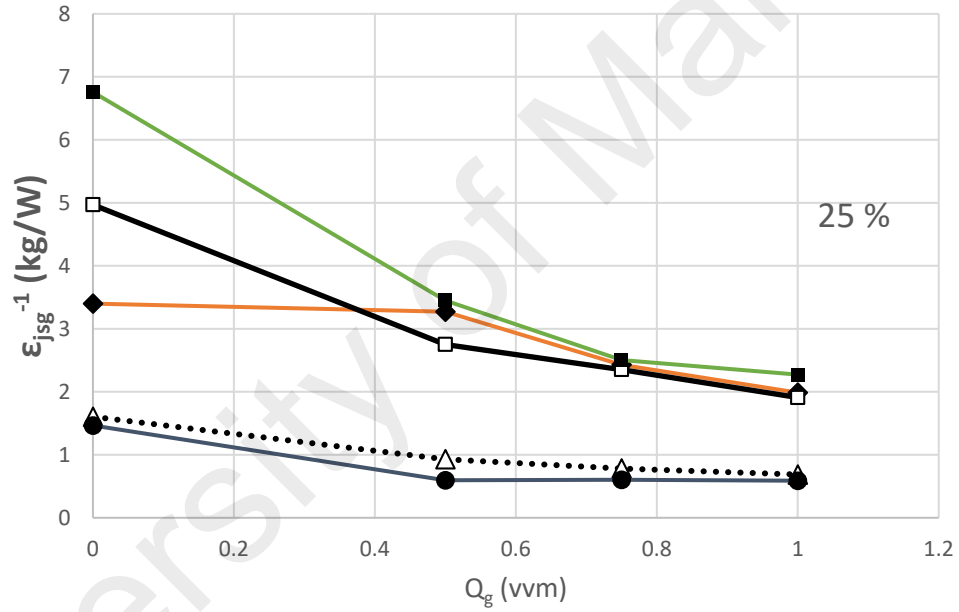


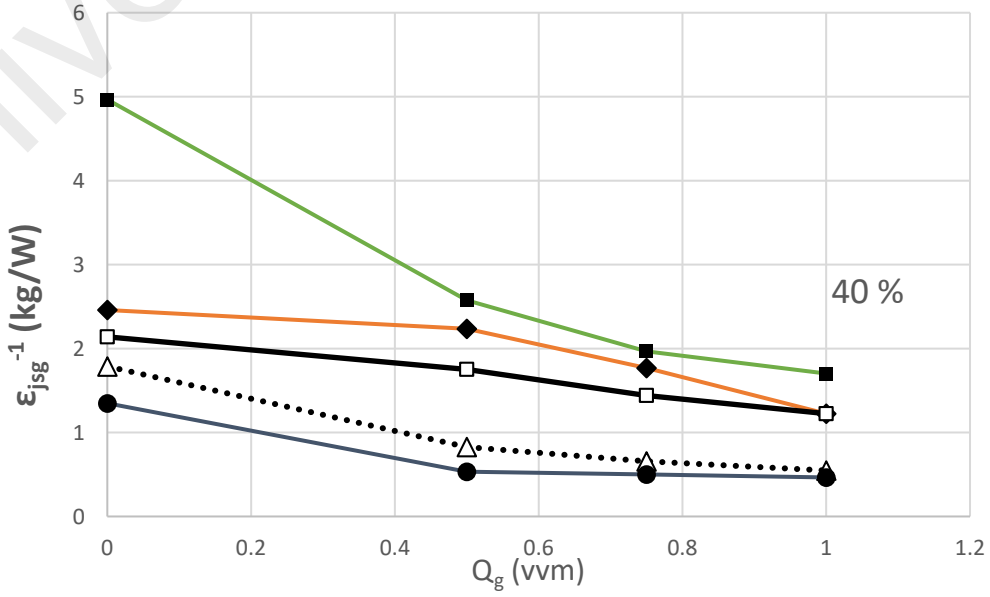

Figure 4.16 Performance of impellers in three suspension regions as a function of Qg

In summary, a mixing tank that is operating at low solid concentrations, as practised in many industries nowadays, is basically underutilised in terms of impeller power efficiency, and its operating cost could be excessively higher due to poor/insufficient usage of the infrastructure. Accordingly, a three-phase mixing system operating within the solids concentration ranges of 0.05 to 0.15, 0.2 to 0.30, and 0.35 to 0.45 can be designated as 'underperforming, 'optimal', and 'overperforming', respectively. It is also noteworthy that mixing intensification, which remarkably enhances the throughput, is not feasible for stirred tanks operating at low/dilute solids concentrations.

### 4.2.7 Effect of baffling configuration on power efficiency factor

It has been reported that significant savings can be achieved by simply removing baffles in solid-liquid stirred tanks. Experiments were carried out in this work to study the effect of baffle removal on power efficiency factor of various impellers in absence and presence of gas. Obtained results are discussed in the following sections.

#### 4.2.7.1 Solid-liquid system

The experiments were repeated under unbaffled configuration to investigate the effect of baffle removal on values of power efficiency factor. Figure 4.17 exhibits the graphs of $C_v$ vs $\varepsilon_{js}^{-1}$ for three impellers of 0.5 RT, 0.5 PB, and A310 operating in a solid-liquid tank.

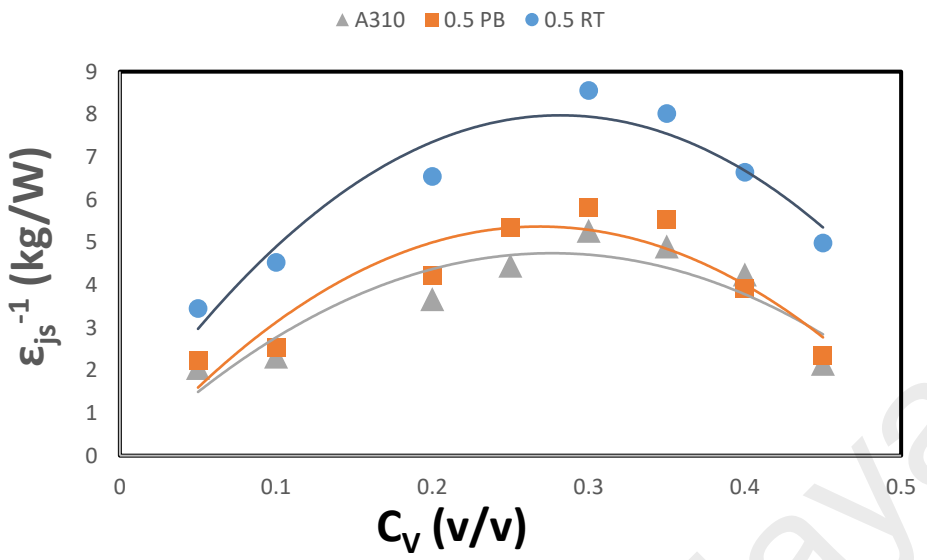


Figure 4.17 Values of power efficiency factor against solids concentration under unbaffled condition

The obtained values revealed three significant findings: i) similar to baffled condition, all impellers exhibited the inverse U-shaped graphs when they were operating in unbaffled tanks; ii) contrary to baffled condition, the values of $\varepsilon_{jsg}^{-1}$ for radial-flow impeller were higher compared to those of axial- and mixed-flow impellers in an unbaffled tank; and iii) in terms of contribution to energy efficiency, removal of baffles had different impacts on impellers' performances.

In order to better study the effect of baffle removal on efficiency of various impellers, a term defined as baffling efficiency factor, R, was used which indicates the percentage of improvement in the values of impeller's energy efficiency factor upon removal of baffles. High values of R reflects significant improvement in energy efficiency of an impeller if the tank is running under unbaffled condition. Values of R were determined using this equation:

$$R = \frac{\Delta \boldsymbol{\varepsilon_{js}^{-1}}}{\varepsilon_{js\,(unbaffled)}^{-1}} = \frac{\varepsilon_{js\,(unbaffled)}^{-1} - \varepsilon_{js\,(baffled)}^{-1}}{\varepsilon_{js\,(unbaffled)}^{-1}} \times 100 \qquad \textbf{4-5}$$

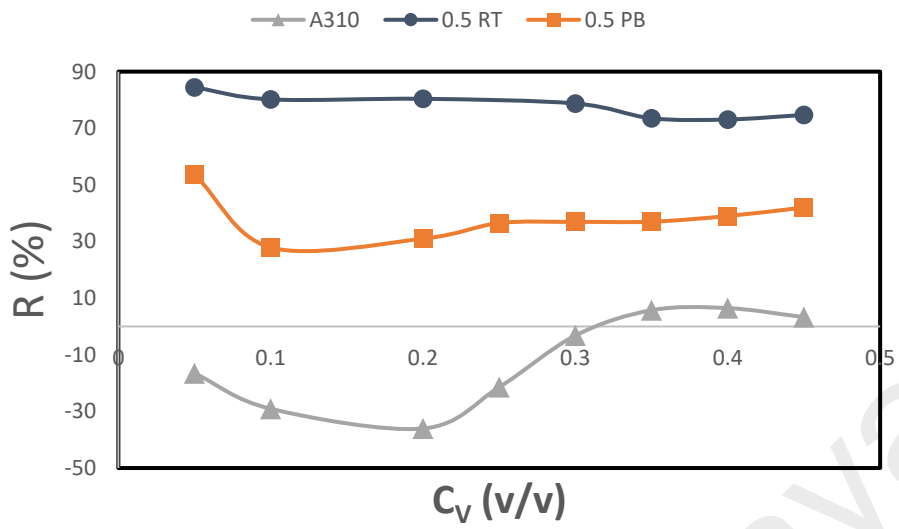


Figure 4.18 Values of baffling efficiency factor for different impellers under various solids concentrations in solid-liquid system

Figure 4.18 presents the values of baffling efficiency factor for A310, 0.5 RT, and 0.5 PB impellers for a wide range of solid concentrations. It was observed that the radial impellers exhibited the highest values of R in all solid loadings. These high values were consistent and they tend to slightly decrease after $C_v$ = 0.3 v/v, which indicated that removal of baffles remarkably improved the efficiency of this impeller in stirred vessels and this advantage was almost independent of $C_v$. The R values of 0.5 PB impeller initially decreased by increasing $C_v$ from 0.05 to 0.1. After that, the R values started to gradually increase with solids concentration. The R values of A310 impeller, however, were found to be inconsistent. It was observed that removal of baffle could cause the axial impeller to suspend lower mass of solids for a given Watt. According to our results, removal of baffles improved the efficiency of A310 when the volumetric concentration of solids inside the vessel was more than $C_v$ = 0.32. When the tank was loaded with lower fraction of solids, removal of baffles led to higher consumption of power using A310 impeller. Therefore, it can be concluded that the order of impellers in terms of efficiency in baffled and unbaffled two-phase stirred tanks are reverse:

$$\left(\left(\varepsilon_{js}^{-1}\right)_{A310} > \left(\varepsilon_{js}^{-1}\right)_{0.5\,PB} > \left(\varepsilon_{js}^{-1}\right)_{0.5\,RT}\right)_{baffled} vs \left(\left(\varepsilon_{js}^{-1}\right)_{0.5\,RT} > \left(\varepsilon_{js}^{-1}\right)_{0.5\,PB} > \left(\varepsilon_{js}^{-1}\right)_{A310}\right)_{unbaffled}$$

### 4.2.8 Gas-solid-liquid system

The experiments were repeated in presence of gas to observe how baffle removal affects power efficiency of three different impellers operating under various aeration conditions.

#### 4.2.8.1 Radial-flow impeller

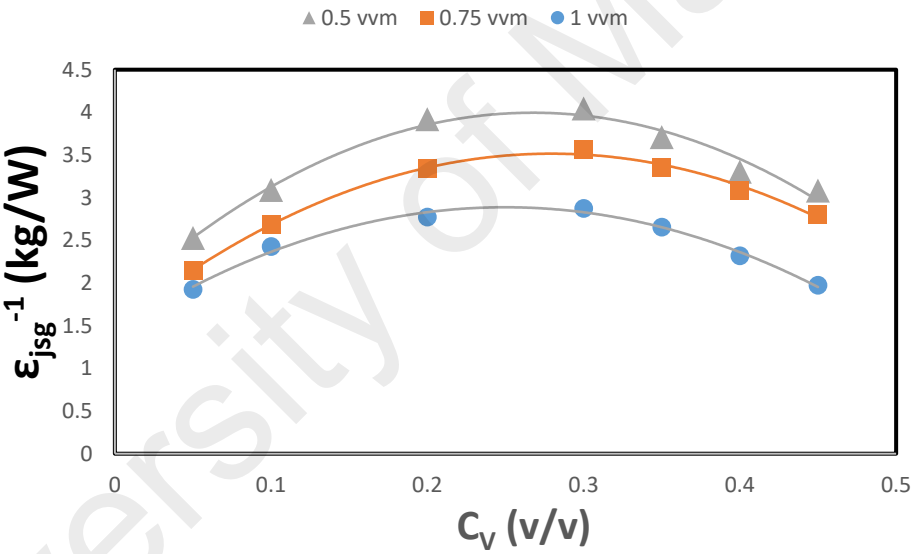


Figure 4.19 Effect of solids concentration on $\varepsilon_{jsg}^{-1}$ of 0.5 RT in presence and absence of gas under unbaffled condition

The experiments in the three-phase tank were repeated after removing the baffles and the obtained values for 0.5 RT are presented in Figure 4.19. 0.5 RT impeller exhibited the same behavior under unbaffled condition, where higher gassing rates resulted in lower values of $\varepsilon_{jsg}^{-1}$. It was found that the 0.5 RT impeller offered higher values of $\varepsilon_{jsg}^{-1}$ upon removal of baffles at any particular gas flow rate and solids concentration. A terms is

defined as baffling efficiency factor, R, which represents the amount of energy that can be saved by operating in unbaffled model. In Figure 4.20, values of R are plotted against $C_v$ to provide a better picture of the amount of energy that is saved by removing baffles in a three-phase stirred vessel agitated by a 0.5 RT impeller. For the sake of comparison, values of the two-phase system are also included.

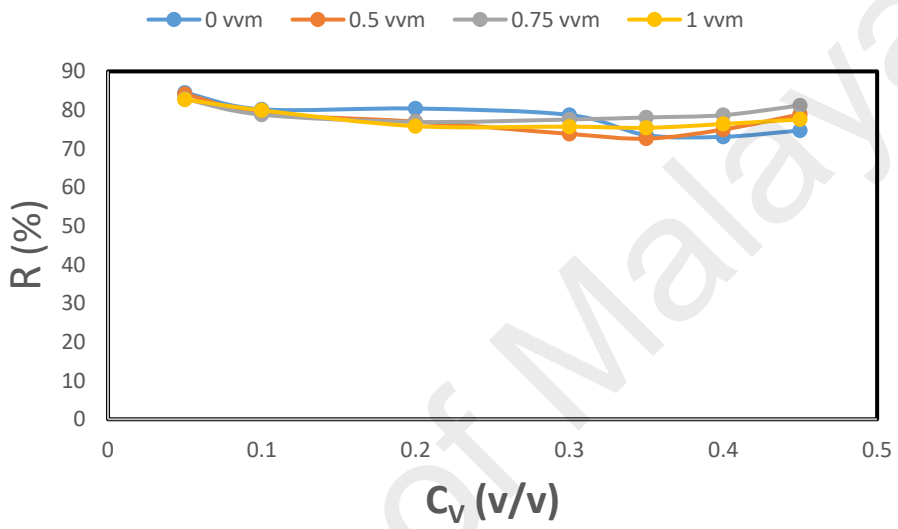


Figure 4.20 Values of baffling efficiency factor for 0.5 RT in absence and presence of gas

It was evident that removal of baffle tremendously enhanced the $(R)_{0.5\,RT}$ values and consequently improved the efficiency of this impeller in both the two- and three-phase systems. Table 4.5 lists the optimum solid concentrations and their corresponding power efficiency factor values in absence and presence of gas under two different baffling designs.

Table 4.5 Effect of baffling configuration on power efficiency of 0.5 RT

| **Gassing rate (vvm)** | **Baffled** | | **Unbaffled** | |
|---|---|---|---|---|
| | **$(C_v)_{OSC}$** | $\left(\varepsilon_{jsg}^{-1}\right)_{(C_v)osc}$ | **$(C_v)_{OSC}$** | $\left(\varepsilon_{jsg}^{-1}\right)_{(C_v)osc}$ |
| 0 | 0.35 | 2.12 | 0.3 | 8.55 |
| 0.5 | 0.3 | 1.06 | 0.3 | 4.04 |
| 0.75 | 0.3 | 0.8 | 0.3 | 3.56 |
| 1 | 0.3 | 0.69 | 0.3 | 2.87 |

According to the data listed in Table 4.5, by consuming 1 Watt of power, 0.5 RT impeller could suspend 1.06 kg of solid at gas flow rate of 0.5 vvm under baffled condition. By consuming the same amount of energy, this impeller could completely lift 4.04 kg of solids off the tank bottom once the baffles were removed, which was almost four times higher compared to the quantity of the suspended solids in a baffled tank. Similar results could be obtained by comparing the data in the other rows of Table 4.5. Thus, it can be concluded that regardless of gassing rate, the percentage of power that can be saved by simply removing baffles in a tank equipped with a 0.5 RT impeller was between 70%-84%. It was also observed that values of $(C_v)_{OSC}$ for this particular impeller were almost similar in all operating and designing conditions.

#### 4.2.8.1.1 Mixed-flow impeller

The obtained $\left(\varepsilon_{js}^{-1}\right)_{0.5\,PB}$ values under unbaffled configuration are plotted as a function of $C_v$ in Figure 4.21, which is followed by Figure 4.22 where efficiency of baffle removal for this impeller is displayed.

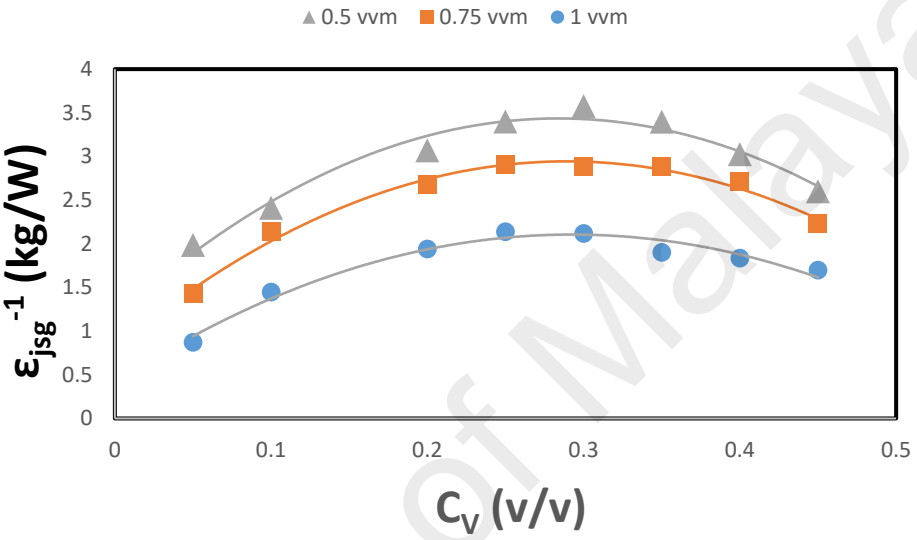


Figure 4.21 Effect of solids concentration on $(\varepsilon_{jsg}^{-1})$0.5 PB values under unbaffled condition

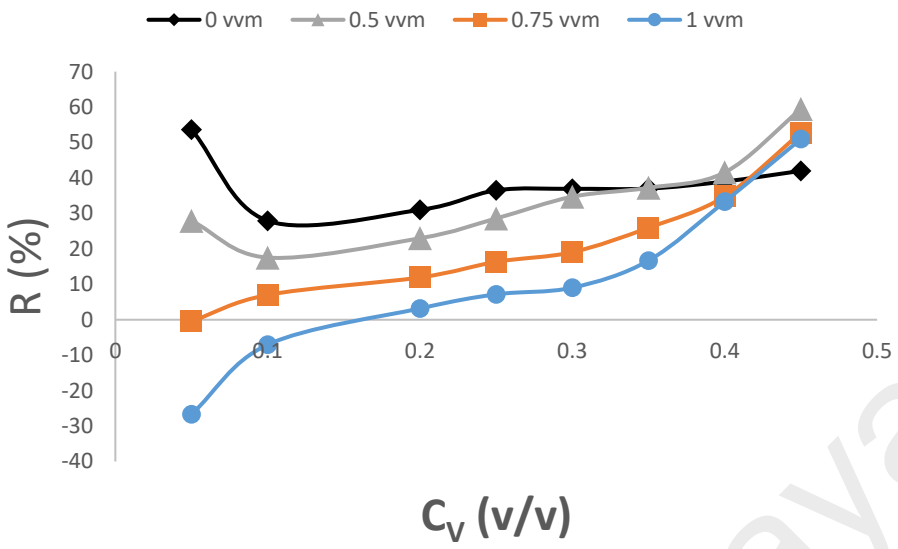


Figure 4.22 Values of unbaffling efficiency factor for 0.5 PB in absence and presence of gas

It was observed that the mixed-flow impeller exhibited the bell-shaped trends in both baffling configurations. Contrary to radial-flow impeller, removal of baffles did not lead to satisfactory results in all operating conditions. Based on Figure 4.22, baffle removal resulted in negative values of R when the tank was operating at high gas flow rate (1 vvm) and low solid concentration (0.05 to 0.17). Therefore, baffles should be kept if a stirred tank equipped with 0.5 PB impeller is operating at the highlighted conditions. In most other cases, increasing solid concentrations and decreasing gas flow rates had positive effects on $R_{0.5\ PB}$ values. $(C_v)_{OSC}$ values of 0.5 PB impeller alongside with the power efficiency factors are listed in Table 4.6. It was observed that increasing gas flow rate resulted in lower values of $\left(\varepsilon_{jsg}^{-1}\right)_{(C_v)osc}$.

Table 4.6 Effect of baffling configuration on power efficiency of 0.5 PB

| **Gassing rate (vvm)** | **Baffled** | | **Unbaffled** | |
|---|---|---|---|---|
| | **$(C_v)$ osc** | $\left(\varepsilon_{jsg}^{-1}\right)_{(C_v)osc}$ | **$(C_v)$ osc** | $\left(\varepsilon_{jsg}^{-1}\right)_{(C_v)osc}$ |
| 0 | 0.3 | 3.66 | 0.3 | 5.8 |
| 0.5 | 0.3 | 3.38 | 0.3 | 3.57 |
| 0.75 | 0.25 | 2.42 | 0.25 | 2.9 |
| 1 | 0.25 | 1.98 | 0.25 | 2.14 |

#### 4.2.8.1.2 Axial-flow impeller

The obtained results for A310 impeller under unbaffled design are depicted in Figures 4.23 and 4-24.

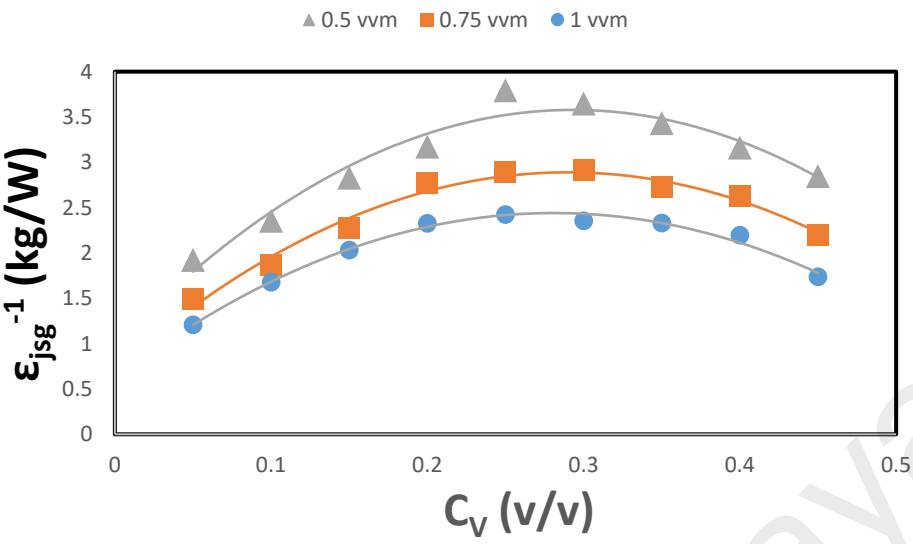


Figure 4.23 Effect of solids concentration on (εjsg-1)0.5 A310 values under unbaffled condition

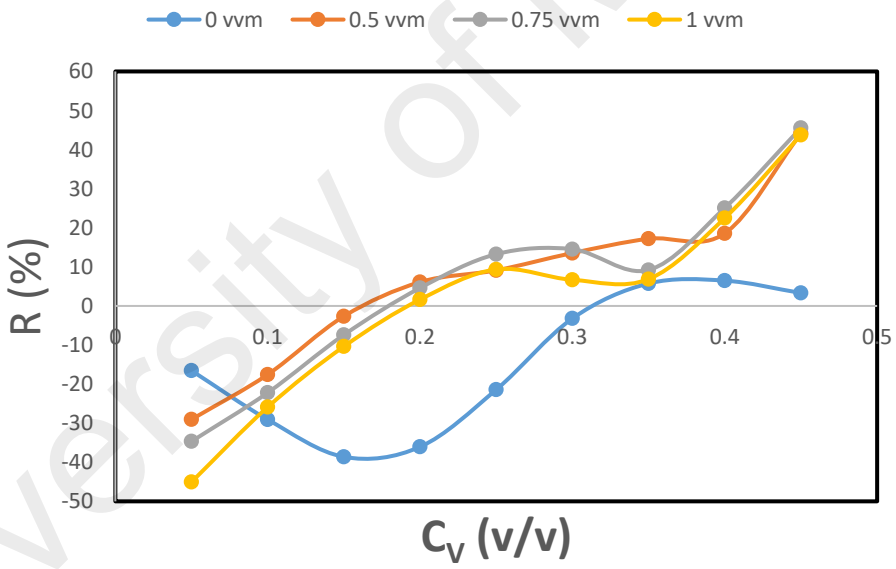


Figure 4.24 Values of unbaffling efficiency factor for A310 in absence and presence of gas

It was found that the impact of baffling configuration on energy efficiency was strictly dictated by the operating conditions. The negative values in all the four graphs indicated that at solids concentrations lower than $C_v$ = 0.16 v/v, amount of solid that A310 impeller suspended in a baffled three-phase tank was higher compared to that under unbaffled

configuration. Accordingly, at higher solid concentrations, positive R values implies that the operation at an unbaffled tank is more energy efficient. Based on these results, A310 impeller had the highest sensitivity to baffling configuration among the impellers studied in this work.

With respect to the graphs plotted in Figure 4.24, increased solids concentration led to improvement in $R_{A310}$ values. Thus, removal of baffles had both positive and detrimental effects on A310 impeller's energy efficiency depending on the fraction of solids suspended in the vessel. This behavior was close to what 0.5 PB impeller exhibited with this difference that range of critical operating conditions, at which removal of baffles is discouraged, is wider for the axial-flow impeller. Table 4.7 lists the $(C_v)_{OSC}$ for A310 impeller and their corresponding power efficiency factors.

Table 4.7 Effect of baffling configuration on power efficiency of A310

| **Gassing rate (vvm)** | **Baffled** | | **Unbaffled** | |
|---|---|---|---|---|
| | **$(C_v)$ osc** | $\left(\varepsilon_{jsg}^{-1}\right)_{(C_v)osc}$ | **$(C_v)$ osc** | $\left(\varepsilon_{jsg}^{-1}\right)_{(C_v)osc}$ |
| 0 | 0.3 | 6.79 | 0.3 | 6.58 |
| 0.5 | 0.25 | 3.44 | 0.25 | 3.79 |
| 0.75 | 0.2 | 2.64 | 0.3 | 2.91 |
| 1 | 0.2 | 2.27 | 0.25 | 2.42 |

Overall, the three impellers studied in this work exhibited different behaviors upon removal of baffles. 0.5 RT impeller was found to be the most suitable impeller for suspension of solids in unbaffled tanks. Removal of baffles resulted in significant enhancement in power efficiency factor values, which was an improvement applicable at

all solids concentrations. 0.5 PB impeller benefited from baffle removal in most cases except for the system with high gas flow rate and low solid concentration. In contrary, the axial-flow impeller exhibited negative values of baffling efficiency factor at low to medium solid concentrations when the tank was operating under unbaffled mode. It was concluded that in dilute systems, removal of baffles decreased the $\varepsilon_{jsg}^{-1}$ values, which indicated that the impeller suspended lower mass of solids per unit of consumed power than it did in a baffled tank.

### 4.2.9 Effect of particle size

Larger particles tend to settle with higher velocity and require higher degree of turbulence to stay in suspension, which inevitably forces the impeller to consume more power to keep the system at $N_{js(g)}$ condition (Drewer et al., 1994). Figure 4.25 compares the $\varepsilon_{jsg}^{-1}$ values of two particles with different sizes ($BGB_{370}$, $BGB_{683}$) in two- and three-phase systems under the absence and presence of baffles. In these experiments solids were glass particles, tap water and compressed air (1 vvm flowrate) served as the liquid and gas phases, respectively, and agitation was provided by A310 impeller.

A

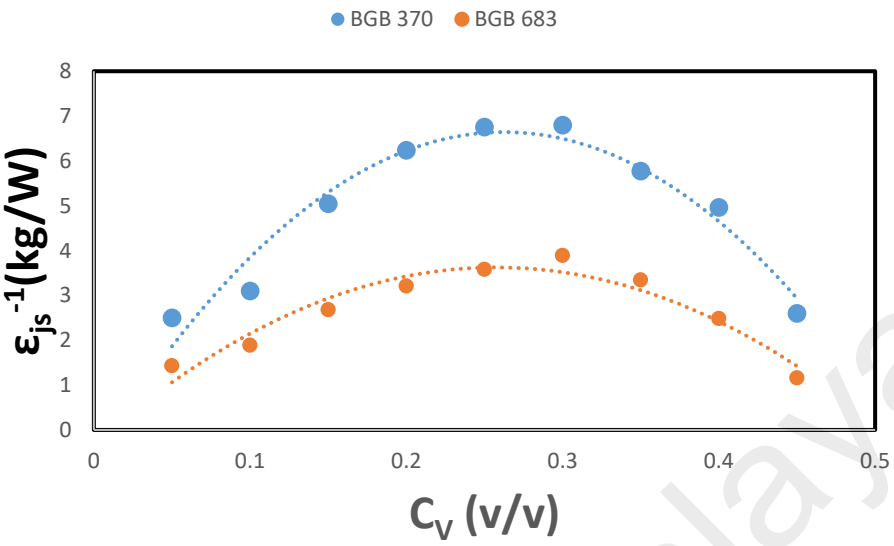


B

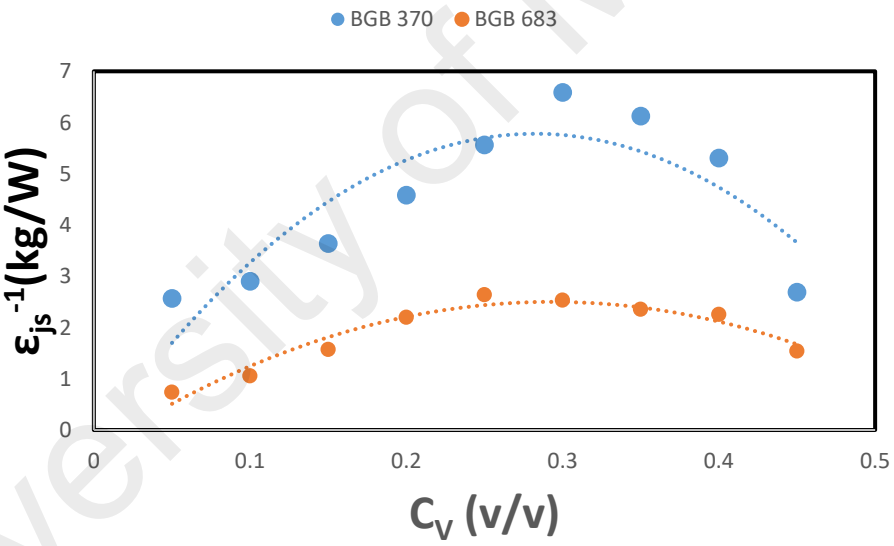

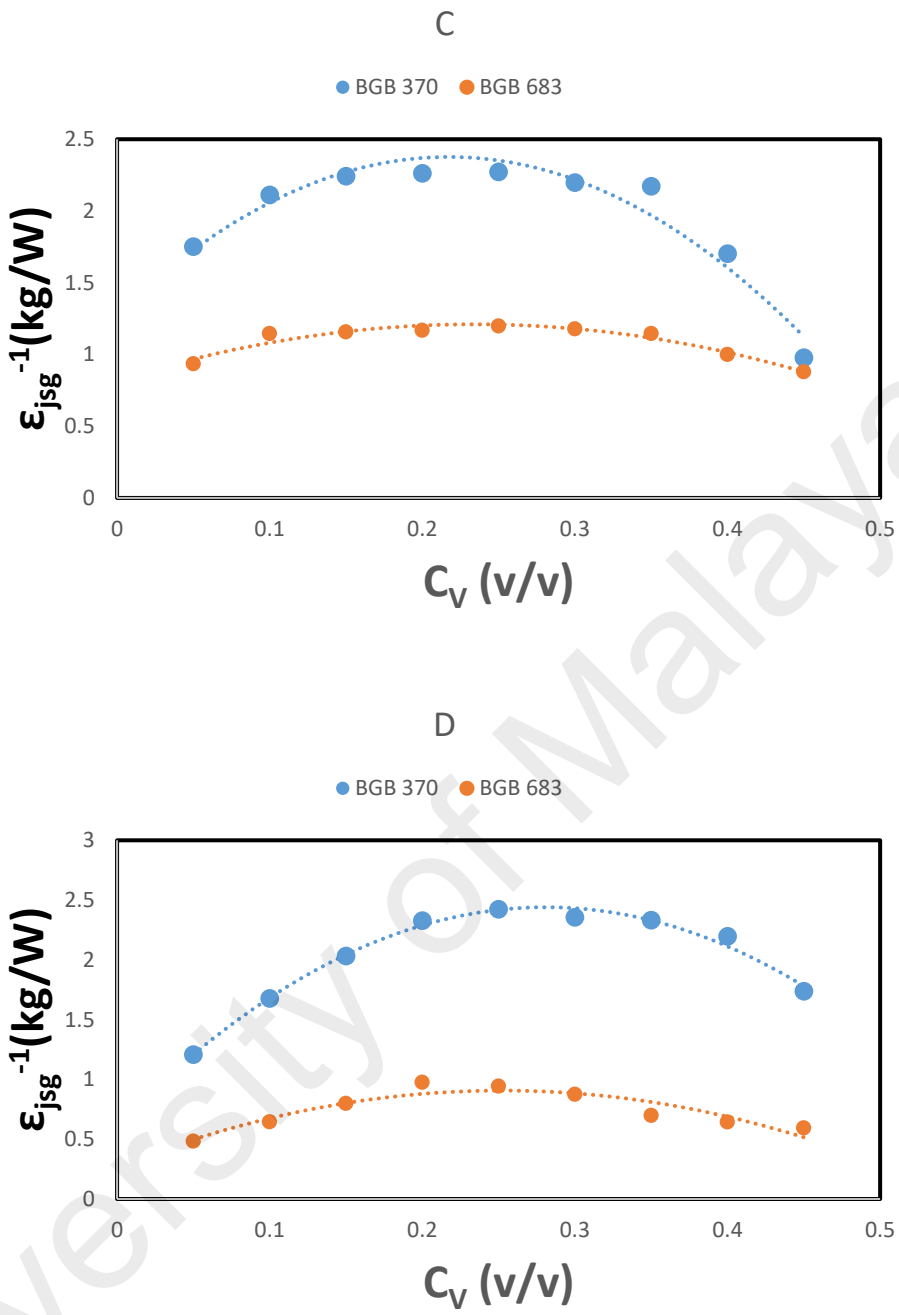


Figure 4.25 Effect of particle size on variations of power efficiency factor values for A310 impeller with solids concentration under two-phase baffled (a) two-phase unbaffled (b) three-phase baffled (c), and three-phase unbaffled (d)

It was observed that with an increase in particle size, the power efficiency values of A310 impeller decreased for all conditions studied in this work. This decline was irrespective of baffling configuration and solid concentration, but was consistent in absence and

presence of gas. In all the four figures, the tank that was operating with larger particles exhibited lower values of $\varepsilon_{jsg}^{-1}$ compared to the tank running with $BGB_{370}$. This difference became more prominent upon removal of baffles, which implied that the upward fluid velocity that large particles require to remain suspended was stronger in unbaffled tanks compared to baffled tanks especially at high solids concentrations ($C_v > 0.25$). Table 4.8 compares the optimum solid concentrations of these two solid particles under different conditions.

Table 4.8 Effect of particle size on optimum solids concentration of A310 under different conditions

| **System** | **Solid-liquid** | | | | **Gas-solid-liquid** | | | |
|---|---|---|---|---|---|---|---|---|
| Baffling condition | Baffled (Figure 4.25a) | | Unbaffled (Figure 4.25b) | | Baffled (Figure 4.25c) | | Unbaffled (Figure 4.25d) | |
| Solid particle | $(C_v)_{OSC}$ | $\varepsilon_{jsg}^{-1}$ | $(C_v)_{OSC}$ | $\varepsilon_{jsg}^{-1}$ | $(C_v)_{OSC}$ | $\varepsilon_{jsg}^{-1}$ | $(C_v)_{OSC}$ | $\varepsilon_{jsg}^{-1}$ |
| $BGB_{370}$ | 0.3 | 6.97 | 0.3 | 6.58 | 0.25 | 2.27 | 0.25 | 2.42 |
| $BGB_{683}$ | 0.3 | 3.89 | 0.25 | 2.64 | 0.25 | 1.19 | 0.2 | 0.975 |

In a solid-liquid system, increase in particle size had no effect on $(C_v)_{OSC}$ when the tank was equipped with baffles. Upon removal of baffles, larger solid particles showed lower values of $(C_v)_{OSC}$. The behavior observed in Figure 4.25a is in agreements with the findings of Drewer et al (2000) who reported that optimum solids concentration was not affected by particle size in a solid-liquid baffled tank, while Wang et al (2012) observed a decline in $(C_v)_{OSC}$ upon increasing particle size in an unbaffled tank, similar to the trend depicted in Figure 4.25b. Our results implied that the same pattern applied to gas-solid-

liquid vessels operating at a similar gas flow rate, where increase in particle size resulted in lower $(C_v)_{OSC}$ if the baffles were removed. Compared to a two-phase system, however, the optimum solid concentration at any given scenario in three-phase systems was lower.

In addition, it is worth mentioning that larger particles have higher settling velocity, which forces the impeller to operate at higher impeller speed and consume more power to keep the solids suspended. This explanation is consistent with mathematical correlations previously report for determination of $N_{js}$:

Zwietering's correlation for $N_{js}$ is given by equation (4-6)[5]:

$$N_{js} = \frac{S v^{0.1} d^{0.2} \left(\frac{g\Delta\rho}{\rho_l}\right)^{0.45} X^A}{D^{0.85}} \qquad 4\text{-}6$$

Where, $N_{js}$ represents the critical impeller speed in solid-liquid systems (rps), $\rho_l$ refers to liquid density (kg/m$^3$), respectively, $\Delta\rho$ denotes the difference in densities of solid and liquid (kg/m$^3$), S is a coefficient based on the impeller type, v refers to the kinematic viscosity of liquid (m$^2$s$^{-1}$), X is the solid loading ratio, and d is particle size (m). It is clear that $N_{js}$ increases with an increase in particle size.

### 4.2.10 Dispersion of solid particles at high solids concentrations

Wang et al (2012) studied the status of solids dispersion based on slurry cloud height ($H_S$), and defined 'complete dispersion' as a condition at which $H_S = H$ and $H_B = 0$. In Figures 4.26 and 4-27, the values of power efficiency factor for 0.5 RT and 0.5 PB impellers are plotted against the ratio of suspension height to liquid height ($H_S/H$) for two- and three-phase systems, respectively. The data of sedimentation bed height ($H_B/H$)

were also plotted on the second y axis to provide a clear picture of the relations between $H_S$ and $H_B$.

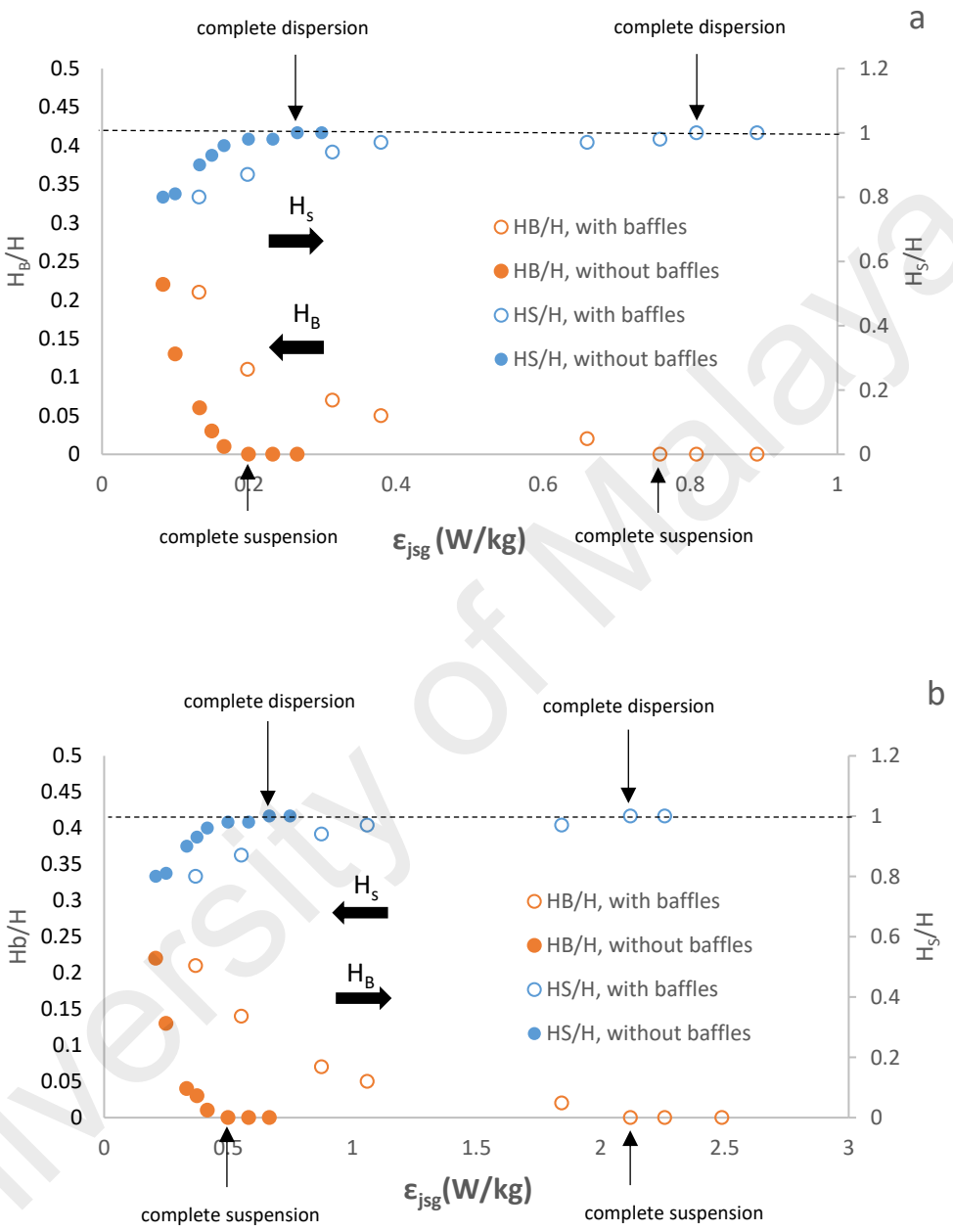


Figure 4.26 Dispersion of solid particles for 0.5 RT impeller in two- (a) and three- (b) phase systems: constant solids concentration (Cv = 0.45 v/v), particle: BGB370, gas flow rate at Figure 4.26 (b): 1 vvm.

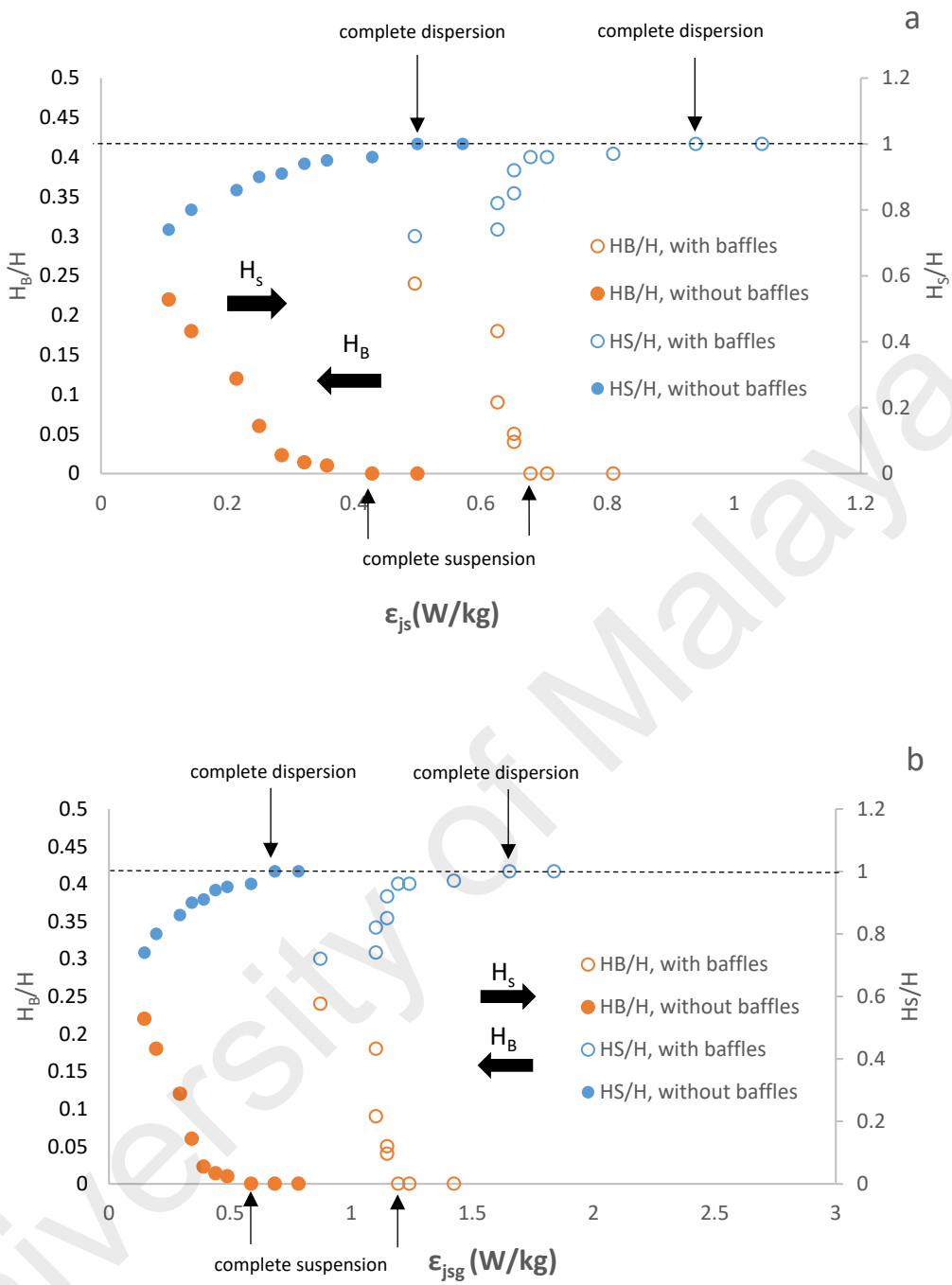


Figure 4.27 Dispersion of solid particles for 0.5 PB impeller in two- (A) and three- (B) phase systems: constant solids concentration (Cv = 0.45 v/v), particle: BGB370, gas flow rate at Figure 4.27 (b): 1 vvm

It can be seen that upon removal of baffles, the graphs in Figures 4.26 and 4.27 shifted to the left, which corresponded to reduction in the power input of impellers for both complete off-bottom suspension and solids dispersion. In both aerated and unaerated systems, the required specific power to provide full solid dispersion (while $H_B = 0$)

reduced significantly upon removal of baffles. For instance, according to Figure 4.26b, the required power to provide complete solid dispersion for a three-phase stirred tank rotating with a 0.5 RT impeller and operating at $C_v$ = 0.45 v/v decreased from 2.12 to 0.63 W/kg once the baffles were removed. As shown in Figure 4.27b, the obtained power saving was less pronounced in the case of 0.5 PB impeller (1.65 to 0.69 W/kg).

Therefore, for both the two- and three-phase stirred vessels, it is possible to obtain a complete solid dispersion with reduced power input, whilst the solids are suspended from tank bottom.

## 4.3 Gas holdup

Gas hold-up is one of the important parameters that determines gas-liquid interfacial area and, therefore, the gas-liquid mass transfer rate. The first attempt to study the effect of solids concentration on gas hold-up was made by Massimillia et al. (1961), who observed a decrease in gas hold-up with an increase in solid loading. They pointed out that high concentration of solids encouraged bubble coalescence and therefore reduced gas holdup. Similar results were reported later by other authors (Yawalkar et al., 2002) (Chapman et al., 1983).

The total volume of three-phase system under aerated and unaerated conditions was measured using an ultrasonic level sensor and used to determine the gas hold-up Øg using the following equation:

$$Øg = \frac{H_A - H}{H_A} \qquad \textbf{4-6}$$

where $H_A$ and H denote the heights of the aerated liquid and the clear liquid, respectively.

Gas hold-up values for 0.5 RT, 0.5 PB, and A310 obtained for a range of solids concentration at $N_{jsg}$ are shown in Figure 4.28. It can be seen that, at any given gas flow rate, an increase in solids concentrations leads to a decrease in gas hold-up. Among the impellers studied, 0.5 RT leads to the highest $\varepsilon_G$ values at all $C_v$ and gassing rates compared to those for 0.5PB and A310. Also, $Ø_g$ values for 0.5PB and A310 are found to be similar at all $C_v$ and gassing rates. At a constant $C_v$, increasing gas flow rate results in higher gas hold-up values for 0.5 RT. This improvement is found to be less pronounced for 0.5PB and A310. These results are in agreement with the gas holdup results reported in literature for three-phase systems (Yawalkar et al., 2002) ((Dohi et al., 1999))

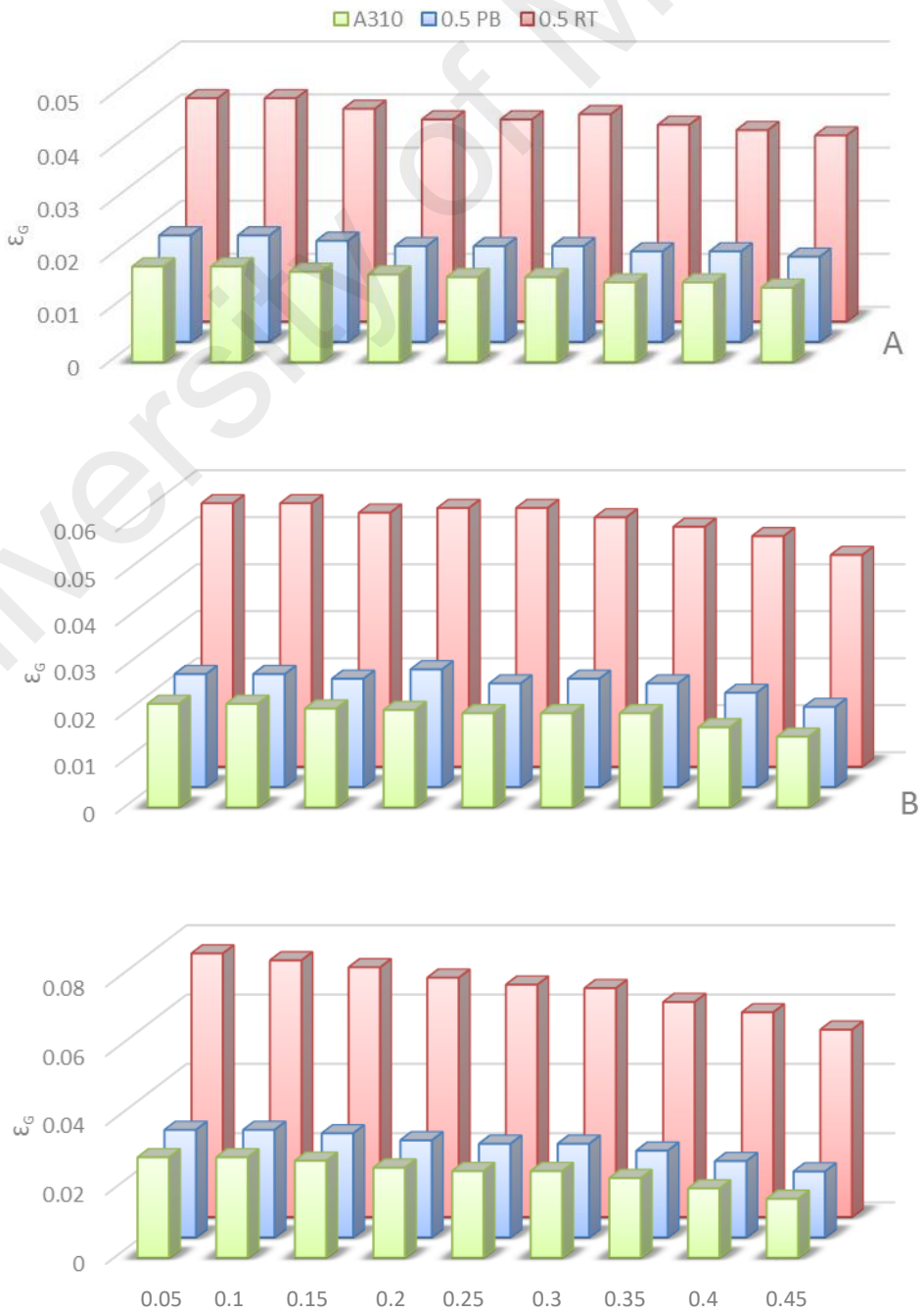

## 4.4 Sauter mean bubble diameter

As explained earlier, an underwater imaging system was used to record videos of simultaneous movement of solid particles and gas bubbles inside the vessel. The camera was able to record high-quality images at various gas flow rates for a wide range of solids concentration ($C_v$ = 0.01-0.25). Quality of images, however, decreased when solids concentration exceeded 0.25 v/v, and bubble shapes were not recognizable in the clouds of dense solids. The recorded images were replayed in slow-motion (10-20% playback rate) and various snapshots were taken. Images that contained bubbles with the highest clarity were selected. Then, diameters of the bubbles in each frame were determined and analyzed using ImageJ software. Figure 4.29 presents some of the images captured using the underwater camera setup. The white particles in these images represent solids and the dark shapes represent gas bubbles. Details of experiment were as follows:

- solids: BGB 370
- camera location: above impeller region
- agitation speed: $N_{jsg}$
- impeller: RT

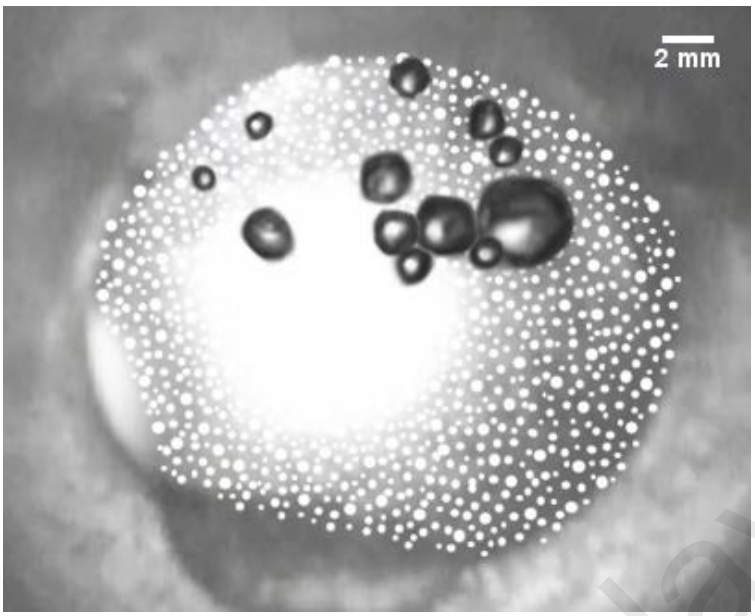


a

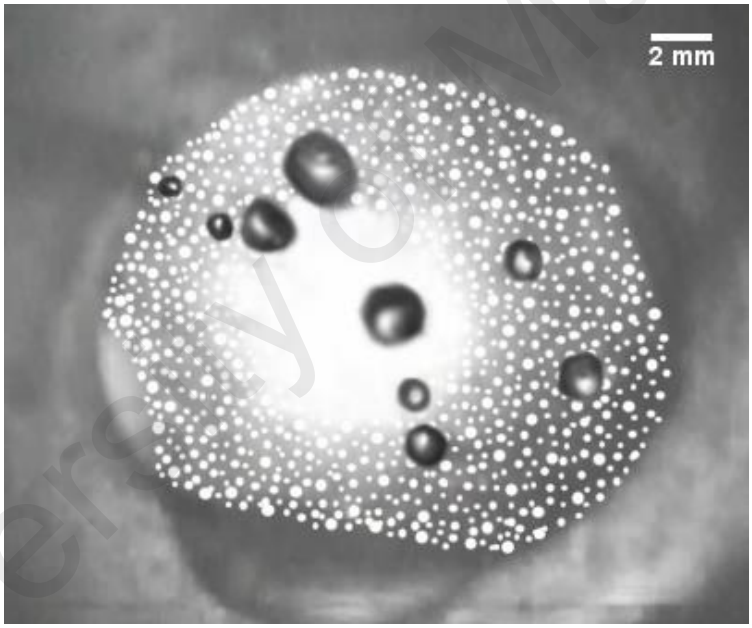


b

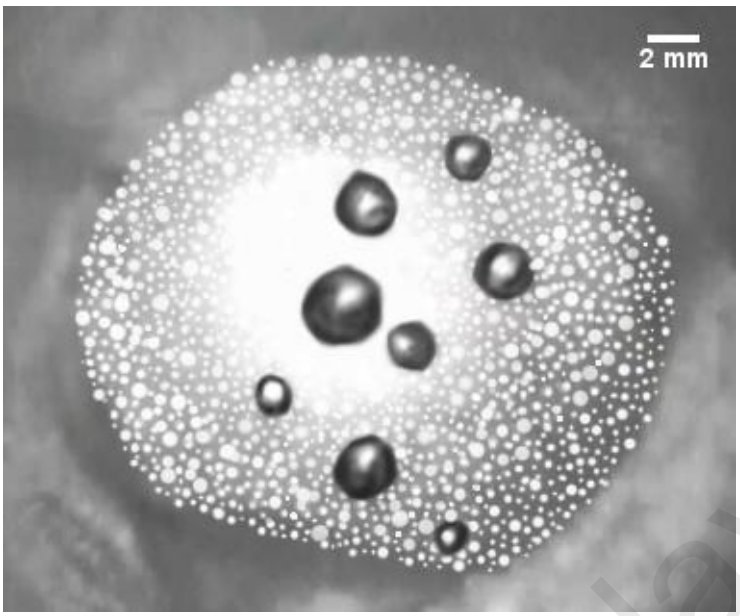


c

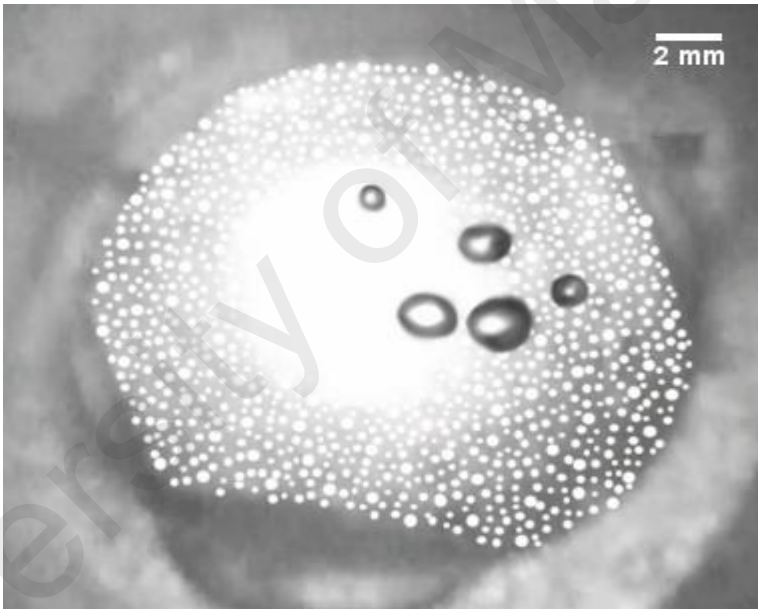


d

Figure 4.29 Gas bubbles in three-phase stirred vessels handling solids concentrations (a) $C_v$= 0.05, $Q_g$ = 0.5 vvm and (b) $C_v$= 0.1, $Q_g$ = 0.5 vvm, (c) $C_v$= 0.12, $Q_g$ = 0.75 vvm, and (d) $C_v$= 0.15 v/v, $Q_g$ = 0.5 vvm

It can be seen that with an increase in $C_v$ (Figures 4.29a to 4.29d), population of white particles found in the images increases, and the average diameter of bubbles decreases. Although solids concentration is increasing, the average bubble size in images 4.29b and 4.29c seem to be nearly the same. This could be attributed to higher gas flow rate in Figure

4.29c, which resulted in the generation of larger bubbles. According to our observations, a majority of bubbles smaller than 2000 µm were spherical, as well as many larger ones. The white circles seen in the middle of the images is the light transmitted through the cylindrical perspex rod. The centralized light led to a uniform illumination of the images produced, which in turn facilitated the reliable bubble size analysis. It is clear that bubbles tend to become smaller with an increase in solids concentration. As explained earlier, diameter of 200 unique bubbles were measured for each $C_v$ and $Q_g$ to obtain a reliable $d_{32}$ value. Number of bubbles in each frame varied according to the volumetric fraction of solids suspended in the tank (e.g. the number of frames analyzed to obtain a reliable $d_{32}$ value were 53 and 93 for an RT impeller operating at $C_v$ = 0.05 and 0.25, respectively). The values of $d_{32}$ for RT and 45 PB impellers are shown as a function of $C_v$ and $Q_g$ in Figures 4.30a and Figure 4.30b, respectively.

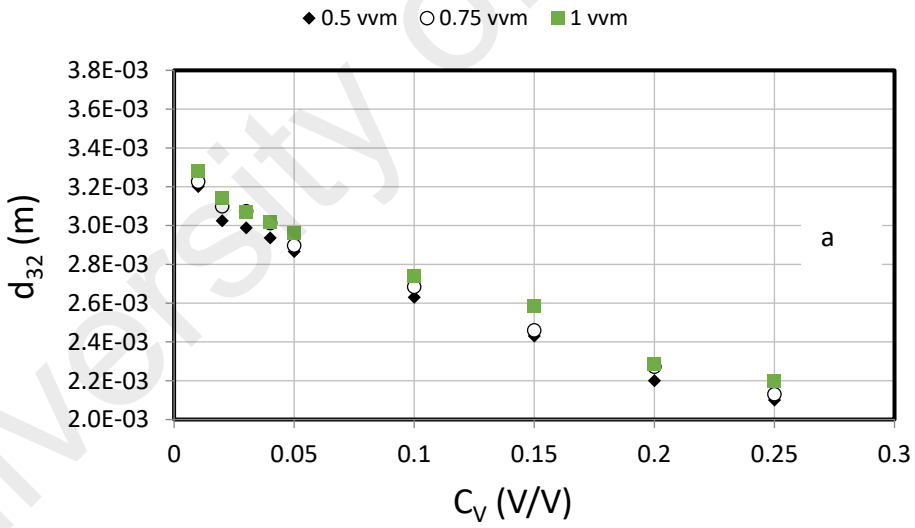

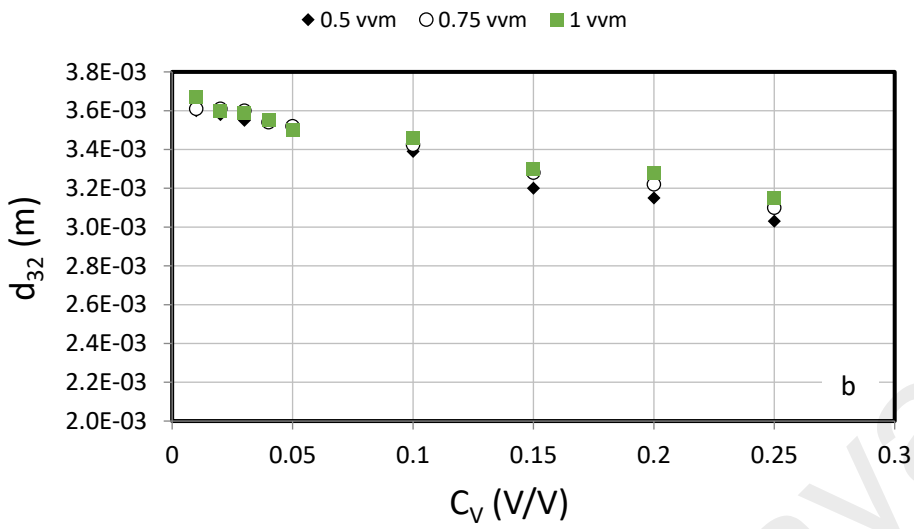


Figure 4.30 Effect of solids concentration on $d_{32}$ at $N_{jsg}$ (a) RT and (b) 45 PB impeller for different gas flow rates

According to Figure 4.30, the $d_{32}$ values for both impellers decreased with an increase in solids concentration at a constant gas flow rate. Moreover, the $d_{32}$ value for a given $C_v$ increased slightly with gas flow rate.

It can be observed that at any given $C_v$ and $Q_g$, the RT impeller leads to smaller bubbles compared to 45 PB impeller. It is interesting to observe that at low solids concentrations ($C_v$ = 0.01-0.05 v/v), the $d_{32}$ values for the mixed-flow impeller remained almost constant regardless of the changes in $C_v$ and $Q_g$, while the $d_{32}$ values for the RT impeller seems to be more sensitive to operating conditions. The $d_{32}$ values for the RT impeller decreases from 3.3 to 2.1 mm as $C_v$ increases from 0.01 to 0.25 v/v.

It can be concluded that RT impeller is able to disperse the bubbles more effectively within the vessel, which is reflected in the larger gas holdup and $d_{32}$ values observed with this impeller. This indicates that the flat blade design of the RT generates stronger liquid

circulation patterns in the vessel as compared to those generated by the blade designs of the 45 PB impeller.

### 4.4.1 Effect of specific power on $d_{32}$

The $d_{32}$ values are plotted against the impeller specific power input (P/V) for the RT and 45 PB impellers in Figures 4.31a and 4.31b, respectively. At $N_{jsg}$ condition, for the same specific power input, $d_{32}$ values obtained at low solids concentrations (0.01-0.05 v/v) were found to be nearly the same for both impellers. As $C_v$ increases, effect of specific power on $d_{32}$ values becomes more pronounced. It is clear from the figures that there is a linear relationship between $d_{32}$ and P/V for both impellers. According to our results, an increase in impeller specific power has stronger influence on $d_{32}$ for a RT impeller than a 45 PB-impeller, which can be verified by comparing the slopes of dotted lines in Figures 4.31a and 4.31b. This difference is noticeable in the selected data listed in Table 4.9.

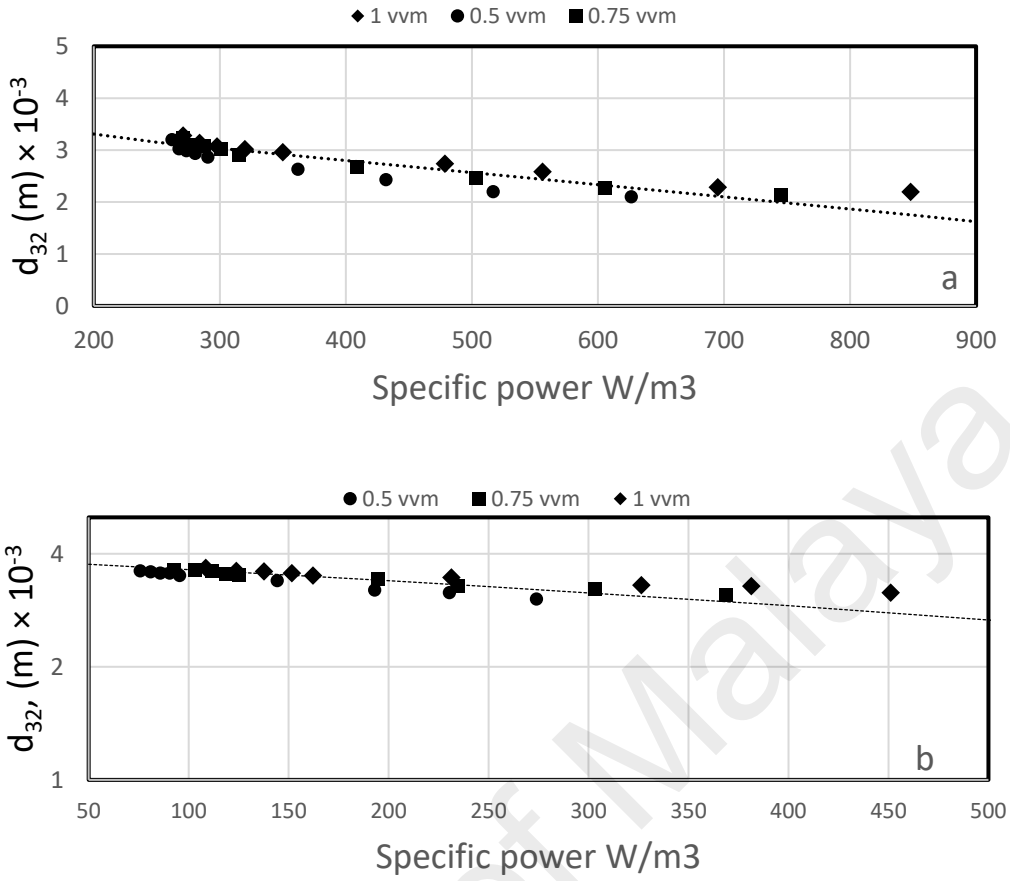


Figure 4.31 Effect of specific power input on $d_{32}$ at $N_{jsg}$ for (a) RT and (b) 45 PB impellers: Qg = 1 vvm

Table 4.9 Effect of gas flow rate and solids concentration on d32 values of two impellers, solids: BGB 370

| Impeller | $C_v$ (v/v) | $Q_g$ (vvm) | $d_{32} \times 10^{-3}$ (m) |
|---|---|---|---|
| RT | 0.01 | 0.5 | 3.2 |
| | 0.05 | 0.5 | 2.8 |
| | 0.25 | 0.5 | 2.1 |
| | 0.01 | 1 | 3.28 |
| | 0.05 | 1 | 2.96 |
| | 0.25 | 1 | 2.19 |
| 45 PB | 0.01 | 0.5 | 3.6 |
| | 0.05 | 0.5 | 3.5 |
| | 0.25 | 0.5 | 3 |
| | 0.01 | 1 | 3.67 |
| | 0.05 | 1 | 3.5 |
| | 0.25 | 1 | 3.15 |

According to the data listed in Table 4.9, the $d_{32}$ values for 45 PB impeller are almost independent of $C_v$ and $Q_g$ at low solids concentration (0.01-0.05 v/v), which suggests that regardless of solids concentration and gas flow rate, the $d_{32}$ value in three-phase dilute systems was only a function of specific power input (P/V). Impact of $C_v$ and $Q_g$ on $d_{32}$ values for the RT impeller is more pronounced as there is a noticeable difference between the $d_{32}$ for $C_v$ = 0.01 compared to that for $C_v$= 0.25 v/v. It is also clear that an increase in solids loading has stronger effect on $d_{32}$ for RT than on $d_{32}$ for 45 PB. Generally, results shown in Figure 4.31 and Table 4.9 indicate that specific power input is one of the main parameters that determine $d_{32}$ in three-phase systems.

It should be noted that as $C_v$ increases, higher impeller speed is required to keep solids in suspension. Consequently, an increase in impeller speed at a constant gas flow rate increases the energy dissipated into the impeller region (i.e., increases $P_g/V$), which leads to the generation of a greater number of smaller bubbles. It can be speculated that an increase in agitation speed at a constant aeration rate increases the turbulence of the trailing gas cavities. On the other hand, increasing the gas flow rate at a constant impeller speed increases the size of the trailing gas cavities, which decreases $P_g/V$ and as a result a greater number of larger bubbles are generated. These results are in agreement with previous reports (Barigou, M & Greaves, 1991, 1992) (Takahashi & Nienow, 1993). These results are also in line with Kolmogoroff's theory of local isotropic turbulence (Kolmogoroff, 1941a, 1941b, 1941c, 1949), which leads to the conclusion that the hydrodynamics in aerated agitated vessels can be attributed to a single parameter, the energy dissipation rate in the impeller zone.

Thus, it is clear that energy input is the most significant factor that influences average bubble diameter is three-phase stirred vessels operating at high solids concentration.

### 4.4.2 Effect of solid particle size on $d_{32}$

The effect of particle size on $d_{32}$ values is shown in Figure 4.32 for the RT impeller. At a constant gas flow rate, $d_{32}$ values of the RT impeller decreases as particle size increases. It could be speculated that particle size influences the average bubble size through increased impeller power draw. It is generally accepted that larger solid particles have higher settling velocity due to which impeller is required to consume more power to keep the particles suspended. Discussions in the previous section indicated that an increase in impeller specific power input leads to the generation of smaller bubbles. Based on that, it can be concluded that suspension involving larger particles leads to smaller bubbles if the impeller is operating at 'complete off-bottom suspension' condition.

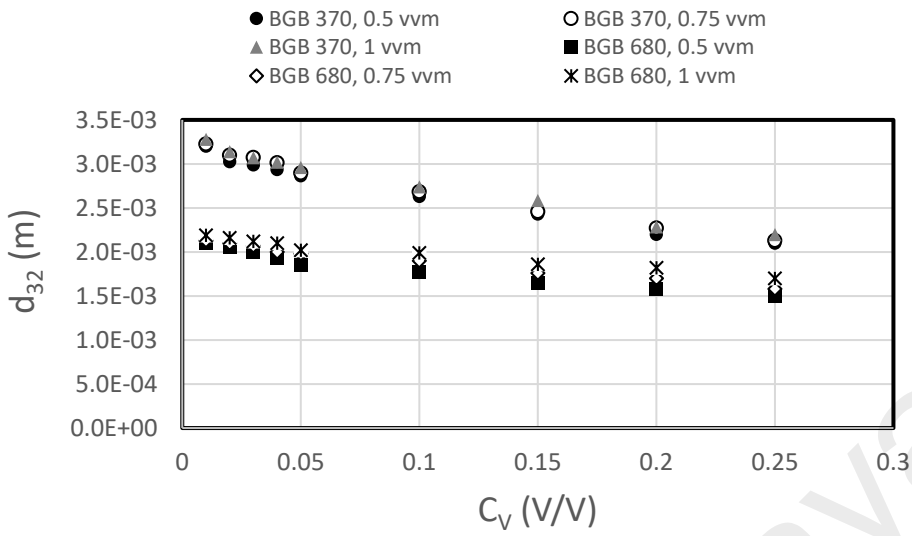


Figure 4.32 Effect of particle size on $d_{32}$ values for RT impeller

It can be reported that particle size influences $d_{32}$ values by changes in impeller power consumption. It can be speculated that particle size has minimal effects on average bubble size if the system under investigation is not operating at $N_{jsg}$ condition.

## 4.5 Gas-liquid interfacial area

By combining gas holdup and Sauter mean bubble diameter, gas-liquid interfacial area ($\alpha_{g\text{-}l}$ ($m^{-1}$)) could be determined using the following equation:

$$a_{g-l} = \frac{6\emptyset_g}{d_{32}} \qquad \textbf{4-7}$$

where $Ø_g$ is the gas holdup and $d_{32}$ is the Sauter mean bubble diameter (m).

Values of $\alpha_{g\text{-}l}$ determined for RT and 45 PB impellers are shown in Figure 4.33.

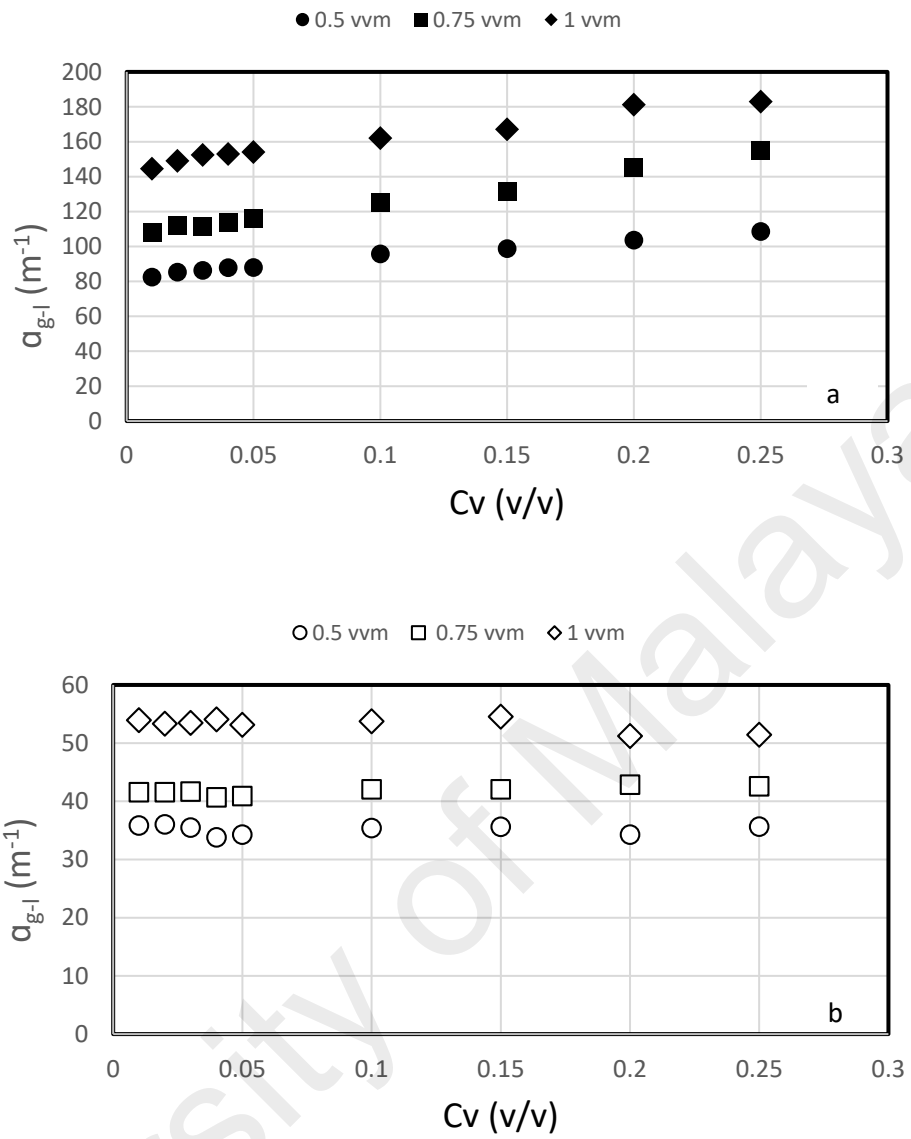


Figure 4.33 Effect of solids concentration and gas flow rate on gas-liquid interfacial area for (a) RT (b) 45 PB impellers, particle size: BGB 370

According to Figure 4.33, RT is able to generate longer $\alpha_{g-l}$ compared to 45 PB impeller at any given $C_v$ and $Q_g$. These results are expected as it has been previously observed that RT impeller shows higher values of gas holdup and lower values of $d_{32}$ compared to 45 PB impeller at any given $C_v$ and $Q_g$. Moreover, an increase in solids concentration results in an increase in $\alpha_{g-l}$ for the RT impeller. However, the $a_{g-l}$ for 45 PB impeller seems to be independent of $C_v$. Based on the results of $Ø_g$, $d_{32}$, and $\alpha_{g-l}$, it seems logical to conclude that radial flow impellers are more efficient in maximizing the contact area between gas

and liquid phases. Nonetheless, it is evident that an increase in solids concentration has no negative influence on gas-liquid interfacial areas generated by both impellers.

### 4.6 Optimum solids concentration

Generally, there are two major strategies to decrease capital and operating costs in three-phase mechanically agitated vessels: decreasing the volume of the vessel or enhancing the throughout through the existing vessel (process intensification) (Chowdry et al., 1995). The second option is more feasible since reducing the volume of existing vessels is not practical due to the high cost involved. Increase in solids concentration, however, demands higher impeller speed to completely suspend the increased amount of solids, which consequently leads to higher impeller power consumption, and potentially, an upgrade of the motor. In some cases, it is possible to maintain the stirrer drive motor by operating the impeller at optimum conditions. Nonetheless, increasing solids concentration and throughout seem to be a more desirable option than scaling up the existing vessel.

According to the experimental results reported in this study, an increase in solids concentration results in smaller average bubble size and causes the gas-liquid contact area to increase, especially in the case of radial-flow impellers. This is, however, achieved by maintaining the system at complete-off bottom condition, which requires higher agitation speed (and consequently higher impeller power draw) when solids concentration is increased.

Figure 4.34 shows the influence of solids concentration on specific impeller power input and gas-liquid interfacial area for different gas flow rates. It was possible in this work to determine the bubble size distribution in the three-phase system only up to $C_v$ = 0.25 v/v. It was difficult to obtain images of bubbles at higher solids loadings. It is the reason why gas-liquid interfacial area data for $C_v$ greater than 0.25 (v/v) are not shown in Figure 4.34.

It can be seen that the $a_{g-l}$ values increase linearly as $C_v$ increases for all gas flow rates (Figure 4.34). Based on this observation, it can be concluded that there is an optimum solids concentration at which impeller's performance in terms of power efficiency and ability to generate large gas-liquid interfacial area can be maximized. Values of $(C_v)_{OPT}$ were found to be 0.25-0.3, 0.3, and 0.3 (v/v) for $Q_g$ = 0.5. 0.75, and 1 vvm, respectively, for the RT impeller. By further increasing the solids concentration, $a_{g-l}$ values would probably enhance, but impeller's performance in terms of energy efficiency starts to decrease. Therefore, it is beneficial to operate the mixing tanks at $(C_v)_{OPT}$ to obtain the most satisfactory performance.

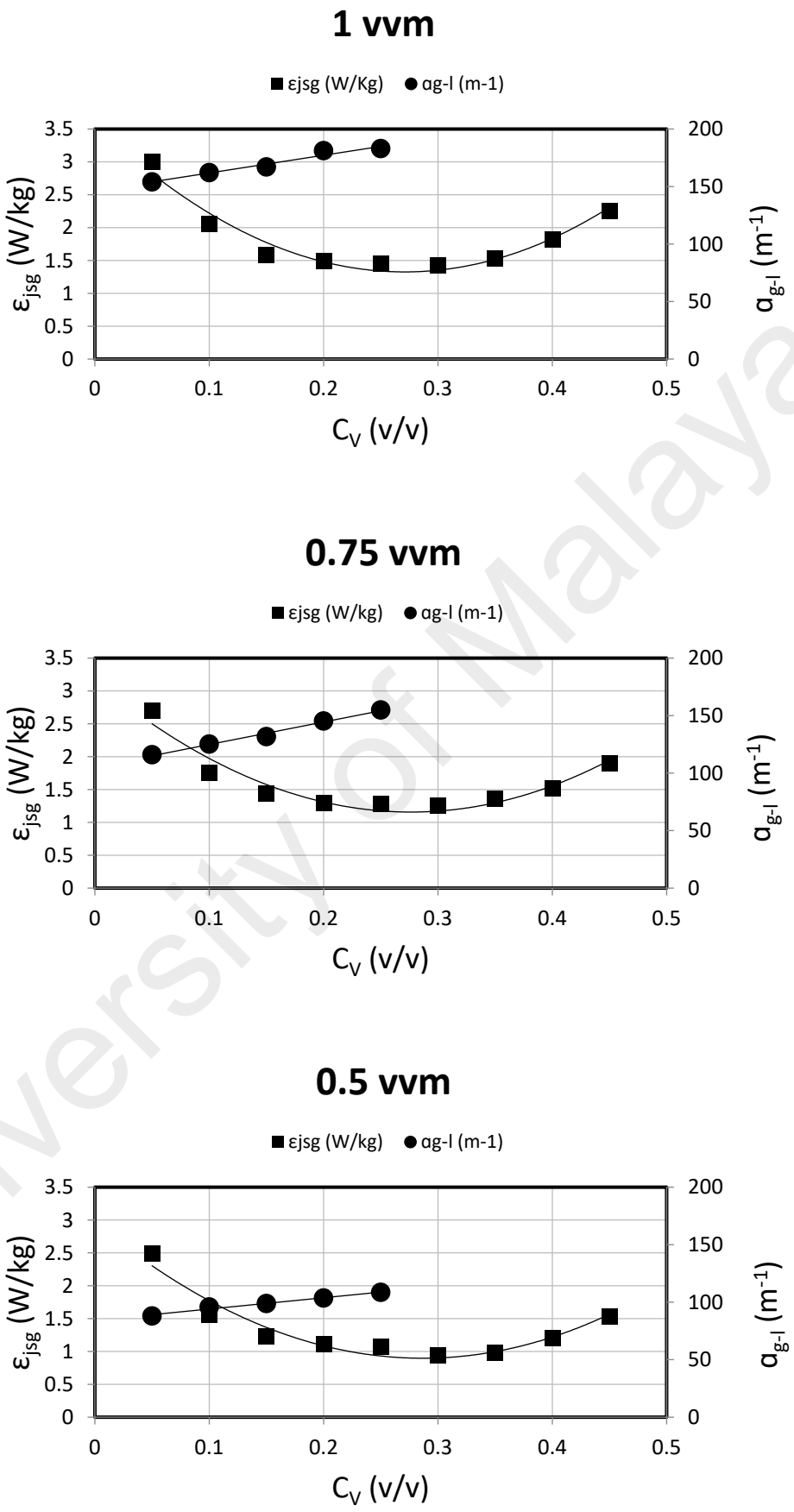


Figure 4.34 Effect of solids concentration on $\varepsilon_{jsg}$ and $\alpha_{g\text{-}l}$ for different gas flow rates: impeller: RT, particles: BGB 370

In short, it was also observed that radial-flow impellers generate smaller bubbles compared to mixed-flow impellers at any given $C_v$ or $Q_g$. It was also noticed that average bubble size in a stirred vessel is highly influenced by power input to the system. Accordingly, an increase in particle size led to generation of smaller gas bubbles due to the fact that keeping larger particles in suspension demands higher power input. It was seen that increase in solids concentration is an effective approach to enhance the gas-liquid interfacial area in three-phase stirred vessels. By taking the role of power consumption into account, it was concluded that there is an optimum solids concentration at which impeller's performance in terms of power efficiency and ability to generate large gas-liquid interfacial area can be maximized.

## 4.7 Proposing mathematical correlations

This part of the study focuses on proposing mathematical correlations to predict values of specific impeller power consumption ($\varepsilon_{jsg}$), Sauter mean bubble diameter ($d_{32}$), and gas-liquid interfacial area ($a_{g\text{-}l}$) in three-phase stirred vessels.

### 4.7.1 Estimation of specific impeller power consumption

Using the experimental data obtained in this work, a mathematical correlation is developed in this section to estimate the specific impeller power input ($\varepsilon_{jsg}$) as a function of $C_v$, gas flow rate ($Q_g$), and impeller and tank geometries.

As explained earlier, Nienow and Bujalski (2002) developed two correlations for the determination of $N_{jsg}$ for down-pumping (equation 4-3) and radial flow impellers (equation 4-4) using $N_{js}$ and gas flow rate.

It should be noted that the presence of solid leads to additional power consumption by the impeller. Bubbico et al. (1998) proposed an empirical correlation that relates impeller power draw and volumetric solid concentration as follows:

$$P = N_p(1 + kC_v)\rho_w N^3 D^5 \quad \textbf{4-8}$$

where P is impeller power required to suspend solids off the tank bottom (W), $N_P$ is impeller power number, $\rho_w$ is density of water (kg/m$^3$), $C_v$ is volumetric solids concentration, N is impeller critical speed (revolutions per second), D is impeller diameter (m), and k is a constant that represents the excessive energy dissipated by particles.

The mass of solids suspended is calculated by:

$$M_s = \rho_S V_s = \rho_s V C_v \quad \textbf{4-9}$$

where $M_s$ is mass of solids, $\rho_s$ is solid density, $V_s$ is volume of solids, and V is liquid volume. The specific power input in terms of the total mass of the suspended solids in a solid-liquid system can be obtained by combining Equation (4-8) with Equation (4-9):

$$\varepsilon_{js} = \frac{P}{M_s} = \left(N_P \frac{\rho_w}{V\rho_s} N^3 D^5\right)\left(\frac{1}{C_v} + k\right) \quad \textbf{4-10}$$

#### 4.7.1.1 Down-pumping impeller

Combined with equation (4-3), equation (4-10) can be written for a three-phase system as:

$$\varepsilon_{jsg} = \frac{P_{jsg}}{M_s} = \left(N_P \frac{\rho_l}{V\rho_s} D^5\right)\left(\frac{1}{C_v} + k\right)\left(N_{js}\left(0.83 + 0.31Q_g\right)\right)^3 \quad \textbf{4-11}$$

Zwietering's correlation for $N_{js}$ is given by equation (4-14):

$$N_{js} = \frac{Sv^{0.1}d^{0.2}\left(\frac{g\Delta\rho}{\rho_l}\right)^{0.45}X^A}{D^{0.85}} \quad \textbf{4-12}$$

where X can be calculated using:

$$X = \left(\frac{\rho_s}{\rho_w}\right)\left(\frac{C_v}{1-C_v}\right) \times 100 \quad \textbf{4-13}$$

In eqs 4-12 and 4-13, $N_{js}$ represents the critical impeller speed in solid-liquid systems (rps), $\rho_l$, $\rho_s$, and $\rho_w$ refer to densities of liquid, solid, and water ($kg/m^3$), respectively, $\Delta\rho$ denotes the difference in densities of solid and liquid ($kg/m^3$), S is a coefficient based on the impeller type, v refers to the kinematic viscosity of liquid ($m^2s^{-1}$), X is the solid loading ratio which is a function of $C_v$, as shown by equation 4-13. The exponent 'A' for low to medium $C_v$ = (= 0.09-0.20 v/v) is approximately equal to 0.13 according to Zweitering[5]. Thus the value of A is assumed 0.13 in this work.

By combining equations (4-11)-(4-13), this work proposes the following equation for the determination of $\varepsilon_{jsg}$ in a three-phase stirred vessel equipped with a down-pumping impeller:

$$\varepsilon_{jsg} = \frac{P_{jsg}}{M_s} =$$

$$v^{0.3}\left(\frac{100C_v\rho_s}{(1-C_v)\rho_l}\right)^{3A} \quad \textbf{4-14}$$

$$\left(\frac{1}{C_v}+k\right)\left(0.83+0.31Q_g\right)^3\left(\frac{Sd^{0.2}\left(\frac{g\Delta\rho}{\rho_l}^{0.45}\right)}{D^{0.85}}\right)^3\left(N_P\frac{\rho_l}{v\rho_s}D^5\right)$$

#### 4.7.1.2 Radial-flow impeller

By combining Equations (4-10) and (4-4), we would have:

$$\varepsilon_{jsg} = \frac{P_{jsg}}{M_s} = \left(N_P \frac{\rho_l}{v\rho_s} D^5\right)\left(\frac{1}{C_v} + k\right)\left(N_{js} + 0.85Q_g\right)^3 \quad \textbf{4-15}$$

Thus, we have proposed the following correlation for determination of $\varepsilon_{jsg}$ in a three-phase stirred vessel involving a radial flow impeller by combing equations 4-12, 4-13, and 4-15:

$$\varepsilon_{jsg} = \frac{P_{jsg}}{M_s} =$$

$$\left(N_P \frac{\rho_l}{v\rho_s} D^5\right)\left(\frac{1}{C_v} + k\right) \quad \textbf{4-16}$$

$$\left(\frac{Sv^{0.1} d^{0.2} \left(\frac{g\Delta\rho}{\rho_l}\right)^{0.45} \left(\left(\frac{\rho_s}{\rho_w}\right)\left(\frac{C_v}{1-C_v}\right) \times 100\right)^A}{D^{0.85}} + 0.85Q_g\right)^3$$

The kinematic viscosity of the slurry can be determined using Thomas's correlation (Thomas, 1965):

$$v = \frac{\mu_{slurry}}{\rho_{slurry}} \quad \textbf{4-17}$$

Where

$$\mu_{slurry} = \mu_l[1 + 2.5C_v + 10.05C_v^2 + 0.0273\exp(16.6C_v)] \quad \textbf{4-18}$$

and according to Behkish et al. (2007):

$$\rho_{slurry} = \left(\emptyset_g \rho_G + \left(1 - \emptyset_g\right)\right)\left(\rho_s C_v + \rho_w (1 - C_v)\right) \quad \textbf{4-19}$$

In equations 4-18 and 4-19, $\mu_l$, $\emptyset_g$, and $\rho_G$ represent liquid viscosity (Pa.s), gas holdup, and gas density (kg/m$^3$), respectively.

Equation 4.14 and 4.16 provide correlations of specific impeller power draw on the basis of solids concentration, gas flow rate, gas holdup, impeller specifications, and particle size for down-pumping and radial-flow impellers, respectively. Zwietering (1958) reported exponent A to be 0.13 for solids concentrations in the range of 0.09 to 0.2 v/v and this value is taken to be applicable for the range of solids concentration used in this work.

The $\varepsilon_{jsg}$ values estimated by equations 4-14 and 4-16 are plotted as a function of $C_v$ for all three impellers in Figure 4.35. The lines represent the values estimated by equations 4-14 and 4-16 and the solid symbols are the corresponding experimental data. It is observed that the proposed equations are able to predict the U-shaped trend in $\varepsilon_{jsg}$ versus $C_v$ results for all impellers reasonably well. Especially, the equations are able to predict the minimum $\varepsilon_{jsg}$ values in the U-shaped curves. The $(C_v)_{OSC}$ values determined corresponding to minimum $\varepsilon_{jsg}$ values using the plots of equations 4-14 and 4-16 are listed in Table 4.10.

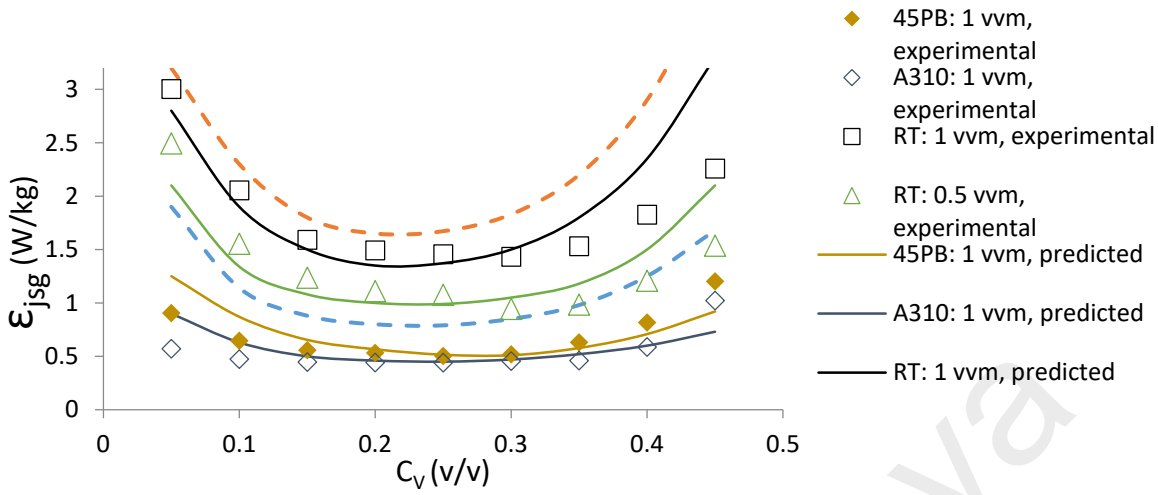


Figure 4.35 Values of impeller specific power predicted by the proposed equations (16) and (18) versus $C_v$ using A= 0.13, $\rho_l$ = 1000 kg/m$^3$, $\rho_s$ = 2500 kg/m$^3$, S = 4.39 (assumed to be constant for all impellers), k = 1.69, 1.315 and 2.44 for A310, 45PB, and RT impellers, respectively

Table 4.10 $(Cv)_{OSC}$ values predicted by equations 4-14 and 4-16 for all mixing systems involved in the present work

| Impellers | $N_p^*$ | $k^*$ | Gas flow rates (vvm) | Predicted $(C_v)_{OSC}$ |
|---|---|---|---|---|
| RT | 3.502 | 2.447 | 0.5 | 0.25 |
| | | | 0.75 | 0.2 |
| | | | 1 | 0.2 |
| 45PB | 1.391 | 1.315 | 0.5 | 0.2 |
| | | | 0.75 | 0.25 |
| | | | 1 | 0.3 |
| A310 | 0.734 | 1.169 | 0.5 | 0.2 |
| | | | 0.75 | 0.2 |
| | | | 1 | 0.25 |

*According to Bubbico et al.

By comparing the results shown in Table 4.10 with the experimental data shown in Table 4.4, it could be concluded that equations 4-14 and 4-16 can estimate $(C_v)_{OSC}$ values with a reasonable accuracy for different mixing systems, in spite of various assumptions made in its development. Furthermore, the equations provide acceptable predictions for systems operating at different gas flow rates. On that note, it would be interesting to assess the interpolation and extrapolation capabilities of the proposed model. Thus, the $\varepsilon_{jsg}$ values predicted by the model for gas flow rates of $Q_g$ = 0.3 and 1.2 vvm are plotted in Figure 4.35. It is clear that model produces acceptable results for unseen data.

### 4.7.2 Estimation of Sauter mean bubble diameter

Experiments were conducted in this work to study the effect of operating parameters and impeller types on $d_{32}$ values. It is of interest to develop a mathematical equation to predict $d_{32}$ values for different operating conditions.

The experimental data obtained in this work were divided into two groups based on the size of solid particles used. The experiments carried out with BGB 370 were used to determine the empirical constants, and the ones obtained using BGB 680 served as a set of 'unseen' data, utilized to validate the mathematical equation and check if the developed equation could be fully predictive.

By assuming that bubble breakage governs bubble size in a turbulent flow, Hinze (1955) proposed a relationship suggesting that surface tension forces balanced the disruptive forces on bubbles that are caused by turbulent fluctuations. Generally, bubbles break when the ratio of two forces exceeds a critical value. Taking into the account of Kolmogoroff's theory of isotropic turbulence, an equation to calculate the maximum stable diameter ($d_{max}$) was proposed (Calderbank, 1958):

$$d_{max} = C\left(\frac{\sigma^{3/5}}{\varepsilon^{2/5}\rho^{3/5}}\right) \qquad \textbf{4-20}$$

where σ, ρ, and ε correspond to surface tension ($Nm^{-1}$), liquid density ($kg/m^3$), and energy dissipation rate per unit mass. It is commonly assumed that Sauter mean diameter ($d_{32}$) is proportional to $d_{max}$ (Parthasarathy et al., 1991) (Alvez et al., 2002), resulting in:

$$d_{32} = C'\left(\frac{\sigma^{3/5}}{\varepsilon^{2/5}\rho^{3/5}}\right) \qquad \textbf{4-21}$$

On empirical ground, this equation was then modified to include the effect of gas holdup (Calderbank, 1958):

$$d_{32} = C'' \left( \frac{\sigma^{3/5}}{\varepsilon^{2/5} \rho^{3/5}} \right) \emptyset_g^{1/2} \qquad \textbf{4-22}$$

In the present work, we replaced ρ with $\rho_{slurry}$ for three-phase systems, which can be calculated using the equation 4-19.

The energy dissipation rate per unit mass in Equation 4-22 is considered as the power consumed by an impeller on the basis of the total mass of the suspended solids:

$$\varepsilon = \frac{P}{M} = \frac{N_p \rho_{slurry} N_{jsg}^3 D^5}{\rho_l V_l} = \frac{N_p \rho_{slurry} N_{jsg}^3 D^5}{\rho_l V (1 - C_v)} \qquad \textbf{4-23}$$

where V and $V_l$ refer to the tank and liquid volumes ($m^3$), respectively. $N_{js}$ in a solid-liquid system can be determined using the well-known correlation proposed by Zwietering (1958) (Eq 4-12 and 4-13)

Thus, an equation for determining $N_{jsg}$ for the RT impeller can be derived as follows:

$$N_{jsg} = \left( \frac{Sv^{0.1} d^{0.2} \left( \frac{g \Delta \rho}{\rho_l} \right)^{0.45}}{D^{0.85}} \right) \left( \left( \frac{\rho_s}{\rho_l} \right) \left( \frac{C_v}{1 - C_v} \right) \times 100 \right)^A + 0.85 \emptyset_g \qquad \textbf{4-24}$$

Dohi et al. (1991) proposed a correlation (Eq 4-25) for determination of $\emptyset_G$ in a three-phase system based on Kolmogoroff's theory of isotropic turbulence:

$$\frac{\emptyset_G}{1-\emptyset_G} = 0.153 \left\{ \frac{\frac{P_g}{Q_g}}{\rho_{leff}\left(\frac{g\mu_{leff}}{\rho_{leff}}\right)^{\frac{2}{3}}} \right\}^{\frac{2}{15}} \left\{ \frac{Q_g}{(gD^5)^{\frac{1}{2}}} \right\}^{\frac{4}{5}} \left(\frac{gD^2\rho_{leff}}{\sigma}\right)^{0.2} \left\{ \frac{\left(\frac{\mu_{leff}}{\rho_{leff}}\right)^2}{gD^3} \right\}^{\frac{2}{45}}$$

**4-25**

$$\left(\frac{\rho_g}{\rho_{leff}}\right)^{1/15} \left(\frac{\rho_{leff}}{\rho_{leff} - p_g}\right) \left(\frac{\mu_{leff}}{\mu_l}\right)^{-1/4}$$

where $P_g$ is the power input in a three-phase system (W) and σ is interfacial tension ($Nm^{-1}$).

Figure 4.36 provides a comparison of the current experimental gas holdup values for the RT impeller with the ones predicted by Equation (4-25) for a wide range of solids concentration (0.01-0.25 v/v). It is clear that almost all experimental data are within 20% of values predicted by equation (4-25).

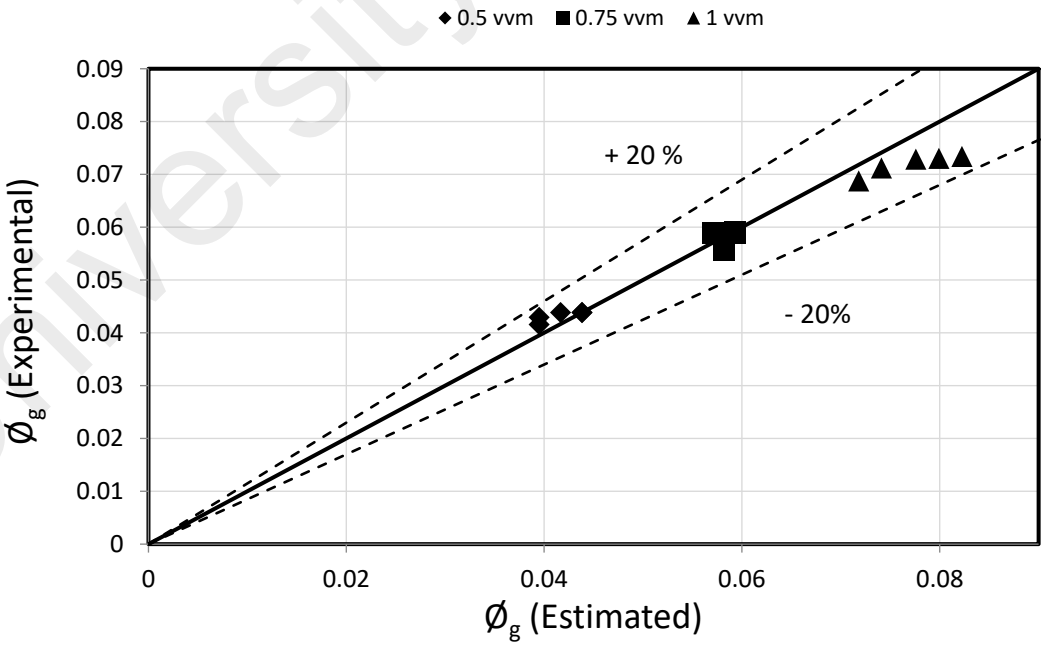


Figure 4.36 Comparison between experimental $\emptyset_g$ values and those obtained using equation (4-25): impeller: RT, particles: BGB 370

Therefore, Equation 4-25 can be used in Equation 4-22 to determine $Ø_g$. Having obtained equation for $\varepsilon$ and $Ø_g$, equation 4-22 can now be used to determine the constant C″.

The experimental values of $d_{32}$ are plotted in Figure 4.37 against the group $\left(\left(\frac{\sigma^{3/5}}{\varepsilon^{2/5}\rho^{3/5}}\right)\emptyset_g^{1/2}\right)$ to determine the constant 'C″' as per equation (4-22).

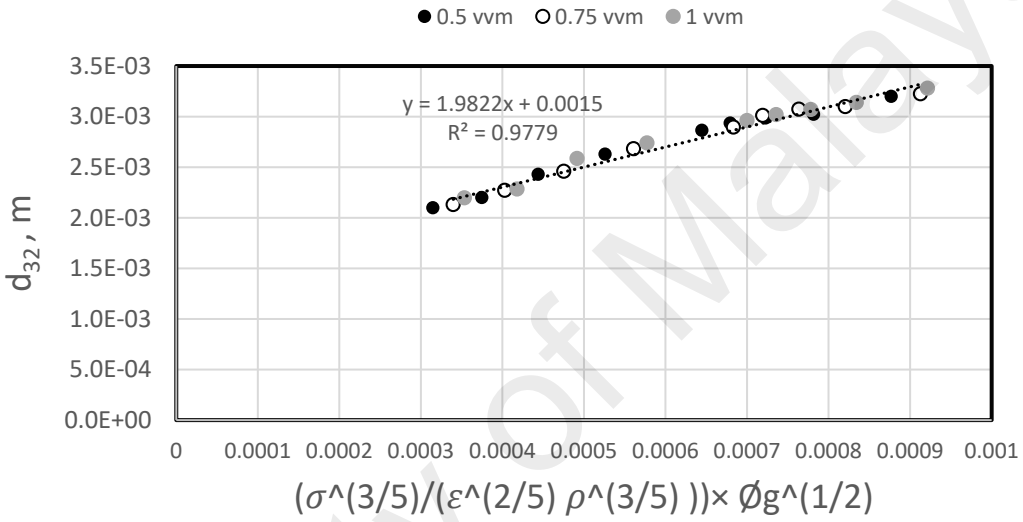


Figure 4.37 $d_{32}$ plotted against group $\left(\frac{\sigma^{3/5}}{\varepsilon^{2/5}\rho^{3/5}}\right)\emptyset_g^{1/2}$, impeller: RT, particle: BGB 370

It can be seen from Figure 4.37 that $d_{32}$ has a linear relationship with the group $\left(\frac{\sigma^{3/5}}{\varepsilon^{2/5}\rho^{3/5}}\right)\emptyset_g^{1/2}$. A linear regression analysis was carried out, and the slope of the straight line was found to be 1.98 which is the value of C″ in equation (4-22). Now equation (4-22) for the estimation of $d_{32}$ value in gas-liquid-solid stirred vessels equipped with RT impeller can be rewritten as:

$$d_{32} = 1.98\left(\frac{\sigma^{3/5}}{\left(\frac{N_p\rho_{slurry}\left(N_{js}+0.85Q_g\right)^3 D^5}{\rho_l V(1-C_v)}\right)^{2/5}\rho_{slurry}^{3/5}}\right)\emptyset_g^{1/2} + 0.0015 \quad \textbf{4-26}$$

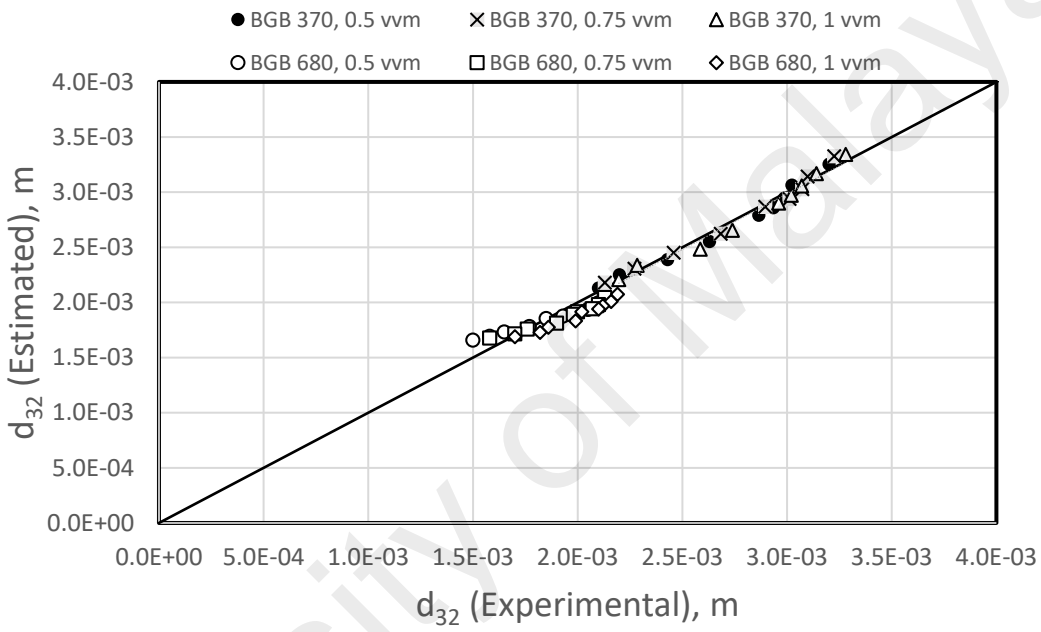


Figure 4.38 Comparison between d32 values estimated by Equation (4-26) with the experimental values, impeller: RT

The proposed correlation can predict $d_{32}$ values for a wide range of parameters. The $d_{32}$ values estimated by Equation (4-26) are compared with the experimental results in Figure 4.38. A least-square analysis on the results gives a straight line with slope of 0.99 and $R^2$ = 0.977, which confirms the validity of the proposed equation in estimating $d_{32}$ values for a wide range of $C_v$ and $Q_g$ in a three-phase stirred vessel agitated by a Rushton turbine impeller.

It was explained earlier that the proportional constant 'C″' in Equation 4-22 was calibrated using the experimental results obtained with BGB 370. In order to validate the estimation capability of the proposed equation, Figure 4.38 also includes the experimental and estimated $d_{32}$ values for BGB 680. The results of BGB 680 were not involved in the original calibration process, and they were solely used to check whether the proposed correlation was fully predictive. It can be observed that Equation (4-26) was able to predict 'unseen' data with satisfactory agreement.

Moreover, Equation 4-26 suggests that an increase in $N_{js}$, and consequently power consumption, results in smaller $d_{32}$ values, which is in agreement with the experimental findings. It can be commented that as the energy input increases, the impeller rotates faster and inserts more energy into the system, which results in generation of a large number of smaller gas bubbles. On that note, increase in solids particle size would leads to formation of smaller bubble as the agitation speed has to be enhanced to keep the solid in suspension form. This explanation is supported by Equations 4-6 and 4-26, which indicate larger particles (d) demand higher impeller speed to stay fully suspended, and higher impeller speed ($N_{js}$) leads to smaller $d_{32}$ values.

### 4.7.3 Estimation of gas-liquid interfacial area

It is now possible to derive an equation for the estimation of gas-liquid interfacial area ($a_{g\text{-}l}$) in the presence of particles by combining Equations 4-7, 4-23, and 4-26:

$$a_{g-l} = \frac{6\emptyset_g}{d_{32}} \qquad 4\text{-}7$$

$$\varepsilon = \frac{P}{M} = \frac{N_p \rho_{slurry} N_{jsg}^3 D^5}{\rho_l V_l} = \frac{N_p \rho_{slurry} N_{jsg}^3 D^5}{\rho_l V (1-C_v)} \qquad 4\text{-}23$$

$$d_{32} = 1.98\left(\frac{\sigma^{3/5}}{\left(\frac{N_p\rho_{slurry}\left(N_{js}+0.85Q_g\right)^3 D^5}{\rho_l V(1-C_v)}\right)^{2/5}\rho_{slurry}{}^{3/5}}\right)\emptyset_g^{1/2} + 0.0015 \qquad 4\text{-}26$$

$$a_{g-l} = \frac{6\emptyset_G}{2\left(\frac{\sigma^{3/5}}{\left(\frac{N_p\rho_{slurry}\left(N_{js}+0.85Q_g\right)^3 D^5}{\rho_l V(1-C_v)}\right)^{2/5}\rho_{slurry}{}^{3/5}}\right)\emptyset_g^{1/2} + 0.0015} \qquad \textbf{4-27}$$

Values of $\alpha_{g\text{-}l}$ estimated by Equation (4-27) are plotted against the experimental data in Figure 4.39. It is clear that equation (4-27) was able to predict $\alpha_{g\text{-}l}$ values with acceptable accuracy.

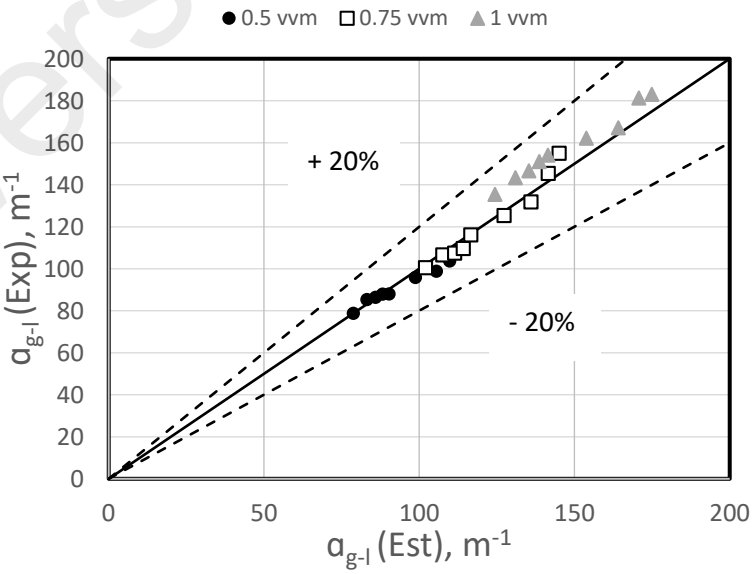


Figure 4.39 Comparison between experimental αg-l values and those estimated by Equation 4-27, impeller: RT, solid particle: BGB 370

Similar analysis was performed to develop equations for $d_{32}$ and $a_{g\text{-}l}$ for the 45PB impeller. The proportionality constant 'C″' in Equation (4-22) was found to be 0.5559 for this impeller. A least-square analysis gives a straight line with slope of 0.97 and $R^2 = 0.97$ in $d_{32}$ (estimated) vs $d_{32}$ (experimental) plot for BGB370 particles for 45PB impeller. The experimental $a_{g\text{-}l}$ values for 45PB impeller were found to lie within ± 25% of the predicted $a_{g\text{-}l}$ values.

According to equation 4-25, an increase in power input leads to higher values of gas holdup. In contrary, an increase in power consumption leads to generation of smaller bubbles based on the relationship shown in equation 4-26. Thus, it can be commented that, at $N_{js}$, an increase in gas holdup results in formation of smaller gas bubble.

In overall, it can be observed that the predictions of the mathematical models proposed in this have acceptable agreement with the experimental results. To the best of author's knowledge, correlations to predict specific impeller power consumption ($\varepsilon_{jsg}$), Sauter mean bubble diameter ($d_{32}$), and gas-liquid interfacial area ($a_{g\text{-}l}$) in three-phase stirred tanks area absent in the literature. The proposed models in this study can be very beneficial in design and operation of stirred tanks as they encompass a wide range of important parameters.

## 4.8 Implementing of the proposed strategies

Using the results reported in the previous sections, optimization strategies can be proposed for power consumption of three-phase stirred vessels through adjusting the design and operating factors. An example is described here to highlight the advantages of implementing some of these strategies. Four mixing systems operating at $N_{jsg}$ are shown in Figure 4.40. Here are details of the four tanks in this Figure:

- existing design 'baffled tank operating with A310'

- modified design ‘unbaffled tank operating with A310’
- modified design ‘baffled tank operating with 0.5 PB’
- modified design ‘unbaffled tank operating with 0.5 RT’

All tanks are 0.4 m (T) in diameter with unaerated liquid height equal to the tank diameter. Four equally spaced baffles with a length of 4 cm (0.1D) were present along the entire height of the baffled tanks. The impeller clearance (C) was 0.25 T for all systems. Values of $N_{jsg}$, $P_{jsg}$, and $\varepsilon_{jsg}$ were determined using the procedures explained earlier in the methodology. Figure 4.40a shows a mixing tank agitated by an A310-impeller operating at $C_v$ = 0.1 v/v and $Q_g$ = 1 vvm. Axial-flow impellers are known for low power numbers, and it is generally believed that baffle removal decreases impeller power input. Therefore, Figure 4.40b depicts a tank operating at similar conditions as the first tank but under unbaffled configurations. It was observed that the minimum energy required by A310 to suspend solid particles off the tank bottom increased upon removal of baffles. In this particular case, the tank with baffles installed was more energy efficient, implying that baffle removal did not always serve as a reliable strategy to minimize the power input of a three-phase stirred vessel.

The mixing tank shown in Figure 4.40d had a 0.5 PB impeller operating at a solid concentration of $C_v$=0.15 v/v and gas flow rate of 0.5 vvm. Although the tank with 0.5 PB was operating at a solid concentration 1.5 times higher than that in the first tank, it was evident that it consumed less power at $N_{jsg}$. Compared to the unbaffled tank shown in Figure 4.40b, the baffled tank agitated by 0.5 PB impeller suspended more solids by consuming less amount of energy. The stirred vessel equipped with 0.5 RT impeller (Figure 4.40c) handled higher solids concentration than the other three ($C_v$ = 0.2), but required the least amount of energy to provide complete off-bottom suspension. Therefore, the tanks with designs ‘a’ and ‘b’ were considered underperforming compared

to the last two designs. By comparing the performance of tanks 'c' and 'd' with the original design (Figure 4.40a), it was logical to conclude that the efficiency of baffle removal strategy for power consumption optimization was strictly dictated by the impeller used and the operating conditions.

A great deal of energy could be saved by using low specific power value ($\varepsilon_{jsg}$ (W/kg)) that could be achieved through proper selection of operating conditions and designing factors. In other words, this example demonstrated that a remarkable improvement in $C_v$ could be obtained with a significant reduction in $\varepsilon_{jsg}$ by following the strategies proposed in this study.

Reduction in power between designs 'a' and 'd' was determined using the following equation:

$$Improvement\ in\ P = \frac{P_{jsg,'a'} - P_{jsg,'d'}}{P_{jsg,'a'}} \times 100 = \frac{127.6 - 118.32}{127.6} \times 100 = 7.3\% \quad \textbf{4-28}$$

where $P_{jsg,\ 'a'}$ and $P_{jsg,\ 'd'}$ (W/m$^3$) refer to the power values of the tanks with designs 'a' and 'd' (depicted in Figures 4.40a and 4.40d), respectively. By expressing the power on the basis of the mass of solid that was suspended in each tank ($\varepsilon_{jsg}$), the reduction in specific power obtained through implementing the strategies was significantly greater:

$$Improvement\ in\ \varepsilon_{jsg} = \frac{\varepsilon_{jsg,'a'} - \varepsilon_{jsg,'d'}}{\varepsilon_{jsg,'a'}} \times 100 = \frac{(\frac{127.6}{11.68}) - (\frac{118.32}{23.36})}{(\frac{127.6}{11.68})} \times 100 = 53.6\% \quad \textbf{4-29}$$

It was obvious that the tank with poor design (Figure 4.40a) was underperforming compared to the tank with 0.5 RT as it required more energy to suspend smaller quantity of solid.

The proposed strategies will lead to greater energy efficiency in three-phase mechanically agitated stirred tanks and minimized their operating costs. Moreover, the enhanced $C_v$ in the optimized tanks may help to improve the product yield and the last two tanks exhibited higher particle dispersion, indicated by higher $H_S$ in the last two designs.

In short, the advantages of proper selection of operating and design factors in three-phase stirred tanks included reduction in impeller speed and power consumption improvement in process yield, enhancement in energy efficiency per unit mass of solid in the tank and enhancement in solid dispersion.

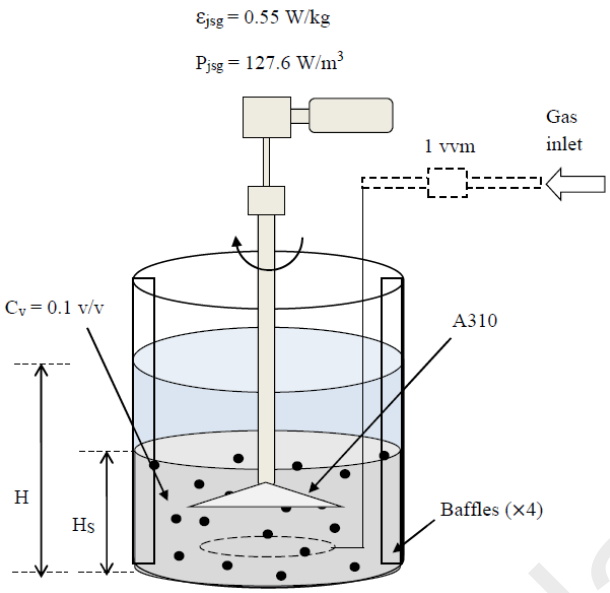


a

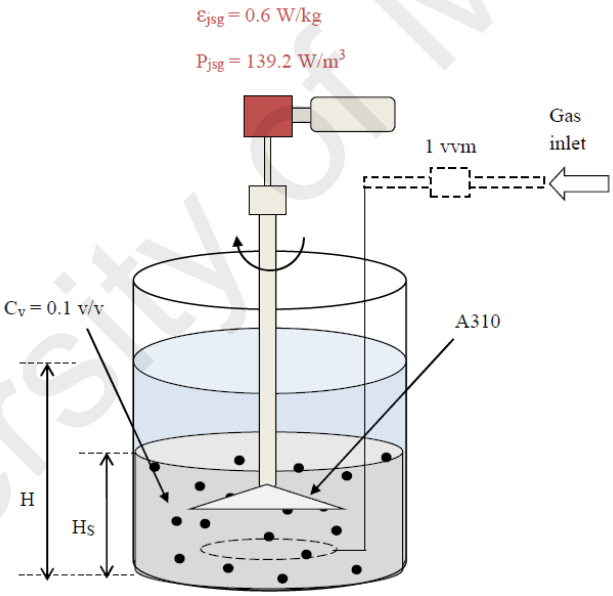


b

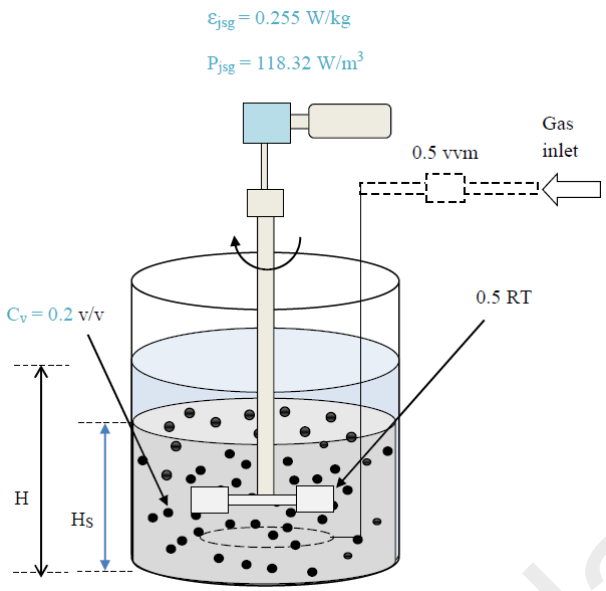


c

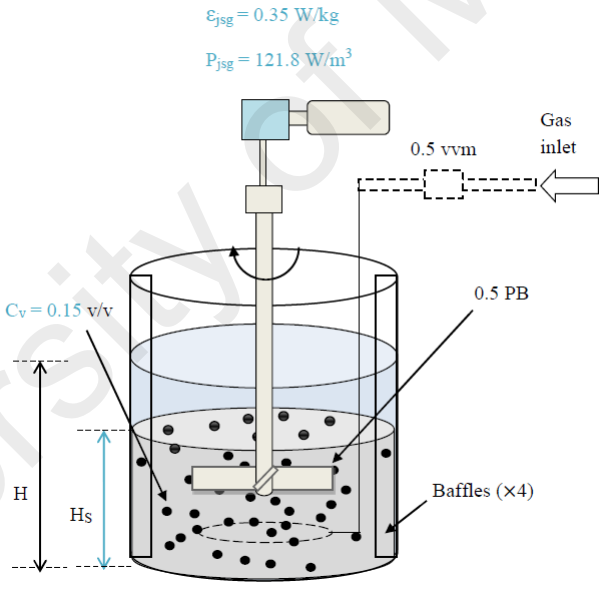


d

Figure 4.40 Improving energy efficiency in three-phase stirred vessels through modifications in design and operating conditions: solid particle : $BGB_{370}$.

## 4.9 Conclusion

In this chapter, through extensive experimentation and mathematical evaluation, systematically investigates the effects of various variables such as solids concentration,

gas flow rate, particle size, impeller type and baffling conditions on specific power consumption in solid-liquid and gas-solid-liquid mechanically agitated vessels.

Experimental results indicate that power per unit solids mass generally decreases with solids concentration, reaches a minimum value and thereafter increases, for all impeller types used. It is found that, therefore, the specific power can be minimized by operating at an optimum solids concentration, in the range of 20 – 30% (v/v) for the slurry properties, impeller types and baffling conditions considered in this paper. These results also suggest that operating the process at higher solids concentration is superior to that with low solids loading owing to relatively low specific power input required for operating the tanks with greater amount of solids.

A baffling efficiency factor $R_\varepsilon$ is defined to determine the savings in specific power input due to the removal of baffles. It is concluded the specific power required to suspend solids from a vessel bottom generally decreases on removal of the baffles if agitation is provided by a radial-flow impeller. R values of mixed- and axial-flow impellers were directly influenced by the operating conditions.

It was also observed that radial-flow impellers generate smaller bubbles compared to mixed-flow impellers at any given $C_v$ or $Q_g$. It was also noticed that average bubble size in a stirred vessel is highly influenced by power input to the system. Accordingly, an increase in particle size led to generation of smaller gas bubbles due to the fact that keeping larger particles in suspension demands higher power input. It was seen that increase in solids concentration is an effective approach to enhance the gas-liquid interfacial area in three-phase stirred vessels. By taking the role of power consumption into account, it was concluded that there is an optimum solids concentration at which impeller's performance in terms of power efficiency and ability to generate large gas-liquid interfacial area can be maximized. This chapter also proposes reliable mathematical

models to estimate specific impeller power input, average bubble size and gas-liquid interfacial area in three-phase systems.

# CHAPTER 5: CONCLUSION AND FUTURE RECOMMENDATION

## 4.10 Conclusion

The first part of the present work was focusing on the suspension of solids in two- and three-phase stirred vessels. The impeller energy efficiency of a mixing system was studied over a range of solids concentrations, solids particle size, gas flow rates, baffling configuration and impeller specifications. Power measurements in this study are linked to the mass of solids suspended in the agitation system based on the consideration that the rates of dissolution and reaction can to a great extent be related to the exposure of maximum surface area to liquid or amount of solids, but actually not be affected by the volume of the system or agitation once complete suspension is achieved.

Our initial observations showed that the specific impeller power consumption under aerated condition (as a function of the total volume of the liquid ($P_{jsg}/V$)) increased with increasing solids concentration. On the contrary, ($P_{jsg}/M_s$) or $\varepsilon_{jsg}$ tended to decrease with increasing $C_v$ up to a critical value, which was labeled as the optimum solid concentration ($C_v$)$_{OSC}$, and started increasing afterwards. These U-shape $\varepsilon_{jsg}$ versus $C_v$ graphs were found for all impellers studied in this work under both aerated and unaerated conditions. A term called as the power efficiency factor (reciprocal of ($P_{jsg}/M_s$)), $\varepsilon_{jsg}^{-1}$ (kg/W) was used as an indicator of the amount of solid particles that could be suspended per unit of the consumed power. It was found that the $\varepsilon_{jsg}^{-1}$ could be maximized by operating the stirred vessel within an optimum range of solids concentration. It was also noted that the introduction of gas has a huge impact on the performance of the impellers studied in this

work. The mixed flow impeller with a large diameter (0.5 PB) exhibited the most satisfactory results under aerated conditions compared to the others. Within a particular range of solids concentration, the $\varepsilon_{jsg}^{-1}$ values for this impeller under aerated conditions were higher compared to those under unaerated conditions. Effects of gassing rate on power consumption of all the five impellers studied were thoroughly examined and discussed.

Another term, known as baffling efficiency factor 'R', was defined to study the effect of baffle removal on $\varepsilon_{jsg}^{-1}$ of different impellers. It was observed that at certain conditions, baffle removal could have negative effects on power efficiency of mixed- and axial-flow impellers. It was also discussed that increase in particle size led to decrease in $\varepsilon_{jsg}^{-1}$ values which was more evident upon removal of baffles. Furthermore, the results indicated that it was possible to obtain complete solid dispersion with reduced power input, whilst the solids were suspended from the tank bottom. Improved energy efficiency is critical for operating the gas-solid-liquid agitated vessels at high solids concentration. This can be achieved by using large power number impellers and the removal of baffles.

It was found that the radial-flow impellers were the most efficient in handling gas phase leading to highest gas hold-up. The gas hold-up increased with gas flow rate but decreased with increasing solids concentration. Based on the experimental results of impeller power consumption, a mathematical correlation that could predict the values of $\varepsilon_{jsg}$ as a function of solid concentration, gas flow rate and impellers geometry was developed and proposed. Predictions of a mathematical equation based on previous correlations demonstrate that all suspensions have an optimum solids concentration where the power per unit mass of solids is at a minimum.

Experimental results obtained in this part of the study provided a clear picture of how gas introduction, gas flow rate, impeller type, impeller diameter, and baffling configuration influence values of optimum solids concentration in multi-phase stirred tanks.

At the next stage of the study, an underwater recording system was designed by which values of $d_{32}$ and gas-liquid interfacial area for a wide range of solids concentration were determined. It was initially observed that an increase in solids concentration led to lower values of $d_{32}$ at any given gas flow rate, while an increase in $Q_g$ resulted in higher $d_{32}$ values at any given $C_v$. By considering the effect of $C_v$ on $Ø_g$ and $d_{32}$ values, it was concluded that increasing volumetric solids concentration was an effective strategy not only to achieve process intensification, but also to maximize the contact area between gas and liquid phases, and thereby to increase the rate of transfer processes. In the next part of the study, another critical aspect, known as impeller power efficiency, was considered in the evaluation of the benefits of process intensification for a multi-phase stirred tank. It was concluded that although $\alpha_{g-l}$ values tend to increase as $C_v$ increases, there were restrictions in terms of impeller's power efficiency to achieve complete off-bottom suspended condition. In the final part of the study, correlations were proposed for the estimation of $d_{32}$ and $\alpha_{g-l}$ in gas-solid-liquid stirred vessels handling solids concentrations for $C_v$=0.01 to 0.25 v/v. The reliability of the proposed correlations was confirmed by the satisfactory agreement between the experimental results and the values estimated by the proposed correlations.

The thesis also discussed an example that demonstrated that significant energy saving could be achieved in three-phase agitated systems by applying proper modifications to the design and operating parameters.

In short, the advantages of process intensification in three-phase stirred tanks include reduction in impeller speed and power consumption, improvement in throughput or

process yield, enhancement in impeller power efficiency per unit mass of solid in the tank, enhancement in solid dispersion, reduction in the average bubble size, and improvement in the gas-liquid interfacial area.

### 4.11 Recommendation for future works

In this work all experiments were carried out in a single-impeller system. Some reports in the literature suggest that using a set of multiple impellers improves the efficiency of solids suspension and gas dispersion in the system. Thus, it would be interesting to study power efficiency and gas-liquid hydrodynamics in three-phase systems agitated by various sets of impellers, and compare the findings with the results presented in this work.

The present study used a tank with a diameter of 0.39 m for all experiments. The values of optimum solids concentration may vary with a change in the tank diameter. Thus, investigations are required using a larger tank to determine the effect of the scale-up on the specific power and gas-liquid hydrodynamics.

In addition, viscous mixing is widely applied in many industrial applications. However, the effect of viscosity on $N_{js}$, specific power consumption, bubble size, and gas hold has been broadly neglected. This absence of information warrants further investigations.

# References


Alves, S. S., Maia, C. I., Vasconcelos, J. M. T., Serralheiro, A. J. (2002) Bubble size in aerated stirred tanks. *Chemical Engineering Journal*, 89, (1–3), 109-117.

Archis A.Y, Viswas G.P. and Anthony A.C.M.B, (2002) "Gas hold-up in stirred tank reactors", Canadian Journal of Chem Eng., vol. 80, page 158-166.

Bates R.L., Fondy, P.L and Fenic, J.G., (1966) "Impeller characteristics on power": Theory and practice volume I, Eds: Unl, V.W. and Gray, J.B, Academic press., New York, Chapter 3.

Bailey, M.; Gomez, C. O.; Finch, J. A. (2005) Development and application of an image analysis method for wide bubble size distributions. *Minerals Engineering*, 18, (12), 1214-1221.

Barigou, M.; Greaves, M. (1991) A capillary suction probe for bubble size measurement. *Measurement Science and Technology*, 2, (4), 318.

Barigou, M.; Greaves, M. (1992) Bubble-size distributions in a mechanically agitated gas—liquid contactor. *Chemical Engineering Science*, 47, (8), 2009-2025.

Behkish, A.; Lemoine, R.; Sehabiague, L.; Oukaci, R.; Morsi, B. I. (2007) Gas holdup and bubble size behavior in a large-scale slurry bubble column reactor operating with an organic liquid under elevated pressures and temperatures. *Chemical Engineering Journal*, 128, (2–3), 69-84.

Boden, S.; Bieberle, M.; Hampel, U. (2008) Quantitative measurement of gas hold-up distribution in a stirred chemical reactor using X-ray cone-beam computed tomography. *Chemical Engineering Journal*, 139, (2), 351-362.

Bohnet, M.; Niesmak, G. (1980) Distribution of solids in stirred suspensions. *Germ. Chem. Eng*, 3, 57–65.

Bombač, A.; Žun, I.; Filipič, B.; Žumer, M. (1997) Gas-filled cavity structures and local void fraction distribution in aerated stirred vessel. *AIChE Journal*, 43, (11), 2921-2931.

Bombač, A.; Žun, I. (2000) Gas-filled cavity structures and local void fraction distribution in vessel with dual-impellers. *Chemical Engineering Science*, 55, (15), 2995-3001.

Bouaifi, M.; Hebrard, G.; Bastoul, D.; Roustan, M. (2001) A comparative study of gas hold-up, bubble size, interfacial area and mass transfer coefficients in stirred gas–liquid reactors and bubble columns. *Chemical Engineering and Processing: Process Intensification*, 40, (2), 97-111.

Bourne, J.R. & Sharma, R.N. (1974) "Homogenous Particle Suspension in Propeller-Agitated Flat Bottom Tanks," Chem. Eng. J. 8, 243-250.

Boyer, C.; Duquenne, A.-M.; Wild, G. (2002) Measuring techniques in gas–liquid and gas–liquid–solid reactors. *Chemical Engineering Science*, 57, (16), 3185-3215.

Brucato, A.; Cipollina, A.; Micale, G.; Scargiali, F.; Tamburini, A. (2010) Particle suspension in top-covered unbaffled tanks. *Chemical Engineering Science*, 65, (10), 3001-3008.

Bruijn, W., Van't Riet, K., and Smith, J.M. (1974) 'Power consumption with aerated Rushton turbines', *Trans IChemE,* vol. 52, pp. 88-104.

Bubbico, R.; Cave, S. D.; Mazzarotta, B. (1998) Agitation power for solid-liquid suspensions containing large particles. *The Canadian Journal of Chemical Engineering*, 76, (3), 428-432.

Bujalski, W., Konno, M., Nienow, A.W., (1988), 'Scale up of 45-degree pitch blade agitators for gas dispersion and solid suspension', *6th European Conference on Mixing, Pavia, Italy: 24-26 May* pp. 389-398.

Busciglio, A.; Grisafi, F.; Scargiali, F.; Brucato, A. (2013) On the measurement of local gas hold-up, interfacial area and bubble size distribution in gas–liquid contactors via light sheet and image analysis: Imaging technique and experimental results. *Chemical Engineering Science*, 102, 551-566.

Buurman, C.; Resoort, G.; Plaschkes, A. (1986) Scaling-up rules for solids suspension in stirred vessels. *Chemical Engineering Science*, 41, (11), 2865-2871.

Cieszkowski, J., and Dylog, M. (1994) "The gas-liquid interface in a three-phase reactor with a mechanical agitator", *International Chemical Engineering*, vol. 34: 527 - 538.

Chapman, C.M., Nienow, A.W., Cook, M. & Middleton, J.C. (1983) "Particle-Gas-Liquid Mixing in Stirred Vessels. Part I: Particle-Liquid Mixing," Chem. Eng. Res. Des. 61, 71-81.

Chowdry, N. H.; Penney, W. R.; Myers, K. J.; Raasano, J. B. (1995) In *An Experimental Investigation of Solids Suspension at High Solids Loadings in Mechanically Agitated Vessels, Industrial Mixing Fundamental with Applications*, AIChE Symp. Ser., pp 131–138.

Dohi, N.; Matsuda, Y.; Itano, N.; Shimizu, K.; Minekawa, K.; Kawase, Y. (1999) MIXING CHARACTERISTICS IN SLURRY STIRRED TANK REACTORS WITH MULTIPLE IMPELLERS. *Chemical Engineering Communications*, 171, (1), 211-229.

Dohi, N.; Takahashi, T.; Minekawa, K.; Kawase, Y. (2004) Power consumption and solid suspension performance of large-scale impellers in gas–liquid–solid three-phase stirred tank reactors. *Chemical Engineering Journal*, 97, (2–3), 103-114.

Drewer, G. R.; Ahmed, N.; Jameson, G. J. (1994) Suspension of High Concentration Solids in Mechanically Stirred Vessels. *IChemE Symp. Ser*, 135, (41).

Drewer, G.R., Ahmed, N. & Jameson, G.J. (2000) "An Optimum Concentration for the Suspension of Solids in Stirred Vessels," *Mixing and Crystallization*.

Einenkel ,W. D., Mersmann, A. Verfahrenstechnik, (1977) 11, p. 90.

Ford, J. J.; Heindel, T. J.; Jensen, T. C.; Drake, J. B. (2008) X-ray computed tomography of a gas-sparged stirred-tank reactor. *Chemical Engineering Science*, 63, (8), 2075-2085.

Frijlink, J.J., Bakker, A. & Smith, J.M. (1990) "Suspension of Solid Particles with Gasses Impellers," *Chem. Eng. Sci*. 45, 1703–1718.

Gao, Z.; Smith, J. M.; Müller-Steinhagen, H. (2001) Void fraction distribution in sparged and boiling reactors with modern impeller configuration. *Chemical Engineering and Processing: Process Intensification*, 40, (6), 489-497.

Gray. D.J., R.E, Treybal and S.M. Bernet. (1987) *AlChe Journal* vol 28, page 195, 1982.

Hampel, U.; Hristov, H. V.; Bieberle, A.; Zippe, C. (2007) Application of high-resolution gamma ray tomography to the measurement of gas hold-up distributions in a stirred chemical reactor. *Flow Measurement and Instrumentation*, 18, (5–6), 184-190.

Hassan I.T.M. and Robinson, K.A.H. ( 1984) "Measurement of bubble size distribution in turbulent gas-liquid dispersions", Chem. Eng. Res. Des, vol. 62, page 3-12.

Hinze, J. O. (1955) Fundamentals of the hydrodynamic mechanism of splitting in dispersion processes. *AIChE Journal*, 1, (3), 289-295.

Honkanen, M.; Eloranta, H.; Saarenrinne, P. (2010) Digital imaging measurement of dense multiphase flows in industrial processes. *Flow Measurement and Instrumentation*, 21, (1), 25-32.

Horn, D., Montante, G., Magelli, F., Paglianti, A. (2007) In *Bubble size distribution and turbulent two-phase flow in aerated stirred vessel*, Proceedings of the 6th International Conference on Multiphase Flow, Leipzig,Germany, 2007; Leipzig,Germany.

Hosseini, S.; Patel, D.; Ein-Mozaffari, F.; Mehrvar, M. (2010) Study of Solid−Liquid Mixing in Agitated Tanks through Computational Fluid Dynamics Modeling. *Industrial & Engineering Chemistry Research*, 49, (9), 4426-4435.

Hicks, M. T.; Myers, K. J.; Bakker, A. (1997) CLOUD HEIGHT IN SOLIDS SUSPENSION AGITATION. *Chemical Engineering Communications*, 160, (1), 137-155.

Ibrahim, S., Nienow, A. W. (2009) The effect of viscosity on particle suspension in an aerated stirred vessel with different impellers and bases. *Chemical Engineering Communications*, 197, (4), 434-454.

Jafari, R. (2010) SOLID SUSPENSION AND GAS DISPERSION IN MECHANICALLY AGITATED VESSELS. University of Montreal.

Jirout, T., Moravec, J., Rieger, F., Sinevic, V., Spidla, M., Sobolic, V., Tihon, J. (2005) Electrochemical measurement of impeller speed for off-bottom suspension. *Inzynieria chemiczna i procesowa*, 26, 485–497.

Kamiwano, M.; Kaminoyama, M.; Nishi, K.; Shirota, D. (2003) The measurement of bubble diameter distributions and liquid side mass transfer coefficients in a gas-liquid agitated vessel using a real-time,high-speed image processing system. *Chemical Engineering Communications*, 190, (9), 1096-1114.

Kasat, G. R.; Pandit, A. B. (2005) Review on Mixing Characteristics in Solid-Liquid and Solid-Liquid-Gas Reactor Vessels. *The Canadian Journal of Chemical Engineering*, 83, (4), 618-643.

Khopkar, A. R.; Rammohan, A. R.; Ranade, V. V.; Dudukovic, M. P. (2005) Gas–liquid flow generated by a Rushton turbine in stirred vessel: CARPT/CT measurements and CFD simulations. *Chemical Engineering Science*, 60, (8–9), 2215-2229.

Kolmogoroff, A. N. (1941) The local structure of turbulence in an incompressible viscous fluid for very large Reynolds numbers. *Compt. Rend. Acad. Sci. USSR*, 30, 301.

Kolmogoroff, A. N. (1941) On degradation of isotropic turbulence in an incompressible viscous liquid. *Compt. Rend. Acad. Sci. USSR*, 31, 538.

Kolmogoroff, A. N. (1941) Dissipation of energy in locally isotropic turbulence. *Compt. Rend. Acad. Sci. USSR*, 32, 16.

Kolmogoroff, A. N. (1949) The breakup of droplets in a turbulent stream. *Dok. Akad. Nauk. USSR*, 66, 825-828.

Kraume, M., (1992) Mixing times in stirred suspensions. *Chemical Engineering & Technology*, 15, (5), 313-318.

Kurten, H., and P. Zehner, "Slurry Reactors." Germ. Chem. Eng., 2, 220 (1979).

Laakkonen, M., Honkanen, M., Saarenrinne, P., Aittamaa, J. (2005) Local bubble size distributions, gas–liquid interfacial areas and gas holdups in a stirred vessel with particle image velocimetry. *Chemical Engineering Journal*, 109, (1–3), 37-47.

Lau, Y. M.; Deen, N. G.; Kuipers, J. A. M. (2013) Development of an image measurement technique for size distribution in dense bubbly flows. *Chemical Engineering Science*, 94, (0), 20-29.

Linek, V.; Moucha, T.; Sinkule, J. (1996) Gas-liquid mass transfer in vessels stirred with multiple impellers—I. Gas-liquid mass transfer characteristics in individual stages. *Chemical Engineering Science*, 51, (12), 3203-3212.

Loiseau, B., Midonx, N, and Charpenter, J.C. (1977) 'Some hydrodynamic and power input data in mechanically agitated gas-liquid contactors', A.Chem,. Eng. Journal, vol 23, page 931-935.

Lu, W.M., Wu, H.Z. & Ju, M.Y., (1997) "Effect of Baffle Design on the Liquid Mixing in an Aerated Stirred Tank with Standard Rushton Turbine Impellers," Chem. Eng. Sci. 52, 3843–3851.

Lucas, D., Krepper, E., Prasser, H. M., (2005) Development of co-current air–water flow in a vertical pipe. *International Journal of Multiphase Flow*, 31, (12), 1304-1328.

Machon, V., Pacek, A. W., Nienow, A. W., (1997) Bubble Sizes in Electrolyte and Alcohol Solutions in a Turbulent Stirred Vessel. *Chemical Engineering Research and Design*, 75, (3), 339-348.

Manera, A., Ozar, B., Paranjape, S., Ishii, M., Prasser, H. M. (2009) Comparison between wire-mesh sensors and conductive needle-probes for measurements of two-phase flow parameters. *Nuclear Engineering and Design*, 239, (9), 1718-1724.

Markopoulos, J., Babalona, E. & Tsiliopoulou E. (2004) "Power Consumption in Agitated Vessels with Dual Rushton Turubines: Baffle Length and Impeller Spacing Effects," Chem. Eng. Technol. 27, 11.

Markopoulos, J., Babalona, E., Tsiliopoulou, E. & Tasopoulou, K. (2005) "Power Consumption in Agitated Vessels with Dual Pitched Blade Turbines: Baffle Length and Impeller Spacing Effects," Chem. Eng. Technol. 28, 9.

Marsden, J.O. & House, C.I., (2006) "Leaching," The Chemistry of Gold Extraction, the Society for Mining, Metallurgy, and Exploration, Inc, USA.

Massimillia, L.; Solimando, A.; Squillace, E. (1961) *British Chemical Engineering*, 6, 232.

Mersmann, A.; Werner, F.; Maurer, S.; Bartosch, K. (1998) Theoretical prediction of the minimum stirrer speed in mechanically agitated suspensions1. *Chemical Engineering and Processing: Process Intensification*, 37, (6), 503-510.

Micale, G.; Grisafi, F.; Brucato, A. (2002) Assessment of Particle Suspension Conditions in Stirred Vessels by Means of Pressure Gauge Technique. *Chemical Engineering Research and Design*, 80, (8), 893-902.

Montante, G.; Horn, D.; Paglianti, A. (2008) Gas–liquid flow and bubble size distribution in stirred tanks. *Chemical Engineering Science*, 63, (8), 2107-2118.

Musil, L.; Vlk, J., (1978) Suspending solid particles in an agitated conical-bottom tank. *Chemical Engineering Science*, 33, (8), 1123-1131.

Nienow, A. W. (1968) 'Suspension of Solid Particles in Turbine Agitated Baffled Vessel' Chem. Eng. Sci. 23, 1453-1459.

Nienow, A. W. and Wisdom, D. J. (1976) Institution of Chemical Engineers, 3rd Annual Research Meeting, Salford,.

Nienow, A.W., Wisdom, D.J., and Middleton, J.C., (1977), 'The effect of scale and geometry on flooding, recirculation and power in gassed stirred vessels,' *Proceedings of the 2nd European Conference on Mixing*, Cambridge, England, pp. F1-1 to F1-16.

Nienow, A. W.; Bujalski, W. (2002) Recent Studies on Agitated Three-Phase (Gas–Solid–Liquid) Systems in the Turbulent Regime. *Chemical Engineering Research and Design*, 80, (8), 832-838.

Nishikawa, M., Ashiwake, K., Hashimoto, N. & Nagata, S. (1979) "Agitation Power and Mixing Time in Off-Centering Mixing," Int. Chem. Eng. 19(1), 153–159.

Paglianti, A.; Pintus, S. (2001) An impedance probe for the measurements of liquid hold-up and mixing time in two/three-phase stirred tank reactors. *Experiments in Fluids*, 31, (4), 417-427.

Pantula, R. R. K.; Ahmed. (1998) N. In *Solid Suspension and Gas Hold-up in Three Phase Mechanically Agitated Contactor*, Proceedings of the 26th Australian Chemical Engineering Conference (Chemica 98), Port Douglas, Australia,; Port Douglas, Australia, 1998.

Paul, E.L., Atiemo-Obeng, V.A. & Kresta, A.M. (2004) Handbook of Industrial Mixing, WileyInterscience, Hobokken, NJ, USA.

Parthasarathy, R.; Jameson, G. J.; Ahmed, N. (1991) Bubble breakup in stirred vessels-predicting the Sauter mean diameter. *Chemical Engineering Research and Design*, 69, 295-301.

Parthasarathy, R.; Ahmed, N. (1994) Bubble Size Distribution in a Gas Sparged Vessel Agitated by a Rushton Turbine. *Industrial & Engineering Chemistry Research*, 33, (3), 703-711.

Raghavo Rao, K.S.M.S., Rewatkar, V.B. & Joshi, J.B. ((1998)) "Critical Impeller Speed for Solid Suspension in Mechanically Agitated Contactors," AIChE, 34, 1332–1340.

Ren, C.; Jiang, X.; Wang, J.; Yang, Y.; Zhang, X. (2008) Determination of critical speed for complete solid suspension using acoustic emission method based on multiscale analysis in stirred tank. *Industrial & Engineering Chemistry Research*, 47, 5323–5327.

Rewatkar, V. B.; Joshi, J. B. (1991) Role of sparger design in mechanically agitated gas-liquid reactors. Part I: Power consumption. *Chemical Engineering & Technology*, 14, (5), 333-347.

Rushton, J.H., Costich, E.W. and Everett H.J. (1950a) "Characteristics of Mixing Impellers, Part 1", Chem. Eng. Progr. 46, 395–404.

Rushton, J.H., E.W. Costich and H.J. Everett (1950b) "Characteristics of Mixing Impellers, Part 2", Chem. Eng. Progr. 46, 467–476.

Rushton J.H. and Bimbinet, J.J. ( 1968) “Holdup and flooding in air liquid mixing”, Can. Journal of Chem. Eng., vol 46, page 16-2.

Sano, Y., H. Usui, (1985) “Interrelations Among Mixing Time, Power Number and Discharge Flow Rate Number in Baffled Mixing Vessels”, J. Chem. Eng. Japan 18, 47–52.

Selima, Y. S.; Fangary, Y. S.; Mahmoud, N. A. (2008) Determination of minimum speed required for solids suspension in stirred vessels using pressure measurements. *The Canadian Journal of Chemical Engineering*, 86, (4), 661-666.

Smith, J.M., (1991) “Simple performance correlations for agitated vessels”, Proc. 7th Eur. Congress on mixing, Brugge, Belgium, page 233 - 241.

Sommerfeld, M.; Bröder, D. (2009) Analysis of Hydrodynamics and Microstructure in a Bubble Column by Planar Shadow Image Velocimetry. *Industrial & Engineering Chemistry Research*, 48, (1), 330-340.

Shiue, S. and C.W. Wong (1984) “Studies on Homogenization Efficiency of Various Agitators in Liquid Blending”, Can. J. Chem. Eng. 62, 602–609.

Takahashi, K.; Nienow, A. W. (1993) Bubble sizes and coalescence rates in an aerated vessel agitated by a Rushton turbine. *Journal of Chemical Engineering of Japan*, 26, (5), 536-542.

Tamburini, A.; Cipollina, A.; Micale, G.; Brucato, A., (2011) Dense solid-liquid suspensions in top-covered unbaffled stirred vessels. *Chemical Engineering Transactions*, 24, 1441–1446.

Tamburini, A.; Cipollina, A.; Micale, G.; Brucato, A. (2012) Measurements of Njs and power requirements in unbaffled bioslurry reactorr. *chemical Engineering Transactions*, 27, 343–348.

Tatterson, G.B., (1991), *Fluid mixing and gas dispersion in agitated tanks*, 1st edn. McGraw-Hill, New York.

Thomas, D. G., (1965) Transport characteristics of suspension: VIII. A note on the viscosity of Newtonian suspensions of uniform spherical particles. *Journal of Colloid Science*, 20, (3), 267-277.

Van't Riet, K., and Smith, J.M., (1973), 'The behaviour of gas-liquid mixtures near Rushton turbine blades', *Chemical Engineering Science*, vol. 28, pp. 1031-1037.

Wang, M.; Dorward, A.; Vlaev, D.; Mann, R. (2000) Measurements of gas–liquid mixing in a stirred vessel using electrical resistance tomography (ERT). *Chemical Engineering Journal*, 77, (1–2), 93-98.

Wang, S.; Boger, D. V.; Wu, J. (2012a) Energy efficient solids suspension in an agitated vessel–water slurry. *Chemical Engineering Science*, 74, 233-243.

Wang, S., Parthasarathy, R., Bong, E. Y., Wu, J., Slatter, P. (2012b) Suspension of ultrahigh concentration solids in an agitated vessel. *AIChE Journal*, 58, (4), 1291-1298.

Wang, S., Parthasarathy, R., Wu, J., Slatter, P. (2014) Optimum Solids Concentration in an Agitated Vessel. *Industrial & Engineering Chemistry Research*, 53, (10), 3959-3973.

Warmoeskerken, M. M. C. G.; Houwelingen, M. C. V.; Frijlink, J. J.; Smith, J. M. (1984) Role of Cavity Formation in Stirred Gas-Liquid-Solid Reactors. *Chemical Engineering Research and Design*, 62, 197-200.

Winterton, R. H. S.; Munaweera, J. S. (2001) Bubble size in two-phase gas–liquid bubbly flow in ducts. *Chemical Engineering and Processing: Process Intensification*, 40, (5), 437-447.

Wu, J., Zhu, Y.G. & Pullum, L. (2002) "Suspension of High Concentration Slurry," AIChE, 48, 6.

Wu, J., Graham, L., Wang, S., Parthasarathy, R. (2010a) Energy efficient slurry holding and transport. *Minerals Engineering*, 23, (9), 705-712.

Wu, J., Nguyen, B. & Graham, L. (2010b) "Mixing Intensification for the Mineral Industry," Canadian Journal of Chemical Engineering, In Press.

Yawalkar, A. A., Pangarkar, V. G., Beenackers, A. A. C. M., (2002) Gas hold-up in stirred tank reactors. *The Canadian Journal of Chemical Engineering*, 80, (1), 158-166.

Yoshida, Y. and Miura, Y. (1963) "Gas absorption in agitated gas-liquid contactors", Ind. Eng. Chem., process Des. Dev., 2, page 263-269.

Yung, C.N., Wong, C.W., and chong, C.L., (1979 ) "Gas holdup and areated power consumption in mechanically stirred tanks", 'Can. Journal of Chem.Eng., vol 57, page 672-676.

Zhu, Y.; Wu, J., (2002) Critical Impeller Speed for Suspending Solids in Aerated Agitation Tanks. *The Canadian Journal of Chemical Engineering*, 80, (4), 1-6.

Zwietering, T. N. (1958) Suspending of solid particles in liquid by agitators. *Chemical Engineering Science*, 8, (3–4), 244-253.

# LIST OF THE PROJECT OUTPUTS

*PATENT*

- 'Probe construction for studying bubble dynamics in three-phase stirred vessels' *Approved for patent registration by ministry of higher education.*

*ISI Journals*

- Meysam Davoody, Abdul Aziz Bin Abdul Raman, Rajarathinam Parthasarathy 'Agitation energy efficiency in gas-solid-liquid stirred vessels operating at ultra-high solids concentrations' *Chemical Engineering Research and Design,* 2016, 111: 34-48.
- Meysam Davoody, Abdul Aziz Abdul Raman, Rajarathinam Parthasarathy 'Maximisng gas-liquid interfacial area in a three-phase stirred vessel operating at high solids concentrations' *Chemical Engineering and Processing: Process Intensification*. 2016, 104: 133-147.
- Meysam Davoody, Abdul Aziz Abdul Raman, Rajarathinam Parthasarathy. 'Maximising impeller power efficiency in gas-solid-liquid stirred vessels through process intensification' *Industrial & Engineering Chemistry Research*. 2015, 54 (47): 11915-11928.
- Meysam Davoody, Abdul Aziz Bin Abdul Raman, Shaliza Ibrahim, Rajarathinam Parthasarathy **'**Prediction of just suspension speed for Rushton turbine agitated vessel using artificial intelligence-based techniques' under review in Iranian Journal of Chemical Engineering.

*Conference Presentations*:

- Meysam Davoody, Abdul Aziz Abdul Raman, Rajarathinam Parthasarathy 'Maximizing power efficiency in gas-solid-liquid stirred vessels handling high solids concentrations' Orally presentation in *Asian Pacific Confederation of Chemical Engineering (APCChE)*, Melbourne, 2015.
- Meysam Davoody, Abdul Aziz Abdul Raman, Rajarathinam Parthasarathy **'**Suspension of high concentration slurry in multiphase agitated vessels' presented in: *INTERNATIONAL SYMPOSIUM ON MIXING IN INDUSTRIAL PROCESSES VIII*, Melbourne, 14-17 September, 2014.